*ENGINEERING TRANSACTIONS* • *Engng. Trans.* • **51**, 2-3, 113–193, 2003
Polish Academy of Sciences • Institute of Fundamental Technological Research
10.24423/engtrans.485.2003

# ADAPTIVE ELASTICITY: A REVIEW AND CRITIQUE OF A BONE TISSUE ADAPTATION MODEL[1)]

S. C. Cowin

**The New York Center for Biomedical Engineering and
The Departments of Biomedical and Mechanical Engineering,
The School of Engineering of The City College and
The Graduate School of The City University of New York**
New York, NY 10031, U. S. A.
e-mail: scccc@cunyvm.cuny.edu

Living bone is continually undergoing processes of growth, reinforcement and resorption. These processes are termed collectively "remodeling". The remodeling processes in living bone are the mechanisms by which the bone adapts its histological structure to changes in long-term loading. The theory of adaptive elasticity was developed as a model for the mechanical load induced adaptation of bone. All three aspects of the theory of adaptive elasticity are reviewed here. These include internal adaptation, surface adaptation and architectural adaptation. The successes of the theory as well as the features of the theory that should now be revised are discussed.

**Key words:** adaptive elasticity, bone, bone strain adaptation, internal remodeling, surface remodeling, architectural remodeling

## Table of contents



[1)]Prepared for the CIM Advanced school and workshop on bone mechanics – mathematical and mechanical models for analysis and synthesis – held at the Instituto Superior Técnico in Lisbon, Portugal on June 24-28, 2002.

5. A summary of the theory
6. Small strain theory of adaptive elasticity
7. Specification of boundary initial value problems for small strain theory of adaptive elasticity
8. Homogeneous processes
9. Approximation of the coefficients
10. Solutions of the remodeling rate equation for steady strain and steady stress
11. The complete solutions to two classes of boundary value problems
12. Devolution of inhomogeneities under steady homogeneous stress
13. Internal bone remodeling induced by a medullary pin
14. An analytical model of Pauwels' functional adaptation mechanism in bone
15. Successes and deficiencies of the theory of adaptive elasticity

## Part II. Surface adaptation

1. The theory of surface remodeling
2. Establishing *in vivo* values for surface remodeling rate coefficients
3. The five animal experiments considered
4. Conceptual formulation of the mechanics problem
5. Estimation of parameters
6. Computational formulation of the problem
7. Summary of surface remodeling results
8. Successes and deficiencies of the surface remodeling theory

## Part III. Architectural adaptation

1. Wolff's law
2. The fabric tensor for cancellous bone tissue
3. The relationship between the fabric tensor and the elasticity tensor
4. Wolff's law at remodeling equilibrium
5. An evolutionary Wolff's law for trabecular architecture
6. Successes and deficiencies of the architectural adaptation theory

Appendix: Special vectors and tensors in six dimensions

## References

## Introduction

The ability of living bone to adapt its material structure and form to its mechanical loading is a well-known example linking biological form and function. The phenomena associated with bone adaptation to mechanical loading have become associated with the name of Julius Wolff because he called it his "law" (COWIN, 2001). In the 1800's a number of investigators made observations about bone form and function as described in WOLFF (1892, 1986) and ROUX (1885). There are two distinct portions to Wolff's "law". The "law" that pertains to trabecular bone architecture relies on the observed similarity of the predominant alignment of trabecular bone struts found internally near the ends of long bone and the approximate principal stress trajectories. The second portion of Wolff's "law" is that the external form of bone is dependent upon its function. For over a century, these observations by Julius Wolff about bone form and function have presented fertile ground for further investigation and criticism.

Models to describe functional adaptation may be classified as phenomenological or mechanistic. The phenomenological models attempt to simulate cause and effect (e.g., changed mechanical loading leading to changed bone architecture) without a consideration of the intermediary mechanisms involved. Phenomenological models allow for convenient testing of the consequences of different hypotheses about bone adaptation. This approach is often useful for eliminating some assumptions that don't match experimental or clinical results and observations (e.g., only compressive static loading leads to bone formation) or stimulate further investigations (e.g., strain rates and spatial gradients may regulate adaptation). The theory of adaptive elasticity considered here is a phenomenological model. This and other phenomenological models for cortical and cancellous bone adaptation have recently been reviewed by HART (2001).

Mechanistic models, on the other hand, start instead with parameters (e.g., bone cell activities and microenvironment) that are linked to portions of the biological processes involved in bone maintenance, turnover, and repair. These models, currently less developed than some of the phenomenological models because they are more complex, may lead to successfully linking mechanical and biological causes and effects. These models offer the promise of not only extending the descriptive and predictive capabilities of phenomenological models, but may offer insights into manipulation of the bone response, and development of pharmacological therapeutic agents. A mechanistic model for bone adaptation is described by COWIN and MOSS (2000). A mechanistic model that relates the effect of mechanical load applied to a whole bone to the bone fluid flow around the cells buried in the bone and, most significantly, to the bone adaptation process has been presented in a series of papers over the last decade: COWIN *et al.* (1991), WEINBAUM *et al.* (1994), COWIN *et al.* (1995), ZHANG *et al.* (1998),

COWIN (1999), WANG *et al.* (1999, 2000), YOU *et al.* (2001) and SMIT *et al.* (2002). Mechanistic models are not reviewed here; aspects of these models are reviewed in COWIN and MOSS (2000), HART (2001) and COWIN (2002).

The distinction made by FROST (1964) between surface and internal remodeling is followed here. Surface remodeling refers to the resorption or deposition of bone material on the external surface of the bone. Internal remodeling refers to the resorption or reinforcement of existing bone by decreasing or increasing respectively, the bulk density of the bone within fixed external boundaries. Part I concerns internal adaptation, Part II, surface adaptation and Part III is on architectural adaptation that concerns trabecular reorientation in cancellous bone.

## Part I. Internal adaptation

### 1. THE ORIGINS OF THE THEORY OF ADAPTIVE ELASTICITY

In 1970 George Hermann participated in the Southwest Mechanics Lecture Series and gave a lecture at Tulane University on the Mechanics of Bone Fracture (HERMANN and LIEBOWITZ, 1972). I was on the faculty at Tulane University at that time and attended the lecture. In that lecture George Hermann showed illustrations of bone plates, plates that were attached to the two ends of a fractured bone by screws to stabilize the fracture. Since it is well known in the mechanics of elastic materials that holes in an object filled with material of a different modulus cause stress concentrations, it was difficult to understand the use of the screws and, more significantly, leaving the screws in the bone indefinitely. To answer that question an area of research was begun that led to the theory of adaptive elasticity. The formal theory of adaptive elasticity originated in three papers (COWIN and HEGEDUS, 1976; HEGEDUS and COWIN, 1976; and COWIN and NACHLINGER, 1978). The objective of these papers was the formulation of a model for the understanding and prediction of the strain-controlled remodeling properties of normal living bone. The bone adaptation to the environmental strain model proposed in these papers was a thermomechanical continuum theory involving a chemical reaction and mass transfer between two constituents. The strain adapting properties of living bone are represented by a strain-controlled chemical reaction that transfers mass, momentum, entropy and energy to and from the porous elastic solid. The addition of mass to the porous solid modifies its porosity. Bone adaptation to environmental strain is a collective phrase for the continual processes of growth, reinforcement and resorption that occur in living bone. The resulting theory describes an elastic material that adapts its structure to applied loading, hence the term *adaptive elasticity.*

## 2. The guiding principles for the 1976 model of bone structural adaptation to environmental strain

The 1976 model was heavily influenced and guided by the book of Harold Frost (1964). The salient physical and biological features of bone adaptation to environmental strain that were identified as attributes of the 1976 model are (Cowin and Hegedus, 1976):

1. There are three basic components of whole bone: the bone cells; extracellular fluid; and the solid extracellular material that is called the bone matrix.
2. The bone matrix is a solid structure with interconnected pores. The mechanical properties of whole bone are essentially the same as the mechanical properties of the matrix.
3. The porosity of the bone matrix is affected by the ambient long-term strain history of the bone.
4. The porosity of the bone matrix is changed by the addition of mass or the removal of mass from the bone matrix. This transfer of mass occurs as the result of a chemical reaction that is mediated by the bone cells. Momentum, energy, and entropy may also be transferred to or from the matrix structure by these chemical reactions.
5. The rates of these chemical reactions depend upon the strain and are very slow. It can be estimated from studies using tetracycline labeling, that the characteristic time for such a reaction is of the order of months.
6. The extracellular fluid is always in contact with the blood plasma. The plasma supplies the materials necessary for the synthesis of bone matrix.
7. The characteristic time of chemical reaction is several orders of magnitude greater than the characteristic time associated with a complete perfusion of the blood plasma in the bone, hence any excess heat generated by the chemical reactions is quickly carried away by the circulation.

A continuum model was developed on the basis of these observations. It was assumed that the load adapting properties of living bone can be modeled by a chemically reacting porous medium in which the rate of reaction is strain controlled. The porous medium has two components: a porous elastic solid representing the matrix structure of bone including the bone cells and a perfusant that represents the extracellular fluid and the blood plasma which flow through the matrix structure. A schematic diagram of this model is shown in Fig. 1.

The fact that living bone is encased in a living organism is reflected in the model by setting the porous structure in a bath of the perfusant. The perfusant bath is assumed to be an isothermal heat reservoir, an assumption that appears to be easily justified by common knowledge concerning living organisms.

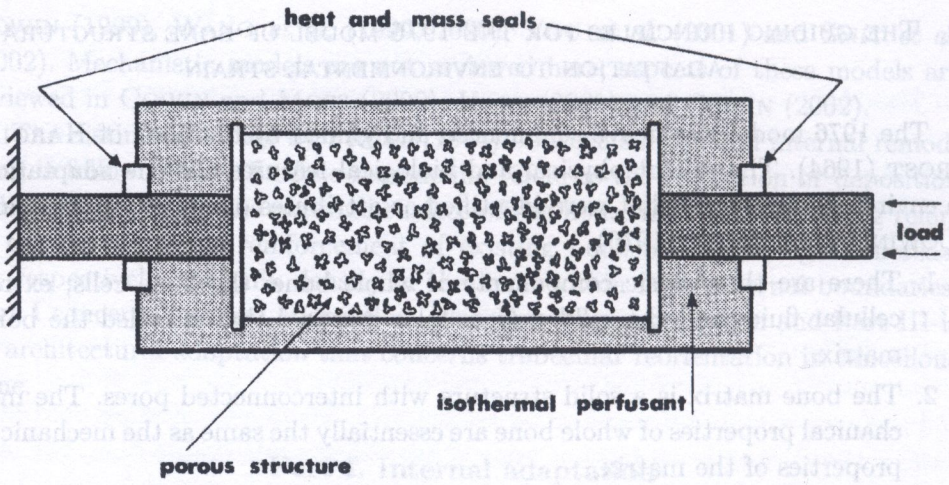


FIG. 1. A schematic diagram of the conceptual model for bone remodeling.

The mechanical load is applied directly to the porous structure across the walls of the perfusant bath as illustrated in Fig. 1. The system consisting of the porous structure and its perfusant bath is considered to be closed with respect to mass, heat energy, and entropy transfer, but open with respect to momentum transfer from loading. The system consisting of only the porous structure without its entrained perfusant is open with respect to momentum transfer as well as mass, energy, and entropy transfer. The bone matrix was considered to be the control system since the mechanical properties of the bone matrix alone determine the mechanical properties of the bone. Balance and constitutive equations were developed only for the bone matrix. The perfusant was accounted for only insofar as it transfers mass, momentum, energy, or entropy to the bone matrix. The rate at which mass, momentum, energy and entropy transfers occur was assumed to depend on the local strain and the other independent variables.

Two assumptions were also made concerning the momentum balance of the porous structure. First, it was assumed that the force of interaction between the porous structure and the perfusant is small compared to the load applied to the porous structure. The second assumption was that only mechanically quasi-static processes are considered. This is justified because the characteristic time of remodeling is so large compared to a characteristic time for inertia effects.

## 3. THE CONTINUUM MODEL, THE BALANCE EQUATIONS AND THE ENTROPY INEQUALITY

The motion $\chi(\mathbf{X}, t)$ gives the place $\mathbf{x}$ of a particle $\mathbf{X}$ at time $t$,

$$\mathbf{x} = \chi(\mathbf{X}, t). \tag{1.1}$$

The velocity $\mathbf{v}$ of a particle $\mathbf{X}$ is given by the time derivative of the motion holding the particle $\mathbf{X}$ fixed,

$$\mathbf{v} = \frac{D\chi}{Dt}_{\mathbf{X}=\text{const}}. \tag{1.2}$$

The deformation gradients $\mathbf{F}$ are defined by

$$\mathbf{F} = \frac{\partial \chi}{\partial \mathbf{X}}, \tag{1.3}$$

and the tensor velocity gradients are denoted by

$$\mathbf{L} = \frac{\partial \mathbf{v}}{\partial \mathbf{x}}. \tag{1.4}$$

The bulk density $\rho$ of the porous structure is expressed as a product

$$\rho = \gamma\nu, \tag{1.5}$$

where $\gamma$ is the density of the material that composes the matrix structure and $\nu$ is the volume fraction of that material present. Both $\gamma$ and $\nu$ can be considered as field variables. The balance of mass for the porous matrix structure without perfusant is given by

$$\frac{D}{Dt}\int_0 \gamma\nu dv = \int_0 c dv, \tag{1.6}$$

where the derivative indicated, $D/Dt$, is the material or substantial time derivative performed holding $\mathbf{X}$ constant; $c$ is the rate at which mass per unit volume is added to or removed from the porous matrix structure; $dv$ is an element of volume and $O$ indicates the porous matrix structure or any portion thereof. If $c$ vanishes, (1.6) reduces to a more familiar statement of mass balance. Because mass is being added to the object, the traditional transport theorem must be modified. If we let $f$ denote an arbitrary field quantity, the modified transport theorem can be stated in the form

$$\frac{D}{Dt}\int_0 \gamma\nu f dv = \int_0 (cf + \gamma\nu \dot{f}) dv. \tag{1.7}$$

This reduces to the usual transport theorem of Reynolds when $c$ vanishes. The balance of momentum for the porous matrix structure is given by

$$\frac{D}{Dt}\int_0 \gamma\nu \mathbf{v} dv = \int_{\partial O} \mathbf{T}\cdot\mathbf{n} ds + \int_0 \gamma\nu \mathbf{b} dv + \int_0 (c\mathbf{v} + \mathbf{p}) dv, \tag{1.8}$$

where $\mathbf{T}$ denotes the stress tensor, $ds$ is an element of surface area, $\partial O$ is the surface of $O$, $\mathbf{n}$ is a unit normal to the surface $\partial O$, $\mathbf{b}$ is the action-at-a-distance force and $\mathbf{p}$ is the force the perfusant applies to the porous matrix structure. The first three integrals in (1.8) are customary; the fourth is a departure. The first term in the fourth integrand represents the force of interaction between the porous matrix structure and the perfusant; the second term, $c\mathbf{v}$, represents the momentum added to the porous matrix structure due to the addition of mass.

The balance of energy for the porous matrix structure is given by

$$\frac{D}{Dt}\int_0 \gamma\nu\left(\varepsilon+\frac{1}{2}\mathbf{v}\cdot\mathbf{v}\right)dv=\int_{\partial O}(\mathbf{v}\cdot\mathbf{T}\cdot\mathbf{n}-\mathbf{q}\cdot\mathbf{n})\,ds + \int_0 \gamma\nu\,(\mathbf{b}\cdot\mathbf{v}+r)\,dv+\int_0\left(c\varepsilon+\frac{1}{2}c\mathbf{v}\cdot\mathbf{v}+\mathbf{p}\cdot\mathbf{v}+\bar{h}\right)dv, \tag{1.9}$$

where $\varepsilon$ is the specific internal energy, $r$ is the specific heat supply function per unit time, $\mathbf{q}$ is the heat flux vector, and $\bar{h}$ is the energy transfer between the matrix and the perfusant which will be discussed below. The first three integrals in (1.9) are customary; the first integral is the sum of the internal and kinetic energy, the second represents the work of the action-at-a-distance force and the heat supply per unit mass and the third represents the work done by the surface tractions and the heat flux. The fourth integrand in (1.9) is associated with the energy transfer between the matrix and the perfusant. The first term in the fourth integrand is the work done by the force of interaction; the second represents the kinetic energy of the added mass; and the third represents the internal energy of the added mass, assuming its specific internal energy is the same as that in the local porous structure. The fourth term represents any energy transfer between the matrix and the perfusant that is not accounted for by the other three terms. For example, $\bar{h}$ may represent the energy transfer due to the fact that the internal energy of the added mass is not the same as that of the local porous structure.

We assume the entropy inequality to be of the form

$$\frac{D}{Dt}\int_0 \gamma\nu\eta dv \geq -\int_{\partial O}\frac{\mathbf{q}\cdot\mathbf{n}}{\theta}ds+\int_0\frac{\gamma\nu r}{\theta}dv+\int_0\left(c\eta+\frac{\tilde{h}}{\theta}\right)dv, \tag{1.10}$$

where $\eta$ is the specific entropy, $\theta$ is temperature and $\tilde{h}$ is defined in the same fashion as $\bar{h}$ above. We distinguish between $\tilde{h}$ and $\bar{h}$ to indicate that all the energy transferred from the perfusant to the matrix need not contribute to the entropy production. As in the case of the balance equations for momentum and energy, the first three integrals are traditional and the last integral represents the entropy

produced by the perfusant and the chemical reaction between the perfusant and the matrix structure. The first integral represents the total entropy, the second is the entropy production associated with the specific heat supply, the third is the entropy production associated with the heat flux and the fourth represents the entropy production due to the interaction between the matrix and perfusant that is not accounted for in the other three terms. For example, this term may represent the difference between the specific entropy of the added mass and the specific entropy of the local porous structure.

The integral equations (1.6), (1.8), (1.9) and (1.10) can be converted to field equations by use of the divergence theorem and the modified transport theorem (1.7). The results of these manipulations are

$$\dot{\gamma\nu} + \gamma\dot{\nu} + \gamma\nu\nabla\cdot\mathbf{v} = c, \tag{1.11}$$

$$\gamma\nu\dot{\mathbf{v}} = \nabla\cdot\mathbf{T} + \gamma\nu\mathbf{b} + \mathbf{p}, \tag{1.12}$$

$$\gamma\nu\dot{\varepsilon} = \mathbf{T}:\mathbf{L} + \gamma\nu r - \nabla\cdot\mathbf{q} + \bar{h}, \tag{1.13}$$

$$\gamma\nu\dot{\eta} \geq \frac{\gamma\nu r}{\theta} - \nabla\cdot\left(\frac{\mathbf{q}}{\theta}\right) + \frac{\tilde{h}}{\theta}, \tag{1.14}$$

which are field equations representing the balance of mass, momentum, energy, and the local form of the entropy inequality. It is convenient to use the specific free energy $\psi$,

$$\psi = \varepsilon - \eta\theta \tag{1.15}$$

rather than the internal energy $\varepsilon$, and to introduce $h$ to denote the difference between $\bar{h}$ and $\tilde{h}$,

$$h = \bar{h} - \tilde{h}. \tag{1.16}$$

A reduced entropy inequality is obtained by using the energy field Eq. (1.14) to eliminate the radiation supply $r$ from the entropy inequality (1.14) and then introducing the notation (1.15) and (1.20), thus

$$-\gamma\nu\dot{\psi} - \gamma\nu\eta\dot{\theta} + \mathbf{T}:\mathbf{L} - \frac{1}{\theta}\mathbf{q}\cdot\nabla\theta + h \geq 0. \tag{1.17}$$

This reduced entropy inequality is one of the arguments used in Sec. 5 to restrict constitutive assumptions made in Sec. 4.

## 4. Constitutive assumptions

The objective was to develop a model for bone as a porous elastic solid and to model the normal adaptive processes that occur in bone remodeling as strain-controlled mass deposition or resorbtion processes which modify the porosity of the porous elastic solid. Constitutive assumptions similar to those made for elastic solids, but with the addition of an independent variable which is a measure of the volume fraction of matrix structure, were assumed. We let $\xi$ denote the volume fraction of the matrix material in an unstrained reference state. The density $\gamma$ of the material composing the matrix is assumed to be constant. Thus the conservation of mass will give the equation governing $\xi$.

Our first important constitutive assumption is that, at constant temperature and zero action-at-a-distance force, there exists a unique zero-strain reference state for all values of $\xi$. Thus $\xi$ may change without changing the reference state for strain. One might imagine a block of porous elastic material with the four points, the vertices of a tetrahedron, marked on the block for the purpose of measuring the strain. When the porosity changes, material is added to or taken away from the pores, but if the material is unstrained it remains so and the distance between the four vertices marked on the block does not change. Thus $\xi$ can change while the zero-strain reference state remains the same. A formal definition of $\xi$ can be made in terms of the volume fraction $v$ associated with the strain state characterized by $\mathbf{F}$, thus

$$\xi = \nu \mathrm{Det}\mathbf{F} = \nu J, \qquad J = \mathrm{Det}\mathbf{F}. \tag{1.18}$$

The definition (1.18) only makes sense for a constant density $\gamma$ of the matrix structure. If the definition (1.18) is substituted into the statement of mass balance (1.11), a relation between $\xi$ and $c$ is obtained,

$$\dot{\xi} = (c/\gamma)\mathrm{Det}\mathbf{F} = (c/\gamma)J. \tag{1.19}$$

Constitutive equations are needed for the specific free energy $\psi$, the entropy $\eta$, the heat flux $\mathbf{q}$, the stress tensor $\mathbf{T}$, the entropy production term $h$, and the rate $c$ at which mass per unit volume is added or removed. The constitutive assumptions made in 1976 were that each of these quantities depends on the temperature $\theta$, the temperature gradient $\nabla\theta$, the zero-strain volume fraction $\xi$ and the deformation gradients $\mathbf{F}$; thus $\psi$, $\eta$, $\mathbf{T}$, $\mathbf{q}$, $h$, and $c$ are all functions of $\theta, \nabla\theta, \xi$ and $\mathbf{F}$.

$$\begin{aligned} \psi &= \psi(\theta, \nabla\theta, \xi, \mathbf{F}), \quad \eta = \eta(\theta, \nabla\theta, \xi, \mathbf{F}), \quad \mathbf{T} = \mathbf{T}(\theta, \nabla\theta, \xi, \mathbf{F}), \\ \mathbf{q} &= \mathbf{q}(\theta, \nabla\theta, \xi, \mathbf{F}), \quad h = h(\theta, \nabla\theta, \xi, \mathbf{F}), \quad c = c(\theta, \nabla\theta, \xi, \mathbf{F}). \end{aligned} \tag{1.20}$$

## 5. A SUMMARY OF THE THEORY

Using the constitutive assumptions, balance equations and thermodynamic arguments it is possible to show that

$$\psi = \psi(\theta, \xi, \mathbf{F}), \quad \eta = -\frac{\partial \psi}{\partial \theta}, \quad \mathbf{T} = \gamma\nu \frac{\partial \psi}{\partial \mathbf{F}}\mathbf{F} = \frac{\xi\gamma}{\det \mathbf{F}} \frac{\partial \psi}{\partial \mathbf{F}}\mathbf{F}. \tag{1.21}$$

An additional constitutive assumption is that there exists a unique zero-strain reference state for all values of $\xi$; this is expressed in equation form as

$$\frac{\partial \psi}{\partial \mathbf{F}}(\theta_0, \xi, \mathbf{1}) = 0 \tag{1.22}$$

for a fixed value of $\theta_0$. To these constitutive equations the balance equations are added. These are the balance of mass in the form (1.18), the balance of momentum (1.16) in the form

$$0 = \nabla \cdot \mathbf{T} + \gamma\nu\mathbf{b}, \tag{1.23}$$

where the inertia term has been neglected because of the quasistatic assumption and where the force $\mathbf{p}$ due to the perfusant has been neglected, and the balance of energy (1.13) with $\psi$ substituted for $\varepsilon$ by (1.15),

$$\gamma\nu(\dot{\psi} + \eta\dot{\theta} + \theta\dot{\eta}) = \mathbf{T} : \mathbf{L} + \gamma\nu r - \nabla \cdot \mathbf{q} + \bar{h}. \tag{1.24}$$

The entropy inequality is reduced to

$$-\xi \frac{\partial \psi}{\partial \xi} c - \frac{1}{\theta}\mathbf{q} \cdot \nabla\theta + h \geq 0. \tag{1.25}$$

For an isothermal process this system of equations simplifies considerably. The mass balance is still expressed by (1.18), the momentum balance by (1.23), the constitutive relation for stress by $(1.21)_3$, but $c$ and $\psi$ are now only functions of $\xi$ and $\mathbf{F}$.

$$c = c(\xi, \mathbf{F}), \qquad \psi = \psi(\xi, \mathbf{F}), \tag{1.26}$$

where $\psi$ must still satisfy (1.22). Equations (1.18), (1.23) and $(1.21)_3$ are a system of 10 scalar equations in the ten unknowns $\xi, \boldsymbol{\chi}$ and $\mathbf{T}$.

## 6. SMALL STRAIN THEORY OF ADAPTIVE ELASTICITY

A non-traditional notation is employed for symmetric second order tensors and for the fourth order tensors in three dimensions (fourth order tensors with

the symmetry of the elasticity tensor), in this and subsequent sections. This notation is explained in the Appendix. It consists of representing quantities that are symmetric second order tensors in three dimensions as vectors in six dimensions and representing quantities that are fourth order tensors in 3 dimensions as second order tensors in 6 dimensions. The six-dimensional quantities are distinguished by a circumflex over the kernel letter; thus $\mathbf{T}$ represents the second rank tensor in three dimensions and $\widehat{\mathbf{T}}$ represents the same quantity as a vector in six dimensions. The three-dimensional fourth order elasticity tensor is represented as the second rank tensor $\hat{\mathbf{c}}$ in six dimensions. This notation thus permits a consistent representation of these three-dimensional fourth rank tensors in matrix notation.

In the case of small strain the basic strain measure is the strain tensor $\mathbf{E}$ that is related to the displacement vector $\mathbf{u}$ by

$$\mathbf{E} = \frac{1}{2}\left(\nabla \otimes \mathbf{u} + (\nabla \otimes \mathbf{u})^T\right). \tag{1.27}$$

The basic system of equations for isothermal small strain adaptive elasticity consist of the equilibrium condition (1.23) where, to terms of first order in strain, $\mathbf{v}$ is given by

$$\nu = (\xi_0 + e)(1 - \mathrm{tr}\mathbf{E}); \tag{1.28}$$

the stress-strain relations,

$$\widehat{\mathbf{T}} = (\xi_0 + e)\hat{\mathbf{c}} \cdot \widehat{\mathbf{E}}, \tag{1.29}$$

where $\hat{\mathbf{c}}$ is the elasticity tensor (see Appendix A for a detailed explanation of this notation); the rate of reaction-strain relation

$$\dot{e} = a(e) + \mathbf{A} : \mathbf{E} = a(e) + \hat{\mathbf{A}} \cdot \widehat{\mathbf{E}}; \tag{1.30}$$

and the strain displacement relations (1.27). This is a system of 16 scalar equations involving the 16 scalar unknowns, $\mathbf{T}$, $\mathbf{E}$, $\mathbf{u}$ and $e$. The inverse of the elasticity tensor $\hat{\mathbf{c}}$ is the compliance tensor $\hat{\mathbf{s}}$, thus

$$(\xi_0 + e)\hat{\mathbf{s}}(e)\hat{\mathbf{c}} = \hat{\mathbf{I}}. \tag{1.31}$$

Using the compliance tensor, the stress-strain relations (1.29) can be inverted for the strains

$$\widehat{\mathbf{E}} = \hat{\mathbf{s}}(e) \cdot \widehat{\mathbf{T}}. \tag{1.32}$$

The expression (1.30) for $\dot{e}$ can also be written in terms of stress; thus from (1.32),

$$\dot{e} = a(e) + \hat{\mathbf{A}} \cdot \hat{\mathbf{s}}(e) \cdot \widehat{\mathbf{T}}. \tag{1.33}$$

Finally, we note that the small strain approximations for $\dot{e}$ and $\psi$ were

$$\dot{e}(e, \widehat{\mathbf{E}}) = a(e) + \hat{\mathbf{A}}(e) \cdot \widehat{\mathbf{E}} + \frac{1}{2}\widehat{\mathbf{E}} \cdot \hat{\mathbf{b}}(e) \cdot \widehat{\mathbf{E}} + \ldots \tag{1.34}$$

$$\psi(e, \widehat{\mathbf{E}}) = \psi(e, 0) + \frac{1}{\gamma}\hat{\mathbf{D}}(e) \cdot \widehat{\mathbf{E}} + \frac{1}{2\gamma}\widehat{\mathbf{E}} \cdot \hat{\mathbf{c}}(e) \cdot \widehat{\mathbf{E}} + \ldots \tag{1.35}$$

## 7. Specification of boundary-initial value problems for small strain theory of adaptive elasticity

In order to specify a displacement boundary value problem in infinitesimal adaptive elasticity, the following data must be given:

a) the geometry of the object $O$ and its material properties $\gamma, a(e), \mathbf{A}(e)$ and $\hat{\mathbf{c}}$,

b) the time interval $[0, t_0)$ for which a solution is desired,

c) the action-at-a-distance force field $\mathbf{b}$,

d) the continuous surface displacement $\breve{\mathbf{u}}(\mathbf{x}, t)$, specified on $\partial O$ for $t \subset [0, t_0)$, and

e) the continuous initial displacement field $\mathbf{u}_0(\mathbf{x})$ and the continuous initial relative volume fraction field $e_0(\mathbf{x})$ for all $\mathbf{x} \subset O$.

With these data, the displacement boundary value problem of quasi-static, isothermal, infinitesimal elasticity is to determine the fields $\mathbf{T}(\mathbf{x}, t), \mathbf{E}(\mathbf{x}, t), \mathbf{u}(\mathbf{x}, t)$ and $e(\mathbf{x}, t)$ corresponding to $\mathbf{b}$ which satisfy the initial conditions

$$\mathbf{u}(\mathbf{x}, 0) = \mathbf{u}_0(\mathbf{x}), \quad e(\mathbf{x}, 0) = e_0(\mathbf{x}) \quad \text{for all} \quad \mathbf{x} \subset O, \tag{1.36}$$

the boundary conditions

$$\mathbf{u}(\mathbf{x}, t) = \breve{\mathbf{u}}(\mathbf{x}, t), \quad \text{for all} \quad \mathbf{x} \subset \partial O, \tag{1.37}$$

and the differential Eqs. (1.23), (1.27), (1.29) and (1.30). The traction boundary value problem is described in a similar way in Hegedus and Cowin (1976).

Cowin and Nachlinger (1978) proved a uniqueness theorem for the theory described above as well as two theorems establishing sufficient conditions for stability. The asymptotic stability theorem on small perturbations requires that the derivative of the remodeling rate Eq. (1.30) with respect to $e$ satisfy an inequality depending upon $\mathbf{A}$ and the derivative of the stress $\mathbf{T}$ with respect to $e$. From a mathematical viewpoint the theory appears to be well behaved. The question of existance and uniqueness for this theory is throughly analyzed by Monnier and Trabucho (1998 a, b) and Trabucho (1999).

## 8. Homogeneous processes

For a boundary-initial value problem involving a homogeneous, isothermal, adaptive infinitesimally elastic material object that is subjected to homogeneous

initial data and no action-at-a-distance forces, two results can be proved. First, one can show that a homogeneous strain field implies a homogeneous stress field and homogeneous adaptation. Second, one can show that a homogeneous stress field implies a homogeneous strain field and homogeneous adaptation.

To see the validity of the first statement one has to observe from (1.30) that if the material is homogeneous (i.e., $a(e)$ and $\mathbf{A}(e)$ are not functions of position), the strain is homogeneous, and since the initial condition on the field $e_0$ is homogeneous, then $e$ is homogeneous for all time. Since the $e$ field and the strain fields are homogeneous for all time, it follows from (1.29) that the strain field is also homogeneous.

## 9. Approximation of the coefficients

The infinitesimal theory involves the functions $a(e)$, $\mathbf{A}(e)$ and the elasticity tensor $\hat{\mathbf{c}}(e)$, or the compliance tensor $\hat{\mathbf{s}}(e)$, characterizing the material properties. From the specification of the two traditional types of boundary value problems, it is clear that knowledge of these functions is necessary in order to solve the boundary value problems. On the other hand there are no experimental data on these functions. To break this unproductive circularity the functions $a(e)$, $\mathbf{A}(e)$ and $\hat{\mathbf{c}}(e)$ are approximated for small values of $e$. To accomplish this approximation we return to the Taylor series expansions (1.34) and (1.35) for $\dot{e}(e, E)$ and $\psi(e, E)$, respectively, and replace our previous series expansions by joint expansions in $e$ and $\mathbf{E}$. In the series expansions, terms of the order $e^3, |\mathbf{E}|e^2$, and $|\mathbf{E}|^2 e$ will be neglected and terms of the order $e$, $|\mathbf{E}|, |\mathbf{E}|e$ and $e^2$ retained. This approximation is a balance between physical plausibility and mathematical tractability. While there is substantial physical justification for assuming that $|\mathbf{E}| < .001$, the value of $e$ is certainly not required to be that small. By its definition $e$ is only required to satisfy the inequality $1 - \xi_0 > e > -\xi_0$, $1 > \xi_0 > 0$. It appears reasonable to assume that for healthy bone one can pick $\xi_0$ so that $|e| < 0.1$; however, for pathological situations which are of interest in the present work, $|e|$ is known to exceed this value. Using the approximation stated above, the expansions (1.34) and (1.35) are replaced by

$$\dot{e}(e, \widehat{\mathbf{E}}) = c_0 + c_1 e + c_2 e^2 + \hat{\mathbf{A}}^0 \cdot \widehat{\mathbf{E}} + e\hat{\mathbf{A}}^1 \cdot \widehat{\mathbf{E}} + \frac{1}{2}\widehat{\mathbf{E}} \cdot \hat{\mathbf{b}}^1 \cdot \widehat{\mathbf{E}} + \ldots, \tag{1.38}$$

and

$$\psi(e, \widehat{\mathbf{E}}) = b_0 + b_1 e + b_2 e^2 + \frac{1}{\gamma}\left\{\widehat{\mathbf{D}}^0 + e\widehat{\mathbf{D}}^1\right\} \cdot \widehat{\mathbf{E}} + \frac{1}{2\gamma}\widehat{\mathbf{E}} \cdot \left\{\hat{\mathbf{c}}^0 + e(\hat{\mathbf{c}}^1 - \hat{\mathbf{c}}^0)\right\} \cdot \widehat{\mathbf{E}} + \ldots, \tag{1.39}$$

respectively. Note that the remodeling rate equation (1.35) for $\dot{e}$ depends not only upon strain, but also has a second order dependence upon a strain energy-like term, $\frac{1}{2}\widehat{\mathbf{E}}\cdot\hat{\mathbf{b}}^1\cdot\widehat{\mathbf{E}}$. Later investigators focused on this strain energy term as the stimulus for $\dot{e}$ and suppressed the dependence upon strain (FYHRIE and CARTER, 1986; HUISKES *et al.* 1987). The argument for strain energy over strain in this situation was that strain energy was easier to compute. That option was not taken in the work reported here because the directional information contained in the strain tensor is lost when the strain energy is computed.

With these approximations outlined above, the stress-strain relation (1.29) takes the form

$$\widehat{\mathbf{T}} = \xi_0\hat{\mathbf{c}}^0\cdot\widehat{\mathbf{E}} + e\hat{\mathbf{c}}^1\cdot\widehat{\mathbf{E}}, \tag{1.40}$$

and the rate of reaction-strain relation (1.30) becomes

$$\dot{e}(e,\widehat{\mathbf{E}}) = c_0 + c_1 e + c_2 e^2 + \hat{\mathbf{A}}^0\cdot\widehat{\mathbf{E}} + e\hat{\mathbf{A}}^1\cdot\widehat{\mathbf{E}}, \tag{1.41}$$

both of which depend upon strain and not strain energy. When this equation is viewed as an ordinary differential equation in time for $e$ it is a Riccati differential equation. The importance of this remark is that, while the Riccati differential equation is a nonlinear first order differential equation, it can be reduced by a simple substitution to a homogeneous linear second order differential equation. Thus if we introduce $u(t)$ such that

$$e = -\frac{\dot{u}}{c_2 u}, \tag{1.42}$$

then (1.41) can be recast as a homogeneous linear second order differential equation in $u$,

$$\ddot{u} - (c_1 + \hat{\mathbf{A}}^1\cdot\widehat{\mathbf{E}})\dot{u} + c_2(c_0 + \hat{\mathbf{A}}^0\cdot\widehat{\mathbf{E}})u = 0. \tag{1.43}$$

If $\widehat{\mathbf{E}}$ is continuous with respect to time, the initial boundary value problem for this differential equation has a unique solution for specified $u(0)$ and $\dot{u}(0)$. Comparison of (1.40) with (1.29) and (1.41) with (1.33) shows that the consistent approximations for the material functions $a(e)$, $\mathbf{A}(e)$ and $\hat{\mathbf{c}}(e)$ are

$$a(e) = c_0 + c_1 e + c_2 e^2, \quad \hat{\mathbf{A}}(e) = \hat{\mathbf{A}}^0 + e\hat{\mathbf{A}}^1, \quad \hat{\mathbf{c}}(e) = \frac{1}{\xi_0 + e}(\xi_0\hat{\mathbf{c}}^0 + e\hat{\mathbf{c}}^1), \tag{1.44}$$

where $c_0, c_1, c_2, \hat{\mathbf{A}}^0, \hat{\mathbf{A}}^1, \hat{\mathbf{c}}^0$, and $\hat{\mathbf{c}}^1$ are all constants representing the material properties. To terms of the order $e$, the inverse $\hat{\mathbf{s}}(e)$ of $(\xi_0 + e)\hat{\mathbf{c}}(e)$ is given by (1.31) as

$$\hat{\mathbf{s}}(e) = \hat{\mathbf{s}}^0 - e\hat{\mathbf{s}}^0\cdot\hat{\mathbf{c}}^1\cdot\hat{\mathbf{s}}^0, \quad \text{where} \quad \xi_0\hat{\mathbf{s}}^0\cdot\hat{\mathbf{c}}^0 = \mathbf{1}. \tag{1.45}$$

## 10. Solutions of the remodeling rate equation for steady strain and steady stress

Not all the solutions of the remodeling rate Eq. (1.30) will yield functions $e(\mathbf{x}, t)$ satisfying the inequality $1 - \xi_0 > e > -\xi_0$. Solutions of the remodeling rate Eq. (1.30) which predict values of $e(\mathbf{x}, t)$ tending to $1 - \xi_0$, or $-\xi_0$, might have physiological interpretation in that well known pathological conditions in bone are characterized by the bone becoming much less porous or much more porous than normal bone. The results of the present analysis are of interest in this regard because the conditions under which the remodeling rate equation (1.30) predicts solutions of $e$ tending to $1 - \xi_0$, or $-\xi_0$, can be calculated and associated with the physical conditions giving rise to these pathologies.

To illustrate the varieties of behavior of $e(\mathbf{x}, t)$ as a function of time we consider the approximate theory of the previous section and the approximate remodeling rate Eq. (1.41) in place of (1.30). The results of the following analysis are then limited by the assumed smallness of $e$. We consider a point $\mathbf{x}$ in an adapting object where, for $t < 0$, the adapting object is in mechanical and remodeling equilibrium. By mechanical and remodeling equilibrium we mean that there exist steady stresses $\mathbf{T}^0(\mathbf{x})$, steady strains $\mathbf{E}^0(\mathbf{x})$ and a steady field $e_0(\mathbf{x})$ satisfying Eqs. (1.23) for zero action-at-a-distance force, the stress-strain relation (1.40), the strain displacement relation (1.27) and the remodeling rate-strain equation (1.41) in the form

$$0 = c_0 + c_1 e(\mathbf{x}) + c_2 e(\mathbf{x})^2 + \hat{\mathbf{A}}^0 \cdot \widehat{\mathbf{E}}^0(\mathbf{x}) + e(\mathbf{x}) \hat{\mathbf{A}}^1 \cdot \widehat{\mathbf{E}}^0(\mathbf{x}). \tag{1.46}$$

For $t \geq 0$ we consider two different situations, the first where the strain is steady and second where the stress is steady. Suppose that at $t = 0$ the strain at the point $\mathbf{x}$ is changed from $\widehat{\mathbf{E}}^0(\mathbf{x})$ to $\widehat{\mathbf{E}}^*(\mathbf{x})$ and held steady at $\widehat{\mathbf{E}}^*(\mathbf{x})$ for all $t > 0$. In this situation $e(\mathbf{x}, t)$ is determined by the differential Eq. (1.42) and the initial condition on $e(x, t)$, thus

$$\dot{e} = a(e^2 - 2be + c), \qquad e(\mathbf{x}, 0) = e_0(\mathbf{x}), \tag{1.47}$$

where

$$a = c_2, \qquad b = -\frac{1}{2c_2}(c_1 + \hat{\mathbf{A}}^1 \cdot \widehat{\mathbf{E}}^*(\mathbf{x})), \qquad c = \frac{1}{c_2}(c_0 + \hat{\mathbf{A}}^0 \cdot \widehat{\mathbf{E}}^*(\mathbf{x})), \tag{1.48}$$

and where $a, b$, and $c$ are independent of time. In formulating (1.46) we have assumed that $c_2$ is not equal to zero. The solution to the problem when $c_2$ is zero is very simple, relatively uninteresting, and not recorded here.

The second situation of interest, that of steady stress, leads again to the differential equation (1.46). We change the above argument for $t \geq 0$ and, rather

than holding $\widehat{\mathbf{E}}^*(\mathbf{x})$ steady, we change the stress $\widehat{\mathbf{T}}^0(\mathbf{x})$ to $\widehat{\mathbf{T}}^*(\mathbf{x})$ at $t = 0$ and hold $\widehat{\mathbf{T}}^*(\mathbf{x})$ steady for all time $t > 0$. From (1.32), (1.44) and (1.40) we again obtain (1.47), but $b$ and $c$ are now given by

$$b = -\frac{1}{2c_2}\left(c_1 + \hat{\mathbf{A}}^1 \cdot \hat{\mathbf{s}}^0 \cdot \widehat{\mathbf{T}}^*(\mathbf{x}) - \hat{\mathbf{A}}^0 \cdot \hat{\mathbf{s}}^0 \cdot \hat{\mathbf{c}}^1 \cdot \hat{\mathbf{s}}^0 \cdot \widehat{\mathbf{T}}^*(\mathbf{x})\right),$$

(1.49)

$$c = \frac{1}{c_2}\left(c_0 + \hat{\mathbf{A}}^0 \cdot \hat{\mathbf{s}}^0 \cdot \widehat{\mathbf{T}}^*(\mathbf{x})\right).$$

Thus, for both the steady stress and steady strain situation the differential equation (1.47) is the object of study.

The solution to the differential equation (1.47) is straightforward. Using the substitution (1.42), (1.47) can be reduced to a linear differential equation of second order with constant coefficients,

$$\ddot{u} + 2ab\dot{u} + a^2cu = 0. \tag{1.50}$$

This differential equation has an associated plane autonomous system obtained by introducing $v$ such that

$$v = \frac{du}{dt}; \tag{1.51}$$

then the matrix equation

$$\begin{bmatrix} \dot{u} \\ \dot{v} \end{bmatrix} = \begin{bmatrix} 0 & 1 \\ -a^2c & -2ba \end{bmatrix} \begin{bmatrix} u \\ v \end{bmatrix} \tag{1.52}$$

is equivalent to (1.50). We let $e_1, e_2$ denote the solutions to the quadratic equation $e^2 - 2be + c = 0$,

$$e_1, e_2 = b \pm \sqrt{b^2 - c}, \tag{1.53}$$

and employ the convention $e_1 \geq e_2$ when $e_1$ and $e_2$ are real. The solutions to Eq. (1.47) are then

$$e = \frac{e_1(e_0 - e_2) + (e_1 - e_0)e_2 e^{-a(e_1 - e_2)t}}{(e_0 - e_2) + (e_1 - e_0)e^{-a(e_1 - e_2)t}} \tag{1.54}$$

for $e_1$ and $e_2$ real and $e_1 > e_2$;

$$e = e_1 - \frac{(e_1 - e_0)}{1 + a(e_1 - e_0)t} \tag{1.55}$$

for $e_1$ and $e_2$ real and $e_1 = e_2$; and

$$e = b + \sqrt{(c - b^2)} \tan \left\{ at\sqrt{(c - b^2)} + \tan^{-1} \frac{\sqrt{(c - b^2)}}{b - e_0} \right\} \tag{1.56}$$

for $e_1$ and $e_2$ complex conjugate. An inspection of these solutions shows that in certain cases $e$ can become infinite in finite time. Specifically, for $a > 0, e$ tends to $+\infty$ as

$$t \to \frac{1}{a(e_1 - e_2)} \ln \frac{(e_0 - e_2)}{(e_0 - e_1)} \tag{1.57}$$

for $e_1$ and $e_2$ real and $e_0 > e_1 > e_2$;

$$t \to \frac{1}{a(e_1 - e_2)} \tag{1.58}$$

for $e_1$ and $e_2$ real and $e_0 > e_1 = e_2$; and

$$t \to \frac{1}{a\sqrt{(c - b^2)}} \left( \frac{\pi}{2} - \tan^{-1} \frac{\sqrt{(c - b^2)}}{b - e_0} \right) \tag{1.59}$$

for $e_1$ and $e_2$ complex conjugate and all values of $e_0$. Also, for $a < 0$, $e$ tends to $-\infty$ as

$$t \to \frac{-1}{a(e_1 - e_2)} \ln \frac{(e_2 - e_0)}{(e_1 - e_0)} \tag{1.60}$$

for $e_1$ and $e_2$ real and $e_1 > e_2 > e_0$; as

$$t \to \frac{-1}{a(e_1 - e_0)} \tag{1.61}$$

for $e_1$ and $e_2$ real and $e_1 = e_2 > e_0$; as

$$t \to \frac{-1}{a\sqrt{(c - b^2)}} \left( \frac{\pi}{2} + \tan^{-1} \frac{\sqrt{(c - b^2)}}{b - e_0} \right) \tag{1.62}$$

for $e_1$ and $e_2$ complex conjugate and all values of $e_0$. Inspection of the solutions (1.54), (1.55) and (1.56) also shows that $e$ tends to certain finite values in infinite time under certain conditions. Specifically $e \to e_2$ as $t \to \infty$ for $a > 0$, $e_1 \geq e_0$ and $e_1$ and $e_2$ real. Also $e \to e_1$ as $t \to \infty$ for $a < 0, e_0 \geq e_2$ and $e_1$ and $e_2$ real.

Some insight into the behavior of these solutions to the remodeling rate Eq. (1.47) can be obtained by considering their representation in the phase plane. In Fig. 2 the solution to the remodeling rate equation (1.47) is plotted in the

case when $e_1$ and $e_2$ are real and unequal for both $a > 0$ and $a < 0$. In this case the remodeling equation is a parabola in $\dot{e}$ and $e$ which crosses the $e$ axis at two points and opens up or down depending on the sign of $a$. These parabolas are sketched in Fig. 2. The arrowheads on the parabolas indicate the direction a solution will evolve in positive time for a given value of $e$. Thus, for example, the fact that $e \to e_2$ in infinite time for $e_1$ and $e_2$ real, $a > 0$ and $e_1 \geq e_0$ is indicated by the arrowheads on the parabola to the left and the right of $e_2$ being directed towards $e_2$. That the arrowheads to the right of $e_1$ are oppositely directed is consistent with the fact that $e \to \infty$ in finite time for $e_1$ and $e_2$ real, $a > 0$ and $e_0 > e_1$. A completely analogous description holds for the case $a < 0$ shown in Fig. 2. When $e_1$ and $e_2$ are complex conjugates, the parabola described by the remodeling rate Eq. (1.47) does not cross the $e$ axis. This situation is illustrated in Fig. 3. The fact that all solutions of (1.47) tend to $\pm\infty$ for $e_1$ and $e_2$ complex conjugate is indicated by the unidirectionality of the arrowheads. When $e_1$ and $e_2$ are real and equal the parabola described by (1.47) is tangent to the $e$ axis at the point $e = e_1 = e_2$. This situation would be illustrated by parabolas exactly like those in Fig. 2, except that they would be tangent at their extremum points to the $e$ axis.

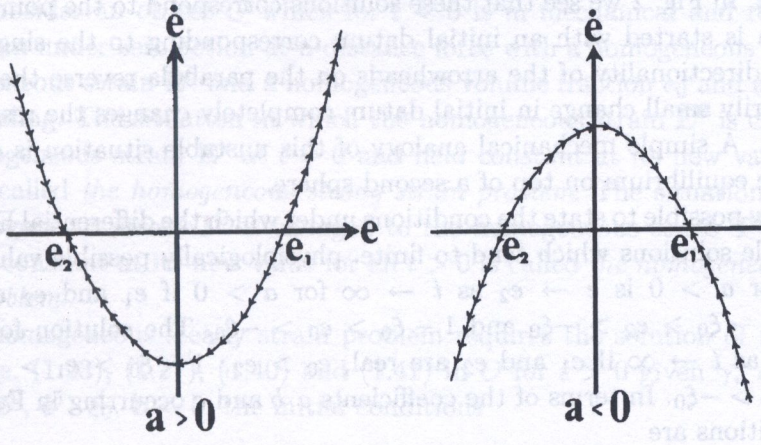


FIG. 2. A phase plane plot of the solution to the remodeling Eq. (1.47) when $e_1$ and $e_2$ are real and unequal.

We have observed that there are two situations in which the solutions of the remodeling Eq. (1.47) tend to finite values. In the first of these situations $e \to e_2$ as $t \to \infty$, $e_1 \geq e_0$ and $e_1$ and $e_2$ real. In the second $e \to e_1$ as $t \to \infty$ for $a < 0$, $e_0 \geq e_2$ and $e_1$ and $e_2$ real. An analysis of the Liapunov type for the stability of these solutions shows that in the first situation ($a > 0$) the solution $e_1 = e_0$ is unstable and all others are stable, while in the second situation ($a < 0$) the solution $e_2 = e_0$ is unstable while all other solutions are stable. The solutions

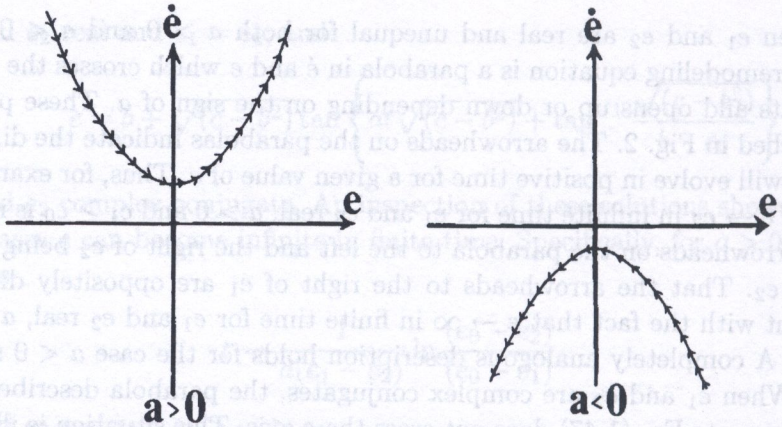


FIG. 3. A phase plane plot of the solution to the remodeling Eq. (1.47) when $e_1$ and $e_2$ are complex conjugates.

that are stable are, in fact, asymptotically stable. This stability analysis is given in the dissertation of Hegedus. The instability of the solutions $e \to e_2$ as $t \to \infty$ for $a > 0$, $e_1 \geq e_0$ and $e \to e_1$ as $t \to \infty$ for $a < 0$, $e_2 = e_0$ can be inferred from Fig. 2. In Fig. 2 we see that these solutions correspond to the points where the system is started with an initial datum corresponding to the single point where the directionality of the arrowheads on the parabola reverse themselves. An arbitrarily small change in initial datum completely changes the response of the system. A simple mechanical analogy of this unstable situation is a sphere in unstable equilibrium on top of a second sphere.

It is now possible to state the conditions under which the differential Eq. (1.47) yields stable solutions which tend to finite, physiologically possible values. The solution for $a > 0$ is $e \to e_2$ as $t \to \infty$ for $a > 0$ if $e_1$ and $e_2$ are real, $e_1 \geq e_0$, $1 - \xi_0 > e_2 > -\xi_0$ and $1 - \xi_0 > e_0 > -\xi_0$. The solution for $a < 0$ is $e \to e_1$ as $t \to \infty$ if $e_1$ and $e_2$ are real, $e_0 > e_2$, $1 - \xi_0 > e_1 > -\xi_0$ and $1 - \xi_0 > e_0 > -\xi_0$. In terms of the coefficients $a, b$ and $c$ occurring in Eq. (1.47) these conditions are

$$(1.63) \qquad a > 0, \quad b^2 > c, \quad b + \sqrt{(b^2 - c)} > e_0, \quad 1 - \xi_0 > b - \sqrt{(b^2 - c)} > -\xi_0,$$

or

$$(1.64) \qquad a < 0, \quad b^2 > c, \quad e_0 > b - \sqrt{(b^2 - c)}, \quad 1 - \xi_0 > b + \sqrt{(b^2 - c)} > -\xi_0.$$

Since the coefficients $a, b, c$ are expressed by Eqs. (1.48) or (1.49) in terms of the material properties and the applied steady strain or steady stress, the conditions (1.63) and (1.64) can be rewritten in terms of these variables. Thus, for a specified material and a specified steady strain or steady stress, it can be

determined at any point of a object whether the value of $e$ will remain finite or tend to one of its pathological extremes.

## 11. The complete solutions to two classes of boundary value problems

The results of the previous section concerning solutions of the remodeling rate equation for steady strain and steady stress may be combined with the results concerning homogeneous processes given in Part I, Sec. 8 to solve two general classes of boundary value problems. The two classes of problems are the same as the two classes considered in the previous section with the exception that the applied strain or applied stress is now homogeneous as well as steady. When this homogeneity assumption is made concerning the applied steady strain or applied steady stress, it follows from Sec. 8 that if the action-at-a-distance forces vanish and the initial data are homogeneous, then all the variables are homogeneous and all the basic equations of the approximate theory of adaptive elasticity are satisfied. In the following paragraphs more details on these solutions are presented.

We consider an object $O$ which for $t < 0$ is in mechanical and remodeling equilibrium under zero action-at-a-distance force with a homogeneous stress $\mathbf{T}^0$, a homogeneous strain $\mathbf{E}^0$ and a homogeneous volume fraction $e_0$ and a zero rate of remodeling. The situation in which the homogeneous strain $\mathbf{E}^0$ is changed to the homogeneous strain $\mathbf{E}^*$ at $t = 0$ and held constant at its new value for all $t > 0$ is called *the homogeneous steady strain problem.* The situation in which the homogeneous stress $\mathbf{T}^0$ is changed to the homogeneous stress $\mathbf{T}^*$ at $t = 0$ and held constant at its new value for all $t > 0$ is called *the homogeneous steady stress problem.*

The homogeneous steady strain problem requires the solution of the differential Eqs. (1.23), (1.27), (1.40) and (1.41) in $O$ for $t > 0$ given $\gamma$, $c_0$, $c_1$, $c_2$, $\hat{\mathbf{A}}^0$, $\hat{\mathbf{A}}^1$, $\hat{\mathbf{c}}^0$, $\hat{\mathbf{c}}^1$, $\xi_0$, $\mathbf{b} = 0$, the initial conditions

$$e(\mathbf{x}, 0) = e_0, \qquad \mathbf{u}(\mathbf{x}, 0) = \mathbf{E}^*\mathbf{x} + \mathbf{W}^*\mathbf{x} + \mathbf{c}, \qquad \mathbf{x} \in O, \tag{1.65}$$

and the boundary conditions

$$\mathbf{u}(\mathbf{x}, t) = \mathbf{E}^*\mathbf{x} + \mathbf{W}^*\mathbf{x} + \mathbf{c}, \qquad t > 0, \qquad \mathbf{x} \in \partial O, \tag{1.66}$$

where $\mathbf{E}^*$ is a constant symmetric tensor, $\mathbf{W}^*$ is a constant skew-symmetric tensor and $\mathbf{c}$ is a constant vector. The tensor $\mathbf{W}^*$ represents a rigid object rotation of the object and the vector $\mathbf{c}$ represents a rigid object translation. We assume that the strain everywhere in the object is constant and equal to $\mathbf{E}^*$. The solution for the field $e(x, t)$ is that given in the previous section with $a, b$ and $c$ as

given by (1.48), the position dependence of $\mathbf{E}^*$ being suppressed. The resulting homogeneous unsteady stress is, from (1.40),

$$\widehat{\mathbf{T}} = \xi_0 \hat{\mathbf{c}}^0 \cdot \widehat{\mathbf{E}}^* + e\hat{\mathbf{c}}^1 \cdot \widehat{\mathbf{E}}^*. \tag{1.67}$$

The strain field $\mathbf{E}^*$, the stress field given by (1.67) and the $e$ field specified in the previous section then satisfy the basic system of equations for the approximate theory of adaptive elasticity and constitute a class of complete solutions.

The homogeneous steady stress problem required the solution of the differential Eqs. (1.23), (1.27), the compatibility conditions and the strain-stress relations

$$\widehat{\mathbf{E}} = \hat{\mathbf{s}}^0 \cdot \widehat{\mathbf{T}} - \hat{\mathbf{s}}^0 \cdot \hat{\mathbf{c}}^1 \cdot \hat{\mathbf{s}}^0 \cdot \widehat{\mathbf{T}} e, \tag{1.68}$$

and the remodeling rate equation in the form

$$\dot{e} = (c_0 + \hat{\mathbf{A}}^0 \cdot \hat{\mathbf{s}}^0 \cdot \widehat{\mathbf{T}}) + (c_1 + \hat{\mathbf{A}}^1 \cdot \hat{\mathbf{s}}^0 \cdot \widehat{\mathbf{T}} - \hat{\mathbf{A}}^0 \cdot \hat{\mathbf{s}}^0 \cdot \hat{\mathbf{c}}^1 \cdot \hat{\mathbf{s}}^0 \cdot \widehat{\mathbf{T}})e + c_2 e^2. \tag{1.69}$$

Equation (1.68) is obtained by substituting (1.45) into (1.32), and (1.69) is obtained by substituting (1.45) into (1.41). The problem is then to solve this system of equations in $O$ for $t > 0$ given

$$e(\mathbf{x}, 0) = e_0, \quad \mathbf{u}(\mathbf{x}, 0) = \mathbf{0}, \quad \mathbf{x} \in O, \tag{1.70}$$

and the boundary conditions

$$\mathbf{t}(\mathbf{x}, t) = \mathbf{T}^* \cdot \mathbf{n}, \quad t \geq 0, \quad \mathbf{x} \in O, \tag{1.71}$$

where $\mathbf{T}^*$ is a constant tensor and $\mathbf{n}$ is the unit normal to the boundary of the object. We assume that the stress everywhere in the object is constant and equal to $\mathbf{T}^*$. When the stress is set equal to $\mathbf{T}^*$ in the differential Eq. (1.69), it reduces to (1.47) with $b$ and $c$ given by (1.49), the position dependence of $\mathbf{T}^*$ being now suppressed. The resulting homogeneous unsteady strain is, from (1.68),

$$\widehat{\mathbf{E}}(t) = \hat{\mathbf{s}}^0 \cdot \widehat{\mathbf{T}}^* - \hat{\mathbf{s}}^0 \cdot \hat{\mathbf{c}}^1 \cdot \hat{\mathbf{s}}^0 \cdot \widehat{\mathbf{T}}^* e(t). \tag{1.72}$$

The stress field $\mathbf{T}^*$ the strain field given by (1.72) and the $e$ field specified in the previous section then satisfy a basic system of equations for the approximate theory of adaptive elasticity and constitute a class of complete solutions.

TSILI (2000) applied the theory described above to the problem of internal bone remodeling induced by casting a broken femur. It is shown that, after the removal of the plastercast, the healing bone became more porous and less stiff. The general nature of the solutions to jumps in the constant, homogeneous applied stress is illustrated in Fig. 4. The responses of the strain, $de/dt$, $e$ and bone stiffness are shown as functions of time.

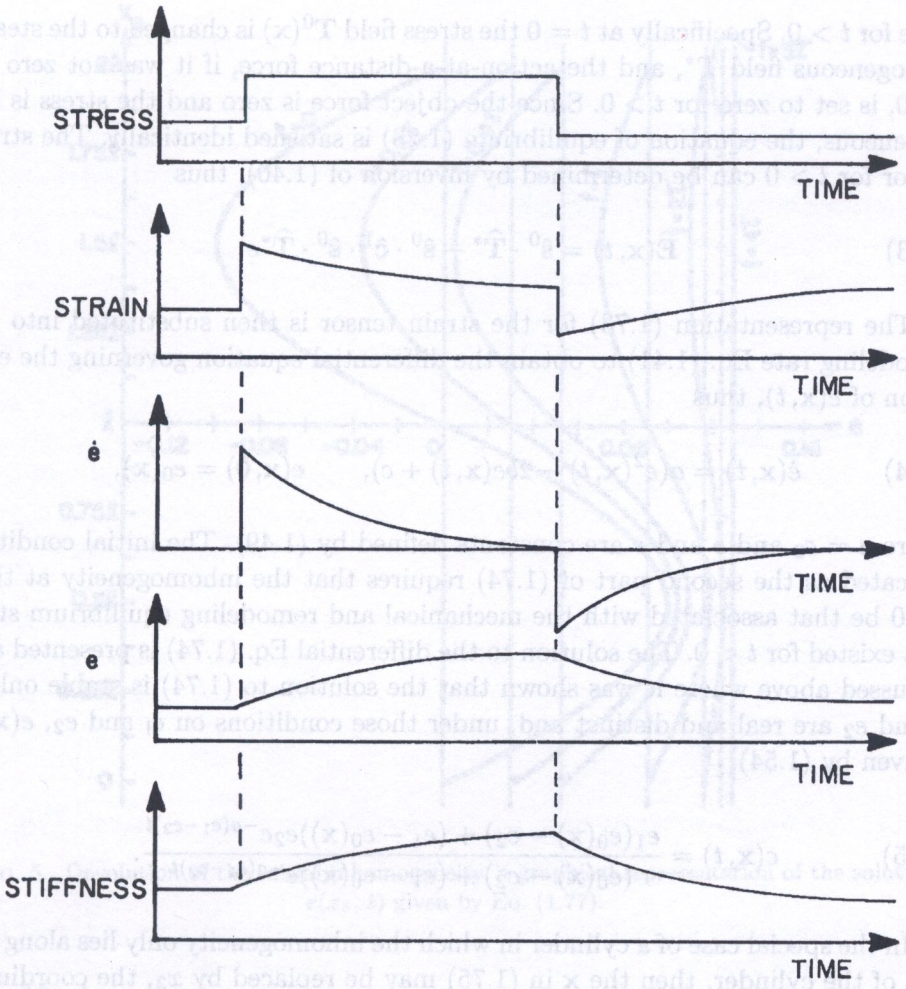


FIG. 4. Internal adaptation responses to jumps in the constant, homogeneous applied stress. The response of the strain, $de/dt$, $e$ and bone stiffness as functions of time.

## 12. DEVOLUTION OF INHOMOGENEITIES UNDER STEADY HOMOGENEOUS STRESS

We consider an inhomogeneous, adaptive elastic material object which is in mechanical and remodeling equilibrium for time $t < 0$. By mechanical and remodeling equilibrium it is meant that there exists a steady stress $\mathbf{T}^0(\mathbf{x})$, a steady strain $\mathbf{E}^0(\mathbf{x})$ and a steady volume fraction $e_0(\mathbf{x})$ which satisfy Eqs. (1.27), (1.23), (1.40) and (1.41) identically. To study the devolution of this inhomogeneous object into a homogeneous one, we subject an inhomogeneous object which is in mechanical and remodeling equilibrium for $t < 0$ to a homogeneous steady stress

state for $t > 0$. Specifically at $t = 0$ the stress field $\mathbf{T}^0(\mathbf{x})$ is changed to the steady homogeneous field $\mathbf{T}^*$, and the action-at-a-distance force, if it was not zero for $t < 0$, is set to zero for $t > 0$. Since the object force is zero and the stress is homogeneous, the equation of equilibrium (1.23) is satisfied identically. The strain tensor for $t > 0$ can be determined by inversion of (1.40), thus

$$\widehat{\mathbf{E}}(\mathbf{x}, t) = \hat{\mathbf{s}}^0 \cdot \widehat{\mathbf{T}}^* - \hat{\mathbf{s}}^0 \cdot \hat{\mathbf{c}}^1 \cdot \hat{\mathbf{s}}^0 \cdot \widehat{\mathbf{T}}^* e. \tag{1.73}$$

The representation (1.73) for the strain tensor is then substituted into the remodeling rate Eq. (1.41) to obtain the differential equation governing the evolution of $e(\mathbf{x}, t)$, thus

$$\dot{e}(\mathbf{x}, t) = a(e^2(\mathbf{x}, t) - 2be(\mathbf{x}, t) + c), \qquad e(\mathbf{x}, 0) = e_0(\mathbf{x}), \tag{1.74}$$

where $a = c_2$ and $b$ and $c$ are constants defined by (1.49). The initial condition indicated as the second part of (1.74) requires that the inhomogeneity at time $t = 0$ be that associated with the mechanical and remodeling equilibrium state that existed for $t < 0$. The solution to the differential Eq. (1.74) is presented and discussed above where it was shown that the solution to (1.74) is stable only if $e_1$ and $e_2$ are real and distinct and, under those conditions on $e_1$ and $e_2$, $e(\mathbf{x}, t)$ is given by (1.54)

$$e(\mathbf{x}, t) = \frac{e_1(e_0(\mathbf{x}) - e_2) + (e_1 - e_0(\mathbf{x}))e_2 e^{-a(e_1 - e_2)t}}{(e_0(\mathbf{x}) - e_2) + (e_1 - e_0(\mathbf{x}))e^{-a(e_1 - e_2)t}}. \tag{1.75}$$

In the special case of a cylinder in which the inhomogeneity only lies along the axis of the cylinder, then the $\mathbf{x}$ in (1.75) may be replaced by $x_3$, the coordinate axis along the axis of the cylinder. If the initial inhomogeneity is sinusoidal in form,

$$e_0(x_3) = 0.1 \sin \frac{\pi x_3}{l}, \tag{1.76}$$

where the cylinder is of length $2l$ and appropriate choices are made for the other coefficients, FIROOZBAKHSH and COWIN (1980), then

$$e(x_3, t) = \frac{(0.129)\left(4.4 - \sin \dfrac{\pi x_3}{l}\right) + (0.44)\left(\sin \dfrac{\pi x_3}{l} - 1.29\right) e_2 e^{-t/\tau}}{\left(4.4 - \sin \dfrac{\pi x_3}{l}\right) + \left(\sin \dfrac{\pi x_3}{l} - 1.29\right) e^{-t/\tau}}, \tag{1.77}$$

where $\tau = 147$ days. This result is plotted in Fig. 5 for various values of time.

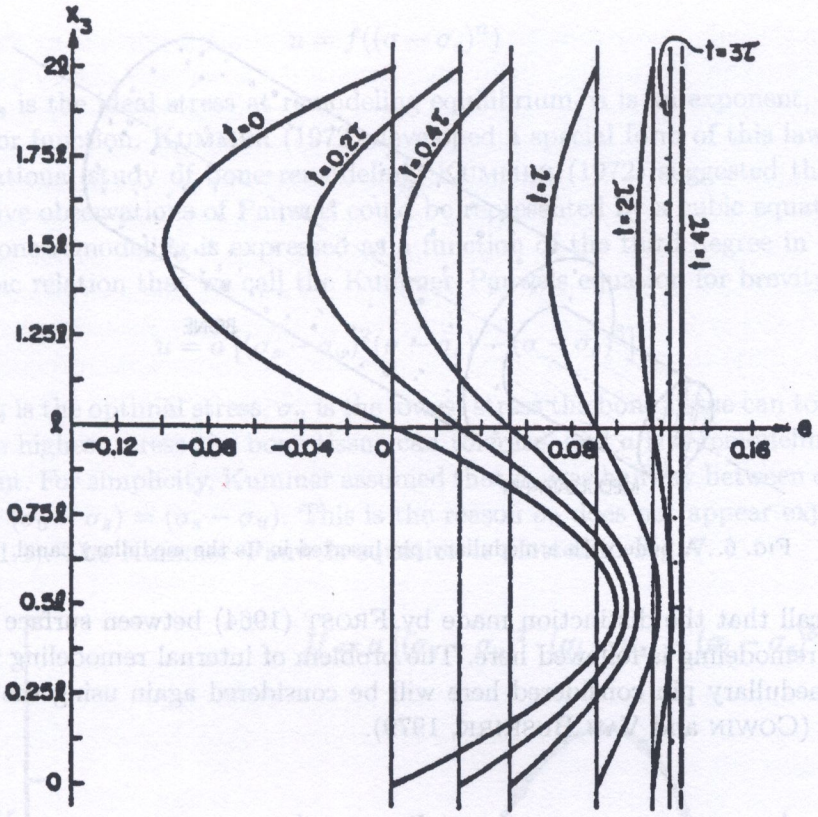


FIG. 5. Devolution of the initial inhomogeneity, a graphical representation of the solution $e(x_3, t)$ given by Eq. (1.77).

## 13. INTERNAL BONE REMODELING INDUCED BY A MEDULLARY PIN

When a metallic pin is fitted into the medullary canal of a long bone as part of a prosthetic device, the bone in the vicinity of the pin will remodel and alter its local structure. A mathematical analysis of the internal bone remodeling induced by a medullary pin according to the theory developed above was given in COWIN and VAN BUSKIRK (1978). The problem is illustrated in Fig. 6. This analysis shows that the force fitting of a medullary pin will necessarily induce one of three following situations: (a) a reduction in stiffness of the bone surrounding the pin, and therefore, a loosening of the pin, (b) osteopetrosis, a pathological bone structure of low porosity or (c) osteoporosis, a pathological bone structure of too high porosity. Although (c) is highly unlikely, it is mathematically possible at the present state of this predictive science. The results of this analysis show that the grip of the bone on the medullary pin will, most likely, loosen in time.

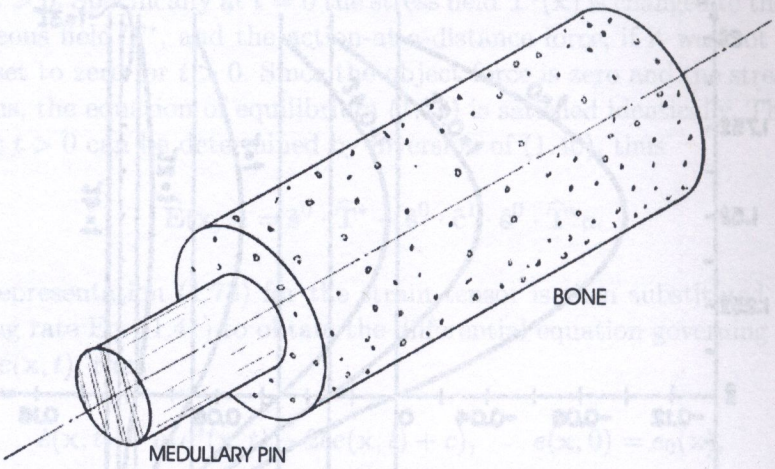


FIG. 6. A bone with a medullary pin inserted in its the medullary canal.

Recall that the distinction made by FROST (1964) between surface and internal remodeling is followed here. The problem of internal remodeling induced by a medullary pin considered here will be considered again using the surface theory (COWIN and VAN BUSKIRK, 1979).

## 14. AN ANALYTICAL MODEL OF PAUWELS' FUNCTIONAL ADAPTATION MECHANISM IN BONE

FIROOZBAKHSH and COWIN (1981) argued and partially demonstrated that the features of Pauwels' qualitative theory of functional adaptation of bone tissue are expressed mathematically by the cubic approximation to the theory of internal remodeling presented by COWIN and HEGEDUS (1976) and described above. The cubic remodeling rate equation is shown to correspond closely to the remodeling equation suggested by Kummer for the qualitative theory of Pauwels, and to a later remodeling suggestion of FUNG (1990).

As a consequence of many studies documenting anatomical bone remodeling effects, PAUWELS (1965, 1980) developed a qualitative theory of the bone remodeling process that he referred to as functional adaptation. In a chapter entitled "Short Survey of the Mechanical Stressing of Bone and Its Significance for Functional Adaptation" Pauwels suggests an analytical model for his qualitative observations of bone remodeling. Pauwels let $u$ denote bone remodeling and $\sigma$ the actual stress experienced by the bone. Positive values of $u$ indicate apposition and negative values indicate resorption. Pauwels suggested that $u$ and $\sigma$ are related by

(1.78) $$u = f((\sigma - \sigma_s)^n)$$

where $\sigma_s$ is the ideal stress at remodeling equilibrium, $n$ is an exponent, and $f$ stands for function. KUMMER (1972) developed a special form of this law for a computational study of bone remodeling; KUMMER (1972) suggested that the qualitative observations of Pauwels could be represented by a cubic equation in which bone remodeling is expressed as a function of the third degree in stress. The cubic relation that we call the Kummer–Pauwels equation for brevity is

(1.79) $$u = a\left[(\sigma_s - \sigma_u)^2(\sigma - \sigma_s) - (\sigma - \sigma_s)^3\right]$$

where $\sigma_s$ is the optimal stress, $\sigma_u$ is the lowest stress the bone tissue can tolerate, $\sigma_0$ is the highest stress the bone tissue can tolerate, and $a$ is a remodeling rate coefficient. For simplicity, Kummer assumed that $\sigma_s$ was halfway between $\sigma_u$ and $\sigma_0$, thus $(\sigma_0 - \sigma_s) = (\sigma_s - \sigma_u)$. This is the reason $\sigma_0$ does not appear explicitly in Eq. (1.1). The Kummer–Pauwels equation is plotted in Fig. 7.

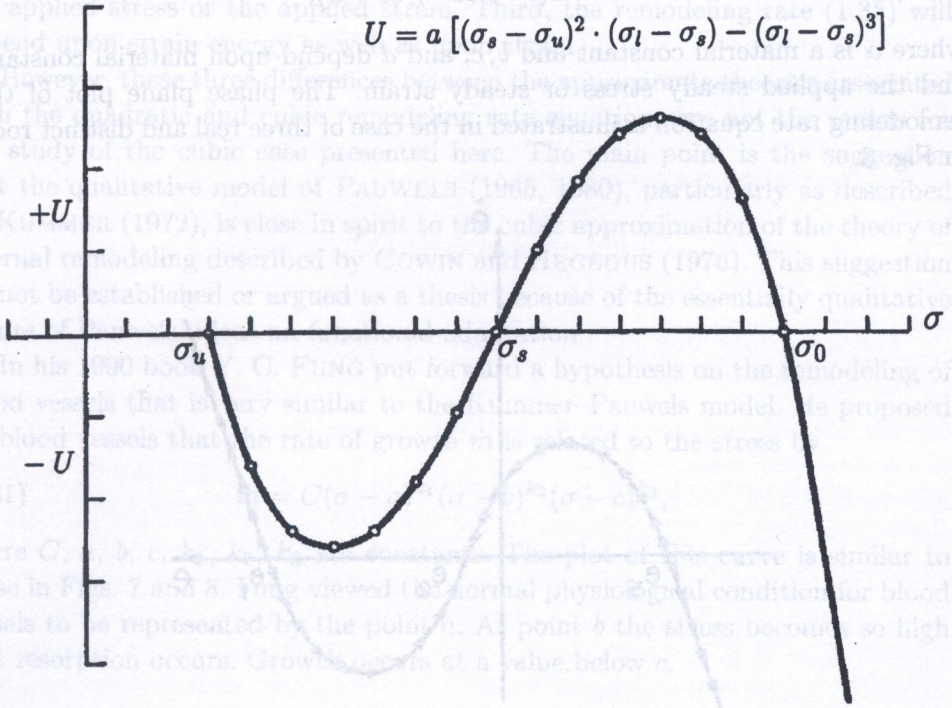


FIG. 7. Plot of the Kummer–Pauwels equation, KUMMER (1972).

The main point of this section is that the qualitative model of PAUWELS (1965, 1980), particularly as described by KUMMER (1972), is essentially the

same as the cubic approximation to the theory of internal remodeling developed by COWIN and HEGEDUS (1976) and described above. The theory presented by COWIN and HEGEDUS (1976) is a general, nonlinear theory. HEGEDUS and COWIN (1976) approximated this general theory so that only terms linear in the strain and quadratic in the change in solid volume fraction $e$ were preserved. This approximation led to a quadratic remodeling rate equation for steady stress or steady strain problems (1.47). This differential equation governed the temporal evolution of the volume fraction change $e$ under new stress or strain conditions imposed at $t = 0$ and held steady indefinitely thereafter. FIROOZBAKHSH and COWIN (1981) developed the next higher approximation of the general theory because it has more of the features of the functional adaptation mechanism of Pauwels, particularly as described by the Kummer–Pauwels Eq. (1.1). In this higher approximation, terms quadratic in strain and cubic in the volume fraction change are retained in the remodeling rate equation. The remodeling rate equation for steady stress or steady strain in problems is then

$$\dot{e} = \alpha(e^3 + be^2 + ce + d), \tag{1.80}$$

where $\alpha$ is a material constant and $b, c$, and $d$ depend upon material constants and the applied steady stress or steady strain. The phase plane plot of this remodeling rate equation is illustrated in the case of three real and distinct roots in Fig. 8.

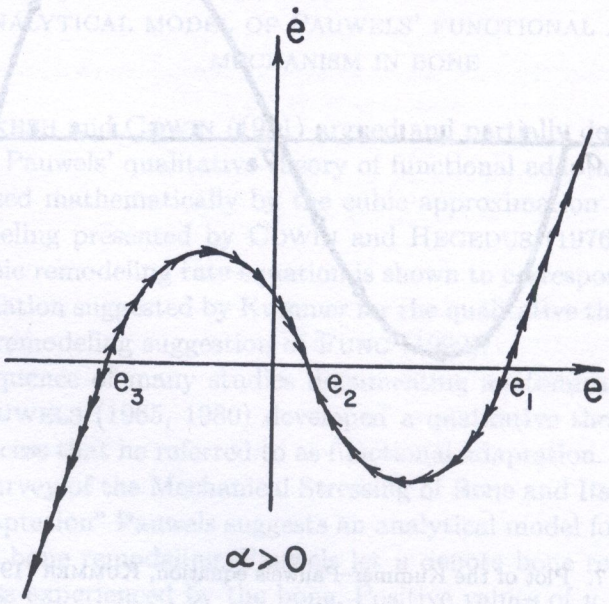


FIG. 8. The cubic remodeling rate equation in the case of three real and distinct roots and $\alpha > 0$.

A significant difference between $b$ and $c$ in Eq. (1.47) and $b, c$ and $d$ in Eq. (1.80) is that $b$ and $c$ in (2.1) are linear in the applied steady stress or the applied steady strain, while $b$, $c$, and $d$ in (1.3) are both linear and quadratic in the applied stress or the applied strain. This particular difference in dependence of the coefficients leads to two important differences in the predictions of the approximate theories associated with the quadratic and cubic remodeling rate equations. First, it was noted in HEGEDUS and COWIN (1976) that, according to the quadratic remodeling rate equation (1.47), pure torsion of an orthotropic adaptive elastic material about one of its preferred material axes will not induce remodeling. This conclusion is not applicable in the case of the cubic remodeling rate Eq. (1.80) because of the dependence of $b, c$ and $d$ in (1.80) upon the square of the applied stress or the applied strain. Second, the approximate theory associated with the quadratic remodeling rate Eq. (1.47) will not predict enhancement of depositional remodeling due to cyclic loading over equivalent steady loading, but the approximate theory associated with the cubic remodeling rate Eq. (1.80) will make such predictions because of its dependence on the terms quadratic in the applied stress or the applied strain. Third, the remodeling rate (1.35) will depend upon strain energy as well as upon strain.

However, these three differences between the approximate theories associated with the quadratic and cubic remodeling rate equations are not the reason for the study of the cubic case presented here. The main point is the suggestion that the qualitative model of PAUWELS (1965, 1980), particularly as described by KUMMER (1972), is close in spirit to the cubic approximation of the theory of internal remodeling described by COWIN and HEGEDUS (1976). This suggestion cannot be established or argued as a thesis because of the essentially qualitative nature of Pauwels' ideas on functional adaptation.

In his 1990 book Y. C. FUNG put forward a hypothesis on the remodeling of blood vessels that is very similar to the Kummer–Pauwels model. He proposed for blood vessels that the rate of growth $\dot{m}$ is related to the stress by

$$\dot{m} = C(\sigma - a)^{k_1}(\sigma - b)^{k_2}(\sigma - c)^{k_3}, \tag{1.81}$$

where $C$, $a$, $b$, $c$, $k_1$, $k_2$, $k_3$ are constants. The plot of this curve is similar to those in Figs. 7 and 8. Fung viewed the normal physiological condition for blood vessels to be represented by the point $a$. At point $b$ the stress becomes so high that resorption occurs. Growth occurs at a value below $c$.

## 15. SUCCESSES AND DEFICIENCIES OF THE THEORY OF ADAPTIVE ELASTICITY

Seen from the perspective of a quarter of a century, there were major successes in the 1976 theory of adaptive elasticity and there were things that should

be done differently if the theory is to be renovated. The largest success was the development of a thermodynamic open-system model of tissue adaptation. This model has been followed, or assumed as a starting point, by most subsequent models of tissue adaptation. Features of this model are illustrated in the discussions of Fig. 1. One of the strongest assumptions made was the assumption that the internal energy of the mass added to the porous tissue was equal to the internal energy of the porous tissue at the site where the mass is added. In retrospect this is a fairly easy assumption to justify if one recalls how bone tissue is deposited and if the bone adaptation is viewed on two time scales. New bone deposition begins with a deposit of osteoid on an existing bone surface. The osteoid is of much lower modulus than the existing bone. Over a time period of a month the osteoid will become mineralized and its modulus will increase approximately linearly with the mineralization. Since the mechanical loading time scale is much, much shorter than the adaptation time scale, the osteoid/bone will undergo many million cycles of mechanical loading in the course of the adaptation tissue deposition time period. It follows that the internal energy can be gradually increased with the mineralization in the tissue deposition time period so that, when viewed from the long term adaptation time scale, it will be equivalent to having the new mass deposited at the same internal energy as the existing mass in the porous bone structure. Other features common to most of the later models of internal adaptation include the formulation of the theory in terms of a constitutive relation for the mass supply term $c$ introduced by the open system formulation of the mass balance equation:

$$\frac{D}{Dt}\int_0 \gamma \nu dv = \int_0 c dv.$$

The volume fraction $\xi$ of the porous structure in various unloaded adaptation states is related to $c$ by

$$\dot{\xi} = (c/\gamma)\mathrm{Det}\mathbf{F} = (c/\gamma)J,$$

and a constitutive equation is then developed for $c = c(\xi, \mathbf{F})$. The increased or decreased mass is then assumed to influence the elastic constants through the constitutive assumption for the free energy $\psi = \psi(\xi, \mathbf{F})$. Constitutive assumptions like these distinguish a phenomenological theory, like adaptive elasticity, from mechanistic or physiological theories that attempt to explain the mechanism (rather than to just postulate it). These different types of theories were discussed in the introduction.

The 1976 model contained a further simplification. As the porosity of the porous structure changes, the area of the interface between the porous structure and the perfusant also changes. There is not a direct relation between the porosity and the area of the interface. In 1976 we considered only porosity changes and did not introduce the area of the interface into the model as a variable. Also, we

did not consider the thermodynamic properties of the interface as different from the thermodynamic properties of interior points in the matrix structure.

One of the assumptions made in the adaptive elasticity theory is acceptable for bone, but not for soft tissue. That is the assumption of a unique zero-strain reference state for all values of $\xi$; this is expressed in equation form as

$$\frac{\partial \psi}{\partial \mathbf{F}}(\theta_0, \xi, 1) = 0,$$

for a fixed value of $\theta_0$. The existence of a unique zero-strain reference state is acceptable for bone tissue because new bone tissue is always laid down on existing bone tissue, that is to say bone adaptation occurs by surface adaptation. This is not the case for soft tissues that may grow by volumetric deposition within existing tissues. When volumetric deposition occurs it changes the existing reference state for the adapting tissue; if material is being continuously added or removed, the possibility of defining a reference state does not exist. Thus, for adapting soft tissue it is not possible to define a reference configuration for strain.

The changes to be recommended if the theory of adaptive elasticity were to be reformulated will now be discussed. A major change would be the introduction of two time scales. These two time scales differ by many orders of magnitude (COWIN *et al.*, 1993). Let $T_A$ denote the time that biological processes take to complete significant growth (or remodeling) associated with a mechanical loading, and let $T_L$ denote the characteristic period of mechanical loading. Rough estimates of these numbers are from two weeks for soft tissue to about six months for mineralized tissue for $T_A$ and about one second for $T_L$; thus $T_L/T_A$ is a small number, on the order $10^{-6}$ to $10^{-7}$. In order to keep these time scales separate let $t$ denote time on the loading time scale and $T$ denote time on the remodeling time scale (COWIN, 1996).

Measures of tissue strain may be constructed using the fact that the tissue is strained on the time scale $T$ and that the gauge length changes on the time scale $T$, a million times longer. Growth is usually inhomogeneous, and it is possible that the gauge length used for the sensing of strain does not change as the tissue grows. For example, the cell may sense the strain itself and not change its length on the time scale $T$. Bone cells (osteocytes) do not change their length on the time scale $T$ as the bone grows. (Actually bone growth occurs by apposition on free surfaces and thus many possible gauge length selections do not change on the time scale $T$.) A gauge length equal to the size of a cell raises the question of strain sensitivity because a change in a specified length must be determined to measure a strain. If the gauge length is as small as a cell, then the change in length will be smaller and greater sensitivity is required. COWIN *et al.* (1991) contains a discussion of the sensitivity of cells to strain. It is noted there that

the behavior of certain marine invertebrates suggests that they are sensitive to changes in their ambient hydrostatic pressure environment corresponding to strains as small as $10^{-6}$, far beyond the sensitivity of any human strain measuring device.

The loading rate of deformation of an object is an instantaneous kinematic measure independent of reference configuration or gauge length, and thus does not have the disadvantage that might exclude strain as a remodeling or growth stimulus. The rate of deformation, $\mathbf{D} = (1/2)(\mathbf{L} + \mathbf{L}^T)$ where the tensor of velocity gradients $\mathbf{L}$ is defined by (1.4), is suggested as a remodeling stimulus for endothelial and bone cells in the sense that the shear stress due to fluid motion over these epithelial cells is a stimulus for their activity and shear stress is proportional to the rate of deformation of a fluid. It is an open question as to how much of the shear rate versus the shear stress is actually transferred to the epithelial cells. The cell layer is compliant and the undulations of the cell contour are observed in laminar shear flows in which the cells are attached to a supporting plate.

The reformulated theory of adaptive elasticity should allow the mass supply $c$ and the free energy $\psi$ to depend upon the remodeling time $T$ and the history of deformation, thus (1.26) should be replaced by functionals of the history of reference solid volume fraction and deformation gradients

$$(1.82) \qquad c = \underset{\tau=-\infty}{\overset{T}{F}} \{\xi(\tau), \mathbf{F}(\tau)\}, \qquad \psi = \underset{\tau=-\infty}{\overset{T}{G}} \{\xi(\tau), \mathbf{F}(\tau)\}.$$

Such strain history dependent relationships are familiar from non-linear viscoelasticity. The reformulated theory would then consist of the usual equations for an elastic object and equations (1.82), which change on a time scale $T$, very slowly adding or subtracting mass and free energy and, thereby, changing the elastic constants.

Perhaps the point most in need of revision in the theory of adaptive elasticity is the stimulus for remodeling. The model pointed to time-averaged-strain and strain-energy as the first measures of stimulus. The experimental literature suggests however that it must be a stimulus that involves the rate-of-strain or the rate-of-loading. SCOTT (1957) has shown that a moderate periodic strain applied to living bone is more effective in causing remodeling than a static strain of the same magnitude. LANYON and RUBIN (1984) showed that a constant load applied with fixed springs to isolated living bone caused it to resorb as if there were no load placed on the bone. In other words, the living bone showed no effect from the constant, non-time varying loading. O'CONNOR *et al.* (1982) gave evidence that the effective stimulus was strain rate. See also RUBIN and LANYON (1984). The mechanistic models (see the Introduction) that relate the effect of mechanical load bone fluid flow around the cells buried in bone to the bone

adaptation process strongly suggest strain rate as a strong mechanical stimulus (WEINBAUM *et al.*, 1994; COWIN and MOSS, 2000).

## Part II. Surface adaptation

### 1. THE THEORY OF SURFACE REMODELING

The phenomenological model for surface remodeling postulates a causal relationship between the rate of surface deposition or resorption and the strain in the surface of the bone. This postulate can be put into equation form using a Cartesian coordinate system at a point on the surface of the bone. Let **n** denote the normal to the bone surface at a surface point **P** and let **t** and **a** be two orthogonal unit vectors in the tangent plane at **P**. These three orthogonal unit vectors constitute a local Cartesian coordinate system as shown in Fig. 9. Let $U$ denote the speed of the remodeling surface normal to the surface, that is to say $U$ is the velocity of the surface in the n direction. The velocity of the surface in any direction in the tangent plane is zero because the surface is not moving tangentially with respect to the object.

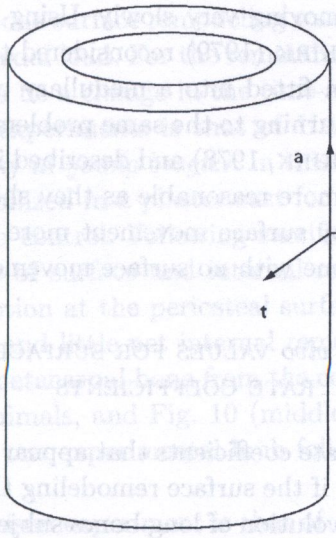


FIG. 9. The local Cartesian coordinate system on the surface of a long bone.

Let $\mathbf{E}(\mathbf{P})$ denote the Cartesian components of the strain tensor at the surface point **P**. Small strains are assumed. The hypothesis for surface remodeling is that the speed of the remodeling surface is linearly proportional to the strain tensor,

$$U = \mathbf{C}(\mathbf{n}, \mathbf{P}) : [E(\mathbf{P}) - E^0(\mathbf{P})], \tag{2.1}$$

where $\mathbf{E}^0(\mathbf{P})$ is a reference value of strain where no remodeling occurs and $\mathbf{C}(\mathbf{n}, \mathbf{P})$ are surface remodeling rate coefficients which are, in general, dependent upon the point $\mathbf{P}$ and the normal $\mathbf{n}$ to the surface at $\mathbf{P}$. The surface remodeling rate coefficients and the reference values of strain are phenomenological coefficients of the bone surface and must be determined by experiment. One would hope that these quantities turn out to be independent of the particular surface point at which they are determined. It is postulated above that surface remodeling rate coefficients are independent of strain. If these coefficients turn out to be strain dependent, the theory will become much more difficult from a manipulative viewpoint. Equation (2.1) gives the normal velocity of the surface at the point $\mathbf{P}$ as a function of the existing strain state at $\mathbf{P}$. If the strain state at $\mathbf{P}$, $\mathbf{E}(\mathbf{P})$, is equal to the reference strain state, $\mathbf{E}^0(\mathbf{P})$, then the velocity of the surface is zero and no remodeling occurs. If the right-hand side of (2.1) is positive, the surface will be growing by deposition of material. If, on the other hand, the right-hand side of (2.1) is negative, the surface will be resorbing.

The complete surface remodeling theory is formed by assuming that bone is a linearly elastic material and that the surface movement of an object is governed by (2.1). Thus, at any point in time the bone is an elastic object whose external boundaries may be moving very slowly. Using the surface remodeling theory COWIN and VAN BUSKIRK (1979) reconsidered the remodeling problem associated with a metallic pin fitted into a medullary canal of a long bone as part of a prosthetic device, returning to the same problem considered only a year earlier (COWIN and VAN BUSKIRK, 1978) and described in Part I, Sec. 13 above. The results in this case were more reasonable as they showed that the observed loosening could be modeled by surface movement more easily than by changes in internal structure of the bone with no surface movement.

## 2. ESTABLISHING *in vivo* VALUES FOR SURFACE REMODELING RATE COEFFICIENTS

Values of the remodeling rate coefficients that appear in the Eq. (2.1) for surface remodeling are necessary if the surface remodeling theory is to be of use for predicting the *in vivo* shape evolution of long bones subjected to changes in their mechanical loading environment. COWIN *et al.* (1985) applied surface remodeling theory to the analysis of five animal bone adaptation experiments in which the temporal evolution of a change in bone shape was documented after a significant change in the mechanical loading environment of the bone. For each of these studies, preliminary estimates of the *in vivo* values of the surface remodeling rate coefficients were established. The preliminary parameter estimates of these

parameters were established by comparison of the published animal experimental results with surface remodeling theory predictions generated by computation. The results of the animal experiments that induced significant net surface remodeling were taken from the literature (UHTHOFF and JAWORSKI, 1978; JAWORSKI *et al.*, 1980; WOO *et al.*, 1981; LANYON *et al.*, 1982; GOODSHIP *et al.*, 1979).

After a brief description of the animal experiments considered in this study, and a brief review of the surface remodeling theory, a description is presented of the conceptual formulation for the application of surface remodeling theory to the five animal experiments considered in this study. A section on the procedures used to estimate the remodeling parameters follows, then a section on the computational formulation of the problem. Following a presentation and discussion of the results, the limitations of the technique as applied here are addressed.

## 3. THE FIVE ANIMAL EXPERIMENTS CONSIDERED

Five animal experiments were considered in this comparison study. These five experiments were divided into two groups on the basis of whether we assumed the axial loading on the bone to be *centric* (i.e. to act along a line passing through the centroid of the cross-section) or *eccentric* (i.e. to act along a line not passing through the centroid). In three of the experiments, the loading change that initiated the net bone surface remodeling was assumed to be a change in the time-averaged centric axial load. For the remaining two experiments, the loading change was assumed to be a change in the time-averaged eccentric axial load.

The first of these experiments is that of UHTHOFF and JAWORSKI (1978) involving disuse atrophy in *young beagles*. In this study one forelimb of one-year old beagles was immobilized in a plaster cast for from 2 to 40 weeks. The other forelimb was used as a control. Following sacrifice, the metacarpal bones were examined for evidence of surface and internal remodeling. The results showed significant bone resorption at the periosteal surface, but little net movement of the endosteal surface, and little net internal remodeling. Figure 10 (top) shows the cross-section of a metacarpal bone from the contralateral control limb of one of the experimental animals, and Fig. 10 (middle) shows the cross-section of a metacarpal bone from one experimental limb following 40 weeks of immobilization.

The second comparison experiment is that of JAWORSKI *et al.* (1980), an experiment that repeated the study described above, but used 8 year old beagles. In contrast to the results with young beagles, the study with older animals showed little net remodeling on the periosteal surface, but significant bone resorption on the endosteal surface. Again, there was little net internal remodeling. Figure 11 (top) shows the cross-section of a metacarpal bone from the contralateral control limb of one of the experimental animals, and Fig. 11 (middle) shows the cross-

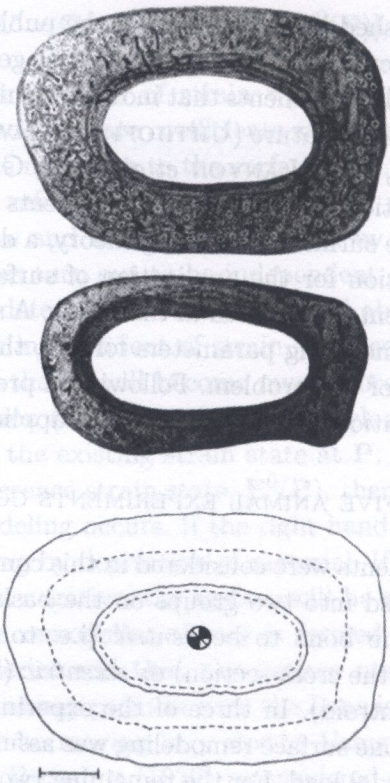

FIG. 10. The young beagle experiment (UHTHOFF and JAWORSKI, 1978). Each illustration represents the cross-section of a metacarpal. (a) (top) The contralateral control metacarpal at 40 weeks. (b) (middle) The experimental metacarpal at 40 weeks, showing marked periosteal resorption and slight endosteal deposition. (c) (bottom) The calculated remodeling. The solid lines represent the surfaces of the control bone, (a, top) above, and the dashed lines represent the predicted geometry at 40 weeks using the constants shown in Table 1. The indicated length is one mm.

section of a metacarpal bone from an experimental limb following 40 weeks of immobilization.

The third experiment considered was that reported by WOO *et al.* (1981). This experiment showed that increased exercise activity in *young pigs* can result in net bone deposition on both the endosteal and periosteal bone surfaces of the femora. The exercise program consisted of forced jogging for one hour every day, and for 30 additional minutes every other day, over a period of one year. Figure 12 (top) shows the cross-section of the femur from one pig in the control group, and Fig. 12 (middle) is the cross-section of a femur from one of the exercised animals. Notice that the periosteal surface appears to have increased slightly in size, and there is also significant new bone deposition on the endosteal surface.

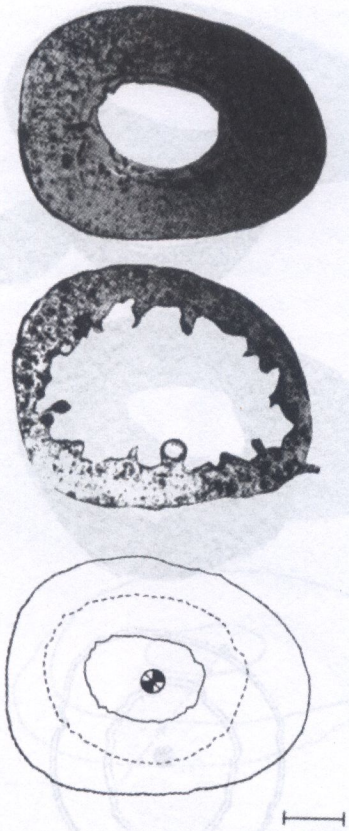

FIG. 11. The old beagle experiment (JAWORSKI *et al.*, 1980). Each illustration represents the cross-section of a metacarpal. (a) (top) The contralateral control metacarpal at 40 weeks. (b) (middle) The experimental metacarpal at 40 weeks, showing marked endosteal resorption. (c) (bottom) The calculated remodeling. The solid lines represent the surfaces of the control bone, (a, top) above, and the dashed lines represent the predicted geometry at 40 weeks using the constants shown in Table 1. The indicated length is one mm.

In each of these three experiments, the observed remodeling is approximately symmetric with respect to the control cross-section. Consequently, the theoretical models for these experiments have assumed that the changes in activity have influenced only the magnitude of the centric axial load, but have not changed the point of application of the load. Thus, in the model the axial loading is assumed to be centric during the entire experimental period.

The fourth and fifth experiments were ulnar ostectomy studies. LANYON *et al.* (1982) conducted a study with the objective of measuring the change in bone strain while inducing the functional adaptation to hyperphysiological stress states. *Mature sheep* were subjected to an ulnar ostectomy (removal of a section of the ulnar diaphysis) on their right limb, and the left forelimb was

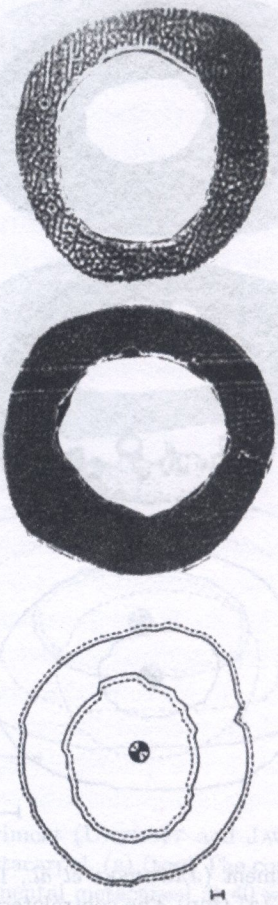

FIG. 12. The exercised young swine experiment (WOO *et al.*, 1981). Each illustration represents the cross-section of a femur. (a) (top) A femur from the control group. (b) (middle) The femur of an experimentally exercised animal after 1 year showing both endosteal and periosteal bone deposition. (c) (bottom) The calculated remodeling. The solid lines represent the surfaces of the control bone, (a, top) above, and the dashed lines represent the predicted geometry at one year using the constants shown in Table 1. The indicated length is one mm.

used as a control. The strain in the radii was monitored by means of *in vivo* strain gauging at the cranial and caudal periosteal surfaces. Figure 13 (top) is a photograph of the cross-section of the intact ulna and radius from the left control limb. Figure 13 (middle) shows the radius from the right experimental limb one year after the removal of the ulna.

Immediately following surgery to remove the ovine ulna, there was, on average, an 8% increase in the compressive strain on the side facing the missing ulna (caudal side), and, on average, a 20% increase in the tensile strain on the

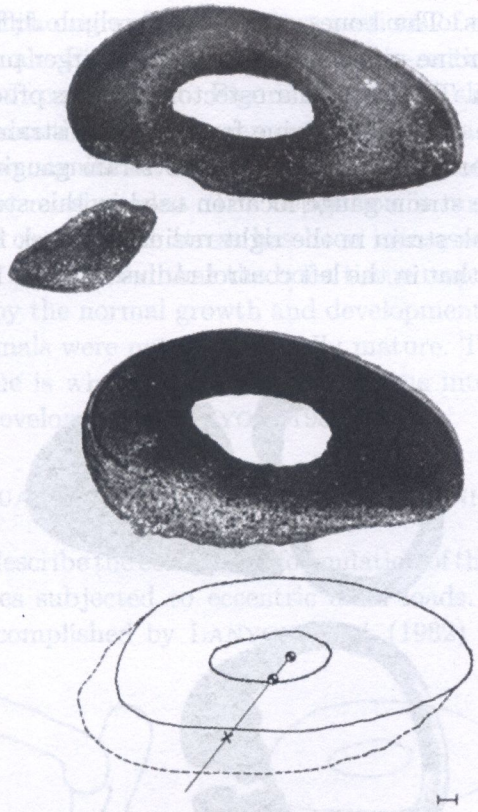

FIG. 13. The ulnar ostectomy experiment with mature sheep (LANYON *et al.*, 1982). Each illustration represents the bone cross-sections in the sheep forelimb. (a) (top) The contralateral control limb at one year showing the radius with the intact ulna. (b) (middle) The experimental radius at one year, showing marked asymmetric periosteal deposition. (c) (bottom) The calculated remodeling, The solid lines represent the surfaces of the control bone, (a, top) above, and the dashed lines represent the predicted geometry at 9 months using the constants shown in Table 1. The indicated length is one mm.

opposite (cranial) side, Fig. 13. One year later, the compressive strain on the face of the radii facing the removed ulna was 10% less than the strain on the control radius. On the opposite side of the radius, the measured tensile strain was 19% less than the opposite control radii. Thus, although most of the bone deposition occurred on the compressive side of the radius that faced the missing ulna, both tensile and compressive strains were reduced to below that recorded on the control radii.

The fifth animal experiment considered here is a similar study conducted by GOODSHIP *et al.* (1979). Again *in vivo* strain gauging was employed to quantify the strains associated with an ulnar ostectomy, but *immature pigs* were the

experimental animals. The bones of the pig forelimb differ from those in the sheep in that the porcine ulna represents a much larger proportion of the total forelimb cross-section. Thus, an ulnar ostectomy in pigs produces a greater strain increase than for the case of the ovine forelimb. The strain in the radii of both forelimbs was monitored by means of *in vivo* strain gauging. The strain gauge results, for the single strain gauge location used in this study, showed that the magnitude of the peak strain in the right radius one week following surgery was approximately twice that in the left control radius. Figures 14 (top) and (middle)

FIG. 14. The ulnar ostectomy experiment with young swine (GOODSHIP *et al.*, 1979). Each illustration represents the bone cross-sections in the forelimb of a pig. (a) (top) The contralateral control limb at one year showing the radius with the intact ulna. The ulna is proportionally much larger than for the sheep forelimb shown in Fig. 4a. (b) (middle) The experimental radius at 3 months, showing marked asymmetric periosteal deposition. (c) (bottom) The calculated remodeling. The solid lines represent the surfaces of the control bone, (a, top) above, and the dashed lines represent the predicted geometry at 3 months using the constants shown in Table 1. The indicated length is one mm.

show reproductions of photographs of the cross-sections of the radii from one of the experimental animals. Figure 14 (top) is the cross-section of the intact ulna and radius from the left control limb. Figure 14 (middle) shows the radius from the right limb three months following removal of the ulna. Comparison of the two photographs shows significant deposition of bone tissue on the right radius on the side facing the missing ulna. The deposition is on the concave side of the radius, where the compressive stress has been increased as a result of axial and bending loads. It is suspected that the bone tissue response observed in this study was enhanced by the normal growth and development of bony tissue since the experimental animals were not yet skeletally mature. The inlet shaped hole in the deposited tissue is where the attachment of the interosseous membrane inhibited new bone development (LANYON, 1982).

## 4. CONCEPTUAL FORMULATION OF THE MECHANICS PROBLEM

In this section we describe the conceptual formulation of the surface-remodeling problem in long bones subjected to eccentric axial loads. A schematic of the ovine ulnaectomy accomplished by LANYON *et al.* (1982) is shown in Fig. 15.

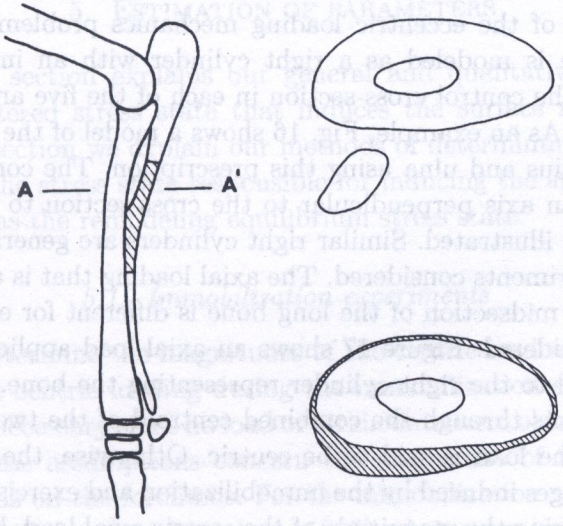


FIG. 15. A schematic diagram of the bone tissue removed in the ulnar ostectomy experiment with mature sheep (LANYON *et al.*, 1982). Above right: The contralateral control limb at one year showing the radius with the intact ulna. Below right: The experimental radius at one year, showing the calculated remodeling.

In the lower right panel of Fig. 15 the remodeling induced by the ulnaectomy is indicated by the shaded area. The mechanics problem with centric axial loads

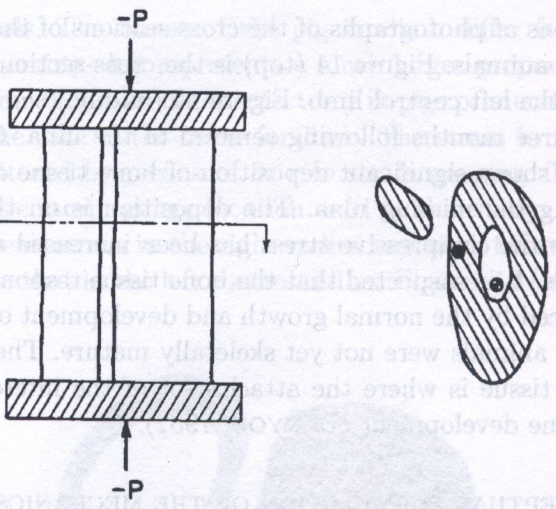


FIG. 16. Model of axial loading. This figure shows an axial load applied via platens to the two right cylinders representing the limb bones. If the axial load, $-P$, acts through the combined centroid of the two bones, indicated by a solid dot, the load is said to be centric. Otherwise, the load is eccentric.

is a special case of the eccentric loading mechanics problem. The midsection of the long bone is modeled as a right cylinder with an initial cross-section coincident with the control cross-section in each of the five animal experiments described above. As an example, Fig. 16 shows a model of the midsection of the control ovine radius and ulna using this prescription. The control cross-section is moved along an axis perpendicular to the cross-section to generate the pair of right cylinders illustrated. Similar right cylinders are generated for the other four animal experiments considered. The axial loading that is assumed to act on the model of the midsection of the long bone is different for each of the animal experiments considered. Figure 17 shows an axial load applied to platens that transmit the load to the right cylinder representing the bone. If the axial load, $-P$, in Fig. 16 acts through the combined centroid of the two bones, indicated by a solid dot, the load is said to be centric. Otherwise, the load is eccentric. The loading changes induced by the immobilization and exercise experiments are modeled by changing the magnitude of the centric axial load, but assuming that it remains centric. The load change in ulnar ostectomy studies are modeled by the removal of the ulna from the model shown in Fig. 16. The resulting model situation is illustrated in Fig. 17. The same load, $-P$, continues to be applied, but only the radius remains to carry it and the loading eccentricity relative to the remaining bone has been increased. In the special case of centric loading, the point of application of the load remains at the centroid and the magnitude of the time-averaged load changes.

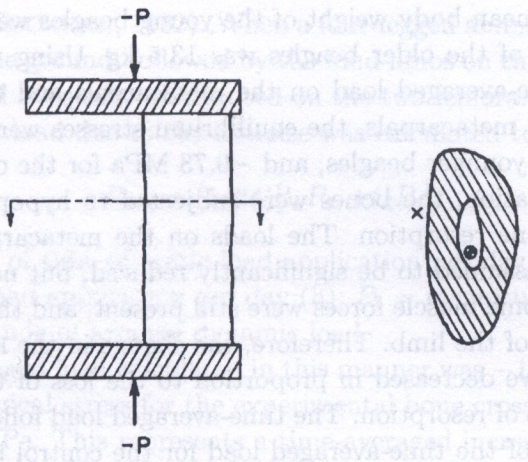


FIG. 17. Model of axial loading. The load change in ulnar ostectomy studies is modeled by the removal of the ulna from the model shown in Fig. 15. The same load, $-P$, continues to be applied, but only the radius remains to carry the load. Since the point of application of the load is no longer the centroid, the loading is eccentric relative to the remaining bone, the radius.

## 5. ESTIMATION OF PARAMETERS

The previous section explains our general and qualitative method of determining the altered stress state that induces the surface remodeling shape changes. In this section we explain our methods of determining quantitative estimates of both the stress state responsible for inducing the surface remodeling response as well as the remodeling equilibrium stress state.

### *5.1. Immobilization experiments*

In order to determine the magnitudes of the centric load and changes in the magnitude of the centric loading during the immobilization experiments, some assumptions are necessary since no load or strain data were obtained during these experiments. These assumptions concern the magnitude of the time-averaged physiological loads on the forelimbs. For the immobilization studies (UHTHOFF and JAWORSKI, 1978; JAWORSKI *et al.*, 1980), the convention that two-thirds of the body weight is distributed over the upper torso of a canine was used (VAN COCHRAN, 1982). Assuming that the load on the upper portion of the body is distributed equally between the left and right sides, one third of the entire body weight is therefore carried by each forelimb. The bone under study in these experiments is the third metacarpal of the right forelimb. Assuming that the load on the limb is distributed equally among the four metacarpals in the canine, then the load on the third metacarpal would equal one twelfth of the

body weight. The mean body weight of the young beagles was 10 kg, while the mean body weight of the older beagles was 13.5 kg. Using these assumptions concerning the time-averaged load on the metacarpals and the cross-sectional areas of the control metacarpals, the equilibrium stresses were calculated to be −0.43 MPa for the younger beagles, and −0.73 MPa for the older beagles.

After immobilization, the bones were subjected to hypophysiological loads that resulted in bone resorption. The loads on the metacarpals following immobilization were assumed to be significantly reduced, but not zero due to the assumptions that some muscle forces were still present, and that casting did not totally prevent use of the limb. Therefore, the change in the loading magnitude was assumed to have decreased in proportion to the loss of the cross-sectional bone area by means of resorption. The time-averaged load following immobilization was thus 45% of the time-averaged load for the control bone in the young beagle, and was 51% of the time-averaged load on the control bone for the old beagle.

Some error may be associated with this scheme if, during the course of the immobilization experiments, the load experienced by the bones was significantly closer to zero than we have assumed for computational purposes. It could be that the experimental bones have reached some genetically determined minimum bone mass (LANYON, 1984a). Experimental measurements of the bone strain would be required to accurately determine the actual loads due to the immobilization created by the plaster casting.

### 5.2. *Exercise experiments*

The exercise experiments of WOO *et al.* (1981) led to increased loads on the femora and to hypertrophy of that bone. The centric load magnitude and the change in the centric loading magnitudes were calculated by assuming that one third of the body weight is distributed equally across the two hind legs, so that the normal time-averaged physiological load on each femur was calculated to be one-sixth of the body weight. From the mean body weight of the exercised swine (66 kg) and from calculated cross-sectional areas of the control femora, the equilibrium stress was calculated to be −0.49 MPa.

The exercise program consisted of forced jogging that was an average of 11 h of running each day for 1 year. Since the loads used in this study are time-averaged, the hyperphysiological load was averaged over a 24 h period. It was assumed that for 22.75 h of each day, the load on the femur was one sixth of the body weight, while for the remaining 1.25 h the load was the hyperphysiological load due to exercise. Using the concept of a dynamic load factor to relate the strains due to dynamic loads to the strains that would be caused by a static load of the same magnitude, the dynamic load was assumed to be twice the

static load (VAN COCHRAN, 1982). When a four-legged animal breaks stride, the forelimbs are on the ground, followed by the hind limbs on the ground. Thus, the total dynamic load is equally distributed on the two femora. The time-averaged hyperphysiological load due to the exercise was calculated to be

$$P_{\text{avg}} = (1/24)[t_s P_s, +t_d P_d], \tag{2.2}$$

where $t_s$ = length of time of static load application per day (h); $t_d$ = length of time of dynamic load application per day (h); $P_s$ = magnitude of average static load; $P_d$ = magnitude of average dynamic load.

The time-averaged load calculated in this manner was $-141.5$ N, and the initial hyperphysiological stress for the experimental bone cross-section considered was thus $-0.64$ MPa. This represents a time-averaged increase in stress of 31% when compared with the control group.

### *5.3. Ulnar ostectomies*

Before the ulna is removed, the radius and the ulna are assumed to be loaded by an axial compressive load, $-P$. In our, now rejected, preliminary analysis the compressive axial load was assumed to act through the centroid of the original combined areas. As described subsequently, the experimental strain gauge data show that there must be an original eccentricity of the axial load due to the distribution of tensile and compressive strains in the control radius. This eccentric loading gives rise to a remodeling equilibrium stress that varies linearly across the cross-sections of the two forelimb bones. The situation before the ulna is removed is illustrated in Fig. 16.

The ulnar ostectomy is then modeled by the removal of the ulna from between the platens, as shown in Fig. 17. The platens are assumed to be constrained to move vertically, allowing no rotation. Therefore, a further eccentricity is added to the initial eccentric axial load now carried entirely by the radius. The effect of this additional eccentricity is an additional bending moment applied to the radius due to the moment arm created by the distance between the current point of load application and the point of initial load application. The magnitude of the time-averaged load is assumed to be constant.

In addition to the experimental strain gauge data reported, several assumptions were required to find the magnitude of the time-averaged load, the change in the average load, as well as the point of load application. The method of determining these time-averaged loads is described below.

### *5.4. Ovine ulnar ostectomy*

The initial assumption of a compressive axial load acting through the centroid of the original combined areas was checked by comparing the calculated

strains with the peak strains measured by LANYON *et al.* (1982) on the cranial and caudal surfaces and found to be inadequate. The strain data showed the radius must sustain significant bending loads while remaining in remodeling equilibrium because tensile strains were measured on the cranial side while compressive strains were measured on the caudal side of the radius. Since the data from only two strain gauges were reported, one on the caudal surface and one on the cranial surface, the approximate locations are represented by the arrows on Fig. 18 – the point of load application could not be uniquely established from the published data (the results from the two experimental radii that had three gauges around the circumference of the bone were not published). Therefore, in order to place a limit on the possible locations of the point of application of the load resultant, a line was constructed connecting the centroids of the radius and the ulna, and it was hypothesized that the point of load application would lie on this line.

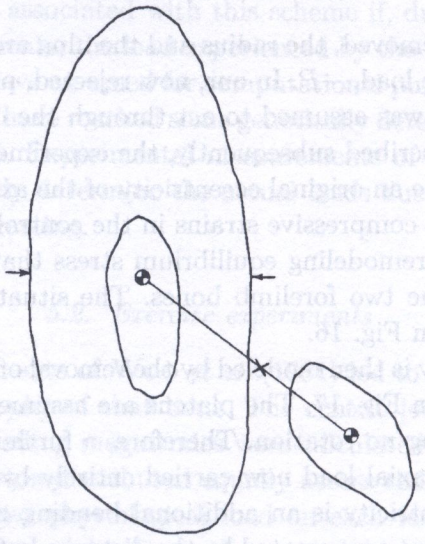

FIG. 18. Cross-section of intact ovine forelimb. Line connects centroids of the radius and ulna, and the point of application of the resultant load is represented by the $X$. Arrows indicate location of strain calculations corresponding to location of experimentally applied strain gauges.

The point of load application was then re-positioned along this centroidal line (Fig. 19) until the strains calculated were close to the peak strains measured by LANYON *et al.* (1982). Since sufficient data were not provided to accurately determine either the magnitude of the peak loading corresponding to the peak strains measured or the point of application of the resultant force, various loading magnitudes were tested as well. It was found that re-location of the point of load

application, represented by an $X$ symbol on Fig. 18, along the line joining the centroids of the radius and ulna, resulted in a linear variation of the strains calculated at cranial and caudal surfaces. The final location chosen shown on Figs. 18 and 19 gave calculated strains close to the peak strains measured with the loading magnitude set equal to 3.5 times the body weight. Further confidence in this choice for the position of the eccentric axial load comes from the lateral view of the longitudinal geometry of a sheep forelimb (LANYON *et al.*, 1982). A line drawn from the middle of the upper joint to the middle of the lower forelimb provides a rough estimation of the line of action of the force due to the weight of the animal. Since there is a gradual curvature of the shaft of the radius at the level where the gauges were attached, the line places the load just outside the periosteum of the radius on the caudal side. This position corresponds closely to the position found by moving the load along the centroidal line and comparing calculated strain with experimentally measured strain.

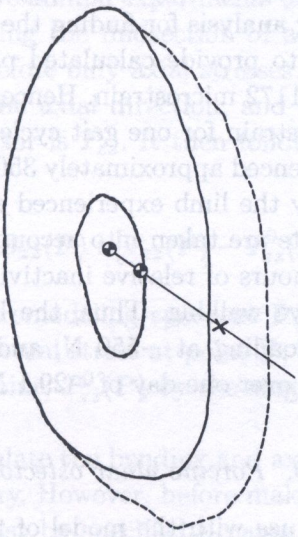

FIG. 19. Cross-section of intact ovine forelimb after the ulnaectomy. Line connects the centroid of the radius and the point of application of the resultant load, represented by the $X$. The dashed line represents the calculated remodeling at one year.

Using the point of load application as indicated on Fig. 18 with a magnitude of 3.5 times body weight gave the calculated values for strain, at the point on the caudal surface corresponding to a strain gauge location, of $-1182$ microstrain as compared to a measured strain of $-1172 \pm 14$ microstrain. Strain calculated at the point on the cranial surface was 419 compared to a measured strain of $635 \pm 5$ microstrain. The loading of 3.5 times body weight was the minimum loading that could generate tensile strains on the cranial surface close to those measured

by LANYON *et al.* (1982). Since for humans (normally with two-legged stance) SEIREG and ARVIKAR (1975) report peak reaction forces of 7.1 times body weight in the knee, the value of 3.5 times body weight for the sheep (normally four-legged stance) did not seem unreasonable. A further assumption required to find the remodeling equilibrium stresses on the radius was that, although the magnitude of the load associated with the remodeling equilibrium stresses would be less than the load associated with the peak strains described above, the point of load application of the two loads would be the same. The load magnitude associated with the remodeling equilibrium stress level was a time-averaged estimate of the dynamic loads, based on strains measured on the radius.

LANYON *et al.* (1982) published plots of the measured principal strains and directions for three gait cycles of normal sheep. The compressive strain on the caudal cortex fluctuates from nearly 0 to a peak value of $-1172$ microstrain. The area between the compressive strain curve and the time axis was approximated giving a time-averaged strain level of approximately 0.4 times the peak value. The previously discussed loading analysis for finding the peak loading gave 3.5 times body weight, or $-1375$ N, to provide calculated peak caudal strains near the experimentally measured $-1172$ microstrain. Hence, a constant force of $-550$ N provides the time-averaged strain for one gait cycle. During one hour of steady walking, the forelimb experienced approximately 3500 loading cycles, and during the other 23 hours each day the limb experienced a total of 950 loading cycles when casual limb movements are taken into account (LANYON *et al.*, 1982). It follows that during the 23 hours of relative inactivity, the forelimb experienced (950/3500) hours of effective walking. Thus, the limb was estimated to have experienced 1.27 hours of loading at $-550$ N, and 22.73 hours with no load, giving a time-averaged load over one day of $-29.1$ N.

### *5.5. Porcine ulnar ostectomy*

Loading parameters for use with the model of the porcine ulnar ostectomy were chosen largely by analogy with the remodeling analysis of the sheep forelimbs since the quantity of load and strain data from the porcine experimental study is rather limited.

For the sheep study, the time-averaged load used to determine the equilibrium and remodeling stress levels was 7.4% of the body weight. The same factor was also used for this porcine model since experimental data are not available to the contrary. The average body weight of the ostectomized group was 44 kg, thus the time-averaged load was set equal to $-32.0$ N.

The location for the loading point was also unknown for this study, and again it was hypothesized that the point of load application was on the line joining the centroids of the ulna and radius.

Due to the lack of strain data and the fact that the experimental animals were not yet skeletally mature, the remodeling parameters could not be rigorously quantified. The main emphasis was thus to choose remodeling parameters and rate constants similar to those used in the sheep study and achieve a remodeled shape similar to that shown in Fig. 14b.

Several locations on the loading line connecting the bone centroids were used to determine the equilibrium and remodeling stress levels on the radial surface. The optimum combination of loading position and remodeling shape is shown in Fig. 14c.

## 6. Computational formulation of the problem

In this section we employ elementary mechanics and the theory of surface remodeling to develop a computational formulation to predict the surface movement in the models of the five animal experiments described above. We consider the right cylinder representing the midsection of a long bone to be subjected to only axial loads and therefore only axial stresses. We select the $z$-coordinate direction to coincide with the axial direction, and therefore the only non-zero component of the stress tensor is $T_{zz}$. It then follows from equation (1.5) that the surface velocity is

$$U = B_{zz}(\mathbf{P}) : \left[T_{zz}(\mathbf{P}) - T^0_{zz}(\mathbf{P})\right]. \tag{2.3}$$

This result shows that the remodeling speed at $\mathbf{P}$, $U(\mathbf{P})$, is determined from the difference between the actual stress at point $\mathbf{P}$, $T_{zz}(\mathbf{P})$, and the remodeling equilibrium stress at that point, $T^0_{zz}(\mathbf{P})$ by the single surface remodeling stress rate coefficient $B_{zz}(\mathbf{P})$.

In the following, we calculate the bending and axial components of the stress $T_{zz}(\mathbf{P})$ using the beam theory. However, before making this calculation the material symmetry of bone must be specified because beam theory is not simple in the many cases involving anisotropic materials. For example, in general, in anisotropic materials a bending moment will induce a twisting of the beam as well as the deflection due to bending alone, and, conversely, a torque on a shaft will induce a bending deflection as well as a twist. However, if the long axis of the beam or shaft, the $z$ axis, is an axis of material symmetry, and if the elastic coefficients $\hat{s}_{34}$ and $\hat{s}_{35}$ vanish, then bending of a beam about the $\theta$ or $r$ axis does not introduce any twisting of the beam, and beam theory can be applied. This result is originally due to Lekhnitskii and is described in books by Hearmon (1961) and Lekhnitskii (1963). It follows then that if the long axis of bone is an axis of material symmetry and if $\hat{s}_{34}$ and $\hat{s}_{35}$ vanish, then beam theory can be applied. In fact, the long axis of the midsection of a long bone is an axis

of material symmetry, and bone can be considered to have orthotropic material symmetry (ASHMAN *et al.*, 1984), a type of symmetry for which both $\hat{s}_{34}$ and $\hat{s}_{35}$ vanish. We shall therefore assume the bone tissue to have orthotropic material symmetry and calculate the axial stress, $T_{zz}(\mathbf{P})$, using beam theory. This result, coupled with the result shown in equation (1.9) simplifies the computational problem considerably. The only material parameter involved in the problem will be the surface remodeling stress rate coefficient, $B_{zz}(\mathbf{P})$. This is the only constant to be determined from each of the five animal experiments, but it is assumed to be different for deposition and for resorption.

To use beam theory to calculate $T_{zz}$, the cross-section of the bone is oriented in a global coordinate system $(x, y)$ as shown in Fig. 20. The coordinates of the centroid are given by $(x_c, y_c)$, and the centroid is the origin of the centroidal coordinate system $(\bar{x}, \bar{y})$ with axes parallel to the global coordinate axes. The point of load application is given in the global coordinates by $(x_p, y_p)$. The general case is that of a beam loaded in unsymmetrical bending with an axial load.

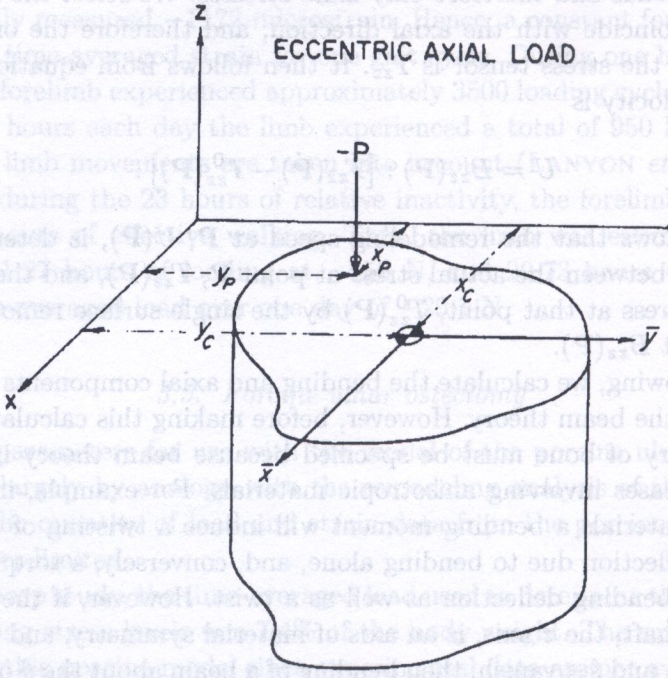


FIG. 20. Cross-sectional bone model. The global coordinate system is the $(x, y)$ system. The coordinates of the centroid are given by $(x_c, y_c)$, and the centroid is the origin of the centroidal coordinate system $(\bar{x}, \bar{y})$ with axes parallel to the global coordinate axes. The point of load application is given in the global coordinates by $(x_p, y_p)$. The general case is that of a beam loaded in unsymmetrical bending with an axial load.

The analysis of this situation is discussed, for example, by TIMOSHENKO (1955). The axial stress is calculated by the formula

$$T_{zz} = -\frac{P}{A} - \frac{P(x_p - x_c)[I_{\bar{x}\bar{y}}(y - y_c) - I_{\bar{x}\bar{x}}(x - x_c)]}{I_{\bar{x}\bar{x}}I_{\bar{y}\bar{y}} - I_{\bar{x}\bar{y}}I_{\bar{x}\bar{y}}} - \frac{P(y_p - y_c)[I_{\bar{x}\bar{y}}(x - x_c) - I_{\bar{y}\bar{y}}(y - y_c)]}{I_{\bar{x}\bar{x}}I_{\bar{y}\bar{y}} - I_{\bar{x}\bar{y}}I_{\bar{x}\bar{y}}}, \tag{2.4}$$

where $T_{zz}$ is the magnitude of the axial stress (acting in the global $z$-direction) at the point defined by global coordinates $(x, y)$, $P$ is the magnitude of the axial load which acts in the $z$-direction, $A$ is the total cross-sectional area of bone in the $x-y$ plane, $(x_p, y_p)$ are the global coordinates of the point of load application, $(x_c, y_c)$ are the global coordinates of the centroid of bone lying in the $x-y$ plane, $I_{\bar{x}\bar{x}}$ is the area moment of inertia of the cross-sectional area with respect to the centroidal $\bar{x}$ axis, $I_{\bar{y}\bar{y}}$ is the area moment of inertia of the cross-sectional area with respect to the centroidal $\bar{y}$ axis, and $I_{\bar{x}\bar{y}}$ is the area product of inertia of the cross-sectional area with respect to the centroidal $\bar{x}$ and $\bar{y}$ axes.

## 7. SUMMARY OF SURFACE REMODELING RESULTS

The results of the computations consist of the computed remodeling coefficients for each of the five animal experiments considered in this study, and the corresponding calculated shape of the remodeled cross-section obtained for each of the experiments. The constants obtained in this study are contained in Table 1. The calculated remodeled cross-sections using the theory of surface remodeling with the constants contained in Table 1 are shown in Figs. 10 left, 11 left, 12 left, 13 left and 14 left. In one case the remodeled cross-section was calculated at two years to see how much it differed from the one-year prediction (Fig. 21).

For each of the five cross-sections, there is good qualitative agreement between the experimentally remodeled shape, shown in Figs. 10 middle, 11 middle, 12 middle, 13 middle and 14 middle and the calculated shape, shown in Figs. 10 left, 11 left, 12 left, 13 left and 14 left. This qualitative agreement prompts two observations: first, the surface remodeling theory is an adequate tool for describing the remodeled bone geometry found from the *in vivo* experiments considered here, and second, coupled with the initial geometry and the loading conditions, the remodeling rate constants reported in Table 1 are adequate for qualitative prediction of each of the remodeled geometries.

The values for the remodeling equilibrium stress, $T^0$, are listed in Table 1. $T^0$ is a different constant for each of the three centric loading experiments, but

**Table 1. Summary of measured data and calculated results.**

| Type of study | Experimental animal | Reference | $T_0$ MPa | $T/T_0$ | $B_{zz}$ mm/day GPa | $U_{avg}$ μm/day | $U_{init}$ μm/day | Remarks |
|---|---|---|---|---|---|---|---|---|
| Immobilization | Young Beagles | Uhthoff and Jaworski | −0.43 | 0.45 | +5.6 (E)<br>−22.2 (P) | +0.4 (E)<br>−2.2 (P) | +1.3 (E)<br>−5.2 (P) | Simultaneous deposition and resorption |
| Immobilization | Old Beagles | Jaworski, Liskova–Kiar, and Uhthoff | −0.73 | 0.51 | −15.3 (E)<br>0.0 (P) | −2.6 (E)<br>0.0 (P) | −5.4 (E)<br>0.0 (P) | Endosteal resorption only |
| Exercise | Young Swine | Woo, Kuei, Dillon, Amiet, White and Akeson | −0.49 | 1.31 | −20.4 (E)<br>−15.3 (P) | +1.7 (E)<br>+1.2 (P) | +3.1 (E)<br>+2.3 (P) | Endosteal and periosteal deposition |
| Ulnar Ostectomy | Mature Sheep | Lanyon, Goodship, Pye and MacFie | −0.05 E<br>−0.27 E<br>+0.17 P<br>−0.48 P | 0.0<br>2.2<br>4.1<br>2.5 | 0.0 ET<br>0.0 EC<br>+5.6 PT<br>−36.0 PC | 0.0<br>0.0<br>+1.1<br>+8.8 | 0.0<br>0.0<br>+2.9<br>+25.9 | Periosteal deposition only. Different rate constants for tension and compression |
| Ulnar Ostectomy | Young Swine | Goodship, Lanyon, and MacFie | −0.10 E<br>−0.23 E<br>−0.07 P<br>−0.25 P | −8.0<br>5.6<br>−15.7<br>6.8 | 0.0 ET<br>0.0 EC<br>0.0 PT<br>−47.2 PC | 0.0<br>0.0<br>0.0<br>43.0 | 0.0<br>0.0<br>0.0<br>70.8 | High velocity reflects quantity of bone deposition |

E denotes Endosteal Surface;
P denotes Periosteal Surface;
T denotes Tension;
C denotes Compression.

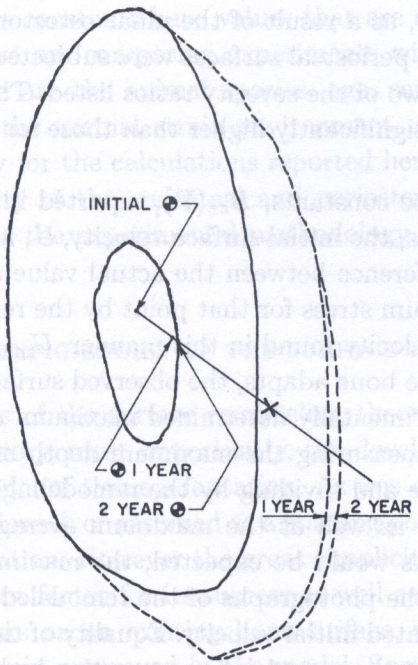


FIG. 21. Cross-section of intact ovine forelimb after the ulnaectomy. Line connects the centroid of the radius and the point of application of the resultant load, represented by the $X$. The dashed lines represent the calculated remodeling at one and two years.

it varies with position on the bone cross-section for the eccentric loading experiments, the ulnar ostectomies. In the case of the ulnar ostectomy studies, the extreme values are listed in Table 1 for both the endosteal and periosteal surfaces. Also listed is the calculated experimental "severity ratio" defined as the ratio of the time-averaged stress calculated at the start of the experiment, $T$, and the calculated time-averaged remodeling equilibrium stress, $T^0$. A negative number for this ratio means that a point on the surface of the bone with a remodeling equilibrium stress that is normally compressive (tensile) is being experimentally loaded so that the point is now in tension (compression). For each of the first three experiments in Table 1, both the remodeling equilibrium stress and the stress at the start of the experimental period were compressive. The ulnar ostectomy experiment with mature sheep shows that a portion of the periosteal bone (cranial surface) has a tensile remodeling equilibrium stress, while the remaining bone has a compressive remodeling equilibrium stress. The magnitude of the time-averaged stresses increased as a result of the ulnar ostectomy, but the sign of the maximum and minimum stresses listed in the table was unchanged. In contrast with the sheep study, the results of the ulnar ostectomy on young swine show that the entire radius has compressive remodeling equilib-

rium stresses. However, as a result of the ulnar ostectomy, portions of bone on both the endosteal and periosteal surfaces were subjected to tensile loads, giving negative numbers for two of the severity ratios listed. The severity ratios for the ostectomy studies are significantly higher than those for the immobilization and exercise experiments.

The remodeling rate constants, $B_{zz}(\mathbf{P})$, reported in Table 1 are in units of mm day – $\text{GPa}^{-1}$. Thus, the initial surface velocity, $U$, in Eq. (2.3) can be found by multiplying the difference between the actual value of stress at a particular point and the equilibrium stress for that point by the remodeling rate constant, $B_{zz}(\mathbf{P})$. The surface velocity found in this manner, $U_{\text{init}}$, is thus the *initial* surface velocity, and as the bone adapts, the observed surface velocity will decrease toward zero. The experimentally determined maximum *average* surface velocity, $U_{\text{avg}}$, is estimated by measuring the maximum depth of the bone deposited or resorbed on the surface and dividing by the remodeling time period. The maximum initial velocities as well as the maximum average surface velocities are reported in Table 1. As would be expected, the maximum average surface velocity measured from the photographs of the remodeled bone cross-sections are smaller than the calculated initial velocity. Equality of the two velocity measures would have implied that the remodeled cross-section had not yet approached the equilibrium configuration since the initial velocity has remained constant.

The sign convention used in Table 1 is as follows. If new bone is deposited on an external surface, then the velocity, $U$, is considered to be positive, while negative surface velocity implies that bone on the external surface is resorbed. If the difference between the actual stress and the remodeling equilibrium stress, $(T-T^0)$, is positive, then $B_{zz}$ positive leads to bone deposition, and $B_{zz}$ negative leads to bone resorption. On the other hand, if the difference between the stresses is negative, then $B_{zz}$ positive leads to bone resorption, and $B_{zz}$ negative leads to bone deposition.

The calculated surface remodeling represented in the left-hand panels of Figs. 10 to 14 all show geometries that have evolved to a shape that is close to the experimental geometry at the time listed with each figure. The evolution of the calculated remodeled geometry is almost complete since, at the time shown, the axial stress is almost equal to the remodeling equilibrium stress, $T^0$. The change in the periosteal surface position and the radius centroid in the time between the predicted geometry at 9 months, shown in the left-hand panel of Fig. 14, and the predicted geometry at 1 year, (not shown) from that value is small. This indicates that the functional adaptation response was almost complete at the end of the 9-month period used in the calculations. This computational result is also in qualitative agreement with the experimental results that showed tetracycline labeling at the end of the six-month experimental group, but an absence of labeling on the twelve month group (LANYON *et al.*, 1982).

The remodeling rate constants have values that are all of the same order of magnitude, although we are comparing experiments with several independent variables. Among these are the animal species, age, severity of experiment in terms of change from the normal strain environment, and the degree of data extrapolation necessary for the calculations reported here. The factor that governs the relative activity of the endosteal and periosteal surfaces seems to be the animal age and not the experimental methodology used to induce the net remodeling response.

## 8. Successes and deficiencies of the surface remodeling theory

Some of the success of the surface remodeling theory is inherited from the internal remodeling theory, most importantly, the development of a thermodynamic open-system model of tissue adaptation. As was noted in Part I, Sec. 15, this model has been followed, or assumed as a starting point, by most subsequent models of tissue adaptation. However the great simplicity of surface remodeling theory is an independent factor for its success as well as the fact that real bone deposition always occurs on an existing bone surface, so the bone remodeling phenomena are accurately portrayed in the model. Some of the major changes to be recommended for a reformulated surface remodeling theory are common with the recommendations made for an internal remodeling theory in Part I, Sec. 15. The common major changes would be the introduction of two time scales, and the introduction of the rate-of-strain or the rate-of-loading as the stimulus, both described in Part I, Sec. 15. A reformulated theory of surface remodeling with a rate-of-strain stimulus was sucessfully developed and applied by Luo *et al.* (1995).

There have been criticisms of the surface remodeling theory that are unjustified from my perspective. Prendergast and Taylor (1994) and Prendergast (2001) criticize the fact that the remodeling rate coefficients for the endosteal and periosteal surfaces are assumed to be different. Their argument is that the remodeling rate coefficients on the endosteal and periosteal surfaces should be the same. However if one looks carefully at the biological structure of the endosteum and periosteum, one sees that the two biological structures are not the same. The endosteum is a fragile single osteoblastic lineage cell layer on the surface of the medullary canal while the periosteum is a relatively (relative to the endosteum) thick fibrous structure whose innermost layer is a single osteoblastic lineage cell layer, but whose interior contains other cell types including fibroblasts. Furthermore the animal experimental data are inconsisent with the equality of the endosteum and periosteum remodeling rate coefficients. An inspection of the results of the animal experiments described here and illustrated by Figs. 10, 11 and 12 demonstrates this inconsistency.

A second unjustified criticism of the surface remodeling theory that is given by MARTIN and BURR (1987). These authors make the following comments (MARTIN and BURR, 1987; p.177): "Obviously, if any theory is to have any practical application, the values of the remodeling rate coefficients must be determined. To that end, Cowin's group compared the predictions of their model to the results of several animal experiments (Figs. 10 to 14). The results were encouraging, but the model is far from biologically useful. The **C** tensor contains coefficients for each component of strain; these must be determined for endosteal and periosteal surfaces. It was found that different coefficients had to be used to predict the results of each experiment. This means that the theory is incapable of describing adaptation to mechanical usage in any sort of generalized way which in turn indicates that the theory is flawed in some way".

MARTIN and BURR (1987) criticize the theory while their real concern is with the fact that the values of the remodeling coefficients determined from the various experiments (as shown in Table 1) are not sufficiently close. The fact that the remodeling coefficients determined from the various experiments (as shown in Table 1) are not sufficiently close is not due to a flaw in the theory as suggested, but rather due to the lack of data on the mechanical loading history in the reports of the animal experiments considered. For four of the experiments, little quantitative data are provided to accurately determine the mechanical loading history estimates on the normal bone or on the abnormally loaded bone (UHTHOFF and JAWORSKI, 1978; JAWORSKI *et al.*, 1980; WOO *et al.*, 1981; GOODSHIP *et al.*, 1979). In addition, strain gauge data provided by LANYON *et al.* (1982) for the sheep ostectomy study did not provide sufficient information to uniquely determine either the points of application or the magnitudes of the loading forces. Consequently, only very approximate mechanical loading history estimates were employed in the study. The ideal experimental information for use with a remodeling theory based on describing and predicting the mechanical objectives of bone remodeling would include sufficient information to accurately determine the loading history on both the experimental and control bones, the geometry of both bones, the material distribution in the bones, and the time course of the remodeling process. The work of COWIN *et al.* (1985) could only proceed by making *ad-hoc* estimates of the mechanical loading history for each animal experiment. The *ad-hoc* methods of estimating the mechanical loading history were described in detail in COWIN *et al.* (1985) and these descriptions have been repeated in Part II, Sec. 5 above. The reader should review the AD-HOC methods under *immobilization experiments, exercise experiments* and *ovine and porcine ulnar ostectomies.* For example, the mechanical loading history for the exercise experiments of WOO *et al.* (1981) were calculated by the method described in the paragraph containing Eq. (2.2). These *ad-hoc* methods produce only gross estimates of the mechanical loading history. They were used because there was

little or no recorded data on the mechanical loading history during these animal experiments. Despite the simplicity of the model and the lack of data that would be required to uniquely define the load environments, the remodeling constants for each of these animal experiments are of approximately the same magnitude. This similarity, despite the differences in loading environment, animal species, and age gives reason to be optimistic about the applicability of the surface remodeling theory as a tool for prediction of *in vivo* bone remodeling.

If MARTIN and BURR (1987) and PRENDERGAST (2001), who also criticized the inconsistency in the values of the remodeling rate coefficients, would think about the information that was available to determine the mechanical loading history for these animal experiments, they will see that the results obtained in COWIN *et al.* (1985) are really quite good and that the theory is simple and not yet either proved or refuted. (The requirement implicitly specified in the paragraph of MARTIN and BURR (1987) quoted above is that the remodeling rate coefficients be the same, independently of the age and species of the animal, is biologically unrealistic.) The unhappy aspect of reconsidering these issues almost twenty years later is that our ability to improve our predictions of the remodeling rate coefficients has not increased. To date there are no animal experiments that report enough information to determine the mechanical loading history. Nothing has changed. I would be happy if these authors will change their opinions. I also would be happy if someone will undertake a properly designed set of animal experiments to prove or refute some version of the surface remodeling theory.

## Part III. Architectural adaptation

### 1. WOLFF'S LAW

An elastic constitutive relation for cancellous bone tissue with an explicit cancellous bone architectural measure was developed in COWIN (1986). This relationship, which only applied at remodeling equilibrium, involves the stress tensor $\mathbf{T}$, the strain tensor $\mathbf{E}$ and a measure of trabecular architecture called the fabric tensor which is denoted by $\mathbf{H}$. As discussed in the next section, the fabric tensor is a symmetric second rank tensor that is a quantitative stereological measure of the microstructural arrangement of trabeculae and pores in the cancellous bone tissue. The constitutive relation obtained is a part of an algebraic formulation of Wolff's law of trabecular architecture in remodeling equilibrium. In particular, with the general constitutive relationship between $\mathbf{T}$, $\mathbf{E}$ and $\mathbf{H}$, the statement of Wolff's law at remodeling equilibrium is simply the requirement of the commutability of the matrix multiplication of the stress tensor and the fabric tensor at remodeling equilibrium, $\mathbf{T}^*\mathbf{H}^* = \mathbf{H}^*\mathbf{T}^*$. The asterisk on the

stress and fabric tensors indicates their values in remodeling equilibrium. It is shown that the constitutive relation also requires that $\mathbf{E}^*\mathbf{H}^* = \mathbf{H}^*\mathbf{E}^*$. Thus, the principal axes of the stress, strain and fabric tensors all coincide at remodeling equilibrium. In the Part III, Sec. 5 the constitutive relations for the evolutionary form of Wolff's law are recorded and graphically illustrated.

## 2. The fabric tensor for cancellous bone tissue

Cancellous bone tissue is an inhomogeneous porous anisotropic structure. The cancellous structure is a lattice of narrow rods and plates (70 to 200 μm in thickness) of calcified bone tissue called trabeculae. The trabeculae are surrounded by marrow that is vascular and provides nutrients and waste disposal for the bone cells. The distinctive structural anisotropy (or architecture) of cancellous bone tissue can be approximately measured by a variety of stereological procedures that produce ellipses, ellipsoids or, equivalently, positive definite second rank tensors. The mean intercept length tensor is one example of such a measure. The mean intercept length $L$ for cancellous bone tissue is measured as a function of direction on polished plane sections. The mean intercept length is the average distance between two bone/marrow interfaces measured along a line. The value of the mean intercept length is a function of the slope of the line, $\theta$, along which the measurement is made; Figure 22 illustrates making such a measurement for a fixed value of $\theta$.

Whitehouse showed that when the mean intercept lengths measured in cancellous bone for different values of $\theta$ were plotted in a polar diagram as a function of the direction (i.e., of the slope of the line along which they were measured), the polar diagram produced ellipses (Fig. 23). If the test lines are rotated through several values of $\theta$ and the corresponding values of mean intercept length $L(\theta)$ are measured, the data are found to fit the equation for an ellipse very closely,

$$\frac{1}{L^2(\theta)} = M_{11}\cos^2\theta + M_{22}\sin^2\theta + 2M_{12}\cos\theta\sin\theta, \tag{3.1}$$

where $M_{11}$, $M_{22}$ and $M_{12}$ are constants when the reference line from which the angle $\theta$ is measured is constant. The subscripts 1 and 2 indicate the axes of the $x_1, x_2$ coordinate system to which the measurements are referred. In three dimensions the mean intercept length is represented by ellipsoids and is therefore equivalent to a positive definite second rank tensor. The constants $M_{ij}$ introduced in the foregoing are then the components of a second-rank tensor $\mathbf{M}$ which are related to the mean intercept length $L(\mathbf{n})$, where $\mathbf{n}$ is a unit vector in the direction of the test line, by

$$\frac{1}{L^2(\theta)} = \mathbf{n}\cdot\mathbf{M}\cdot\mathbf{n}. \tag{3.2}$$

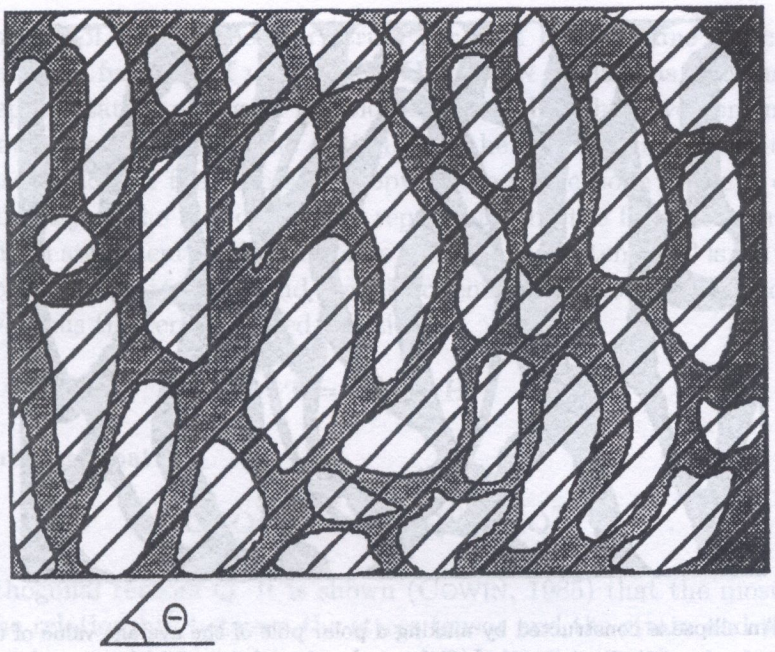


FIG. 22. Test lines superimposed on a cancellous bone specimen. The test lines are oriented at the angle $\theta$. The mean intercept length measured at this angle is denoted $L(\theta)$.

The fabric tensor is denoted by $\mathbf{H}$ and has components $H_{ij}$ relative to a Cartesian coordinate system. $\mathbf{H}$ is related to the mean intercept length tensor $\mathbf{M}$ by

$$\mathbf{H} = \left(\sqrt{\mathbf{M}}\right)^{-1}. \tag{3.3}$$

The positive square root of the inverse of $\mathbf{M}$ is well defined because $\mathbf{M}$ is a positive definite symmetric tensor. $\mathbf{M}$ is a positive definite symmetric tensor because it represents an ellipsoid. The motivation for defining a measure of fabric that depends inversely on the mean intercept length will be discussed later. The fabric tensor or mean intercept ellipsoid can be measured using a cubic specimen. On each of three orthogonal faces of a cubic specimen an ellipse will be determined from the directional variation of mean intercept length on that face. The fabric tensor can be constructed from these three ellipses that are the projections of the ellipsoid on three perpendicular planes of the cube.

The results presented here do not depend upon the precise details of the definition of the fabric tensor. It is only required that the fabric tensor be a positive definite second rank tensor that is a quantitative stereological measure of the trabecular architecture, a measure whose principal axes are coincident with the principal trabecular directions and whose eigenvalues are proportional to

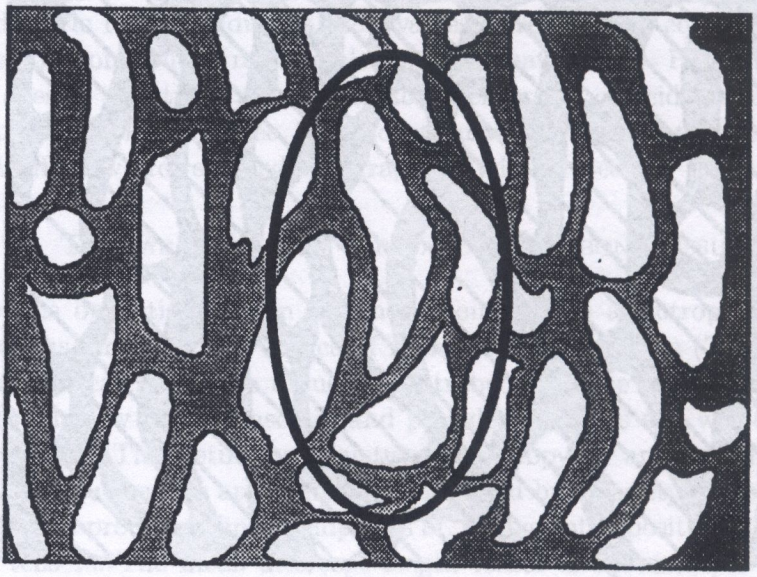

FIG. 23. An ellipse is constructed by making a polar pole of the average value of the mean intercept length $L(\theta)$ for each value of the angle $\theta$.

the massiveness of the trabecular structure in the associated principal direction. The many ways to construct a fabric tensor for bone are described by ODGAARD (1997; 2001).

## 3. THE RELATIONSHIP BETWEEN THE FABRIC TENSOR AND THE ELASTICITY TENSOR

Bone tissue is modeled satisfactorily as an orthotropic, linearly elastic material. The six-dimensional second rank elasticity tensor $\hat{\mathbf{c}}$ relates the six-dimensional stress vector $\widehat{\mathbf{T}}$ to the six-dimensional infinitesimal strain vector $\widehat{\mathbf{E}}$ in the linear anisotropic form of Hooke's law,

$$\widehat{\mathbf{T}} = \hat{\mathbf{c}}\widehat{\mathbf{E}}. \tag{3.4}$$

The elasticity tensor $\hat{\mathbf{c}}$ completely characterizes the linear elastic mechanical behavior of the cancellous bone tissue. If it is assumed that all the anisotropy of cancellous bone is due to the anisotropy of its trabecular structure, that is to say that the matrix material is itself isotropic, then a relationship between the components of the elasticity tensor $\hat{\mathbf{c}}$ and $\mathbf{H}$ can be constructed. From previous studies of cancellous bone it is known that its elastic properties are strongly dependent upon its apparent density or, equivalently, the solid volume fraction of trabecular structure. This solid volume fraction is denoted by $\nu$ and is defined

as the volume of solid trabecular struts per unit bulk volume of the tissue. Thus $\hat{\mathbf{c}}$ will be a function of $\nu$ as well as $\mathbf{H}$. COWIN (1985) has constructed the general representation of $\hat{\mathbf{c}}$ as a function of $\nu$ and $\mathbf{H}$. The development of this representation was based on the notion that the matrix material of the bone tissue is isotropic and that the anisotropy of the whole bone tissue is due only to the geometry of the microstructure represented by the fabric tensor $\mathbf{H}$. The mathematical statement of this notion is that the stress tensor $\mathbf{T}$ is an isotropic function of the strain tensor $\mathbf{E}$ and the fabric tensor $\mathbf{H}$ as well as the solid volume fraction $\nu$. Thus the tensor-valued function

$$\mathbf{T} = \mathbf{T}(\nu, \mathbf{E}, \mathbf{H}) \tag{3.5}$$

has the property that

$$\mathbf{Q}\mathbf{T}\mathbf{Q}^T = \mathbf{T}(\nu, \mathbf{Q}\mathbf{E}\mathbf{Q}^T, \mathbf{Q}\mathbf{H}\mathbf{Q}^T) \tag{3.6}$$

for all orthogonal tensors $\mathbf{Q}$. It is shown (COWIN, 1985) that the most general form of the relationship between the stress tensor and the strain and the fabric tensors consistent with the isotropy assumption (3.6) described in the foregoing is

$$\begin{aligned}\mathbf{T} = {} & a_1 \mathbf{1}\mathrm{tr}\mathbf{E} + a_2 (\mathbf{H}\mathrm{tr}\mathbf{E} + \mathbf{1}\mathrm{tr}[\mathbf{E}\mathbf{H}]) + a_3 \left(\mathbf{1}\mathrm{tr}[\mathbf{H}\mathbf{E}\mathbf{H}] + (\mathrm{tr}\mathbf{E})\,\mathbf{H}^2\right) \\ & + b_1 \mathbf{H}\mathrm{tr}[\mathbf{H}\mathbf{E}] + b_2 \left(\mathbf{H}\mathrm{tr}[\mathbf{H}\mathbf{E}\mathbf{H}] + (\mathrm{tr}\mathbf{E}\mathbf{H})\,\mathbf{H}^2\right) + b_3 \left(\mathbf{H}^2\mathrm{tr}[\mathbf{H}\mathbf{E}\mathbf{H}]\right) \\ & + 2c_1 \mathbf{E} + 2c_2 (\mathbf{H}\mathbf{E} + \mathbf{E}\mathbf{H}) + 2c_3 \left(\mathbf{H}^2\mathbf{E} + \mathbf{E}\mathbf{H}^2\right),\end{aligned} \tag{3.7}$$

where $a_1$, $a_2$, $a_3$, $b_1$, $b_2$, $b_3$, $c_1$, $c_2$, and $c_3$ are functions of $\nu$, $\mathrm{tr}\mathbf{H}$, $\mathrm{tr}\mathbf{H}^2$ and $\mathrm{tr}\mathbf{H}^3$.

## 4. WOLFF'S LAW AT REMODELING EQUILIBRIUM

The absence of bone remodeling is remodeling equilibrium. Specifically, remodeling equilibrium (RE) is the set of conditions under which there is no realignment of trabecular architecture and no net deposition or resorption of cancellous bone tissue. RE is thus characterized by a particular equilibrium architecture, denoted by v* and $\mathbf{H}^*$, and a particular stress and strain state, denoted by $\mathbf{T}^*$ and $\mathbf{E}^*$, respectively. The RE stress $\mathbf{T}^*$ and strain $\mathbf{E}^*$ may actually be ranges of stress and strain, or some special measures of stress and strain history. When this theory was formulated, $\mathbf{T}^*$ and $\mathbf{E}^*$ were considered to be long time averages of the environmental stress and strain, although they may be more specific functions of the stress and strain history of the bone tissue.

In the introduction it was noted that Wolff's law of trabecular architecture states that the principal stress axes coincide with the principal trabecular directions in cancellous bone in RE. This means that, in RE, the principal axes

of stress $\mathbf{T}^*$ must coincide with the principal axes of fabric $\mathbf{H}^*$. This coincidence of principal axes is assured if the matrix multiplication of $\mathbf{T}^*$ and $\mathbf{H}^*$ is commutative, i.e., if

$$\mathbf{T}^*\mathbf{H}^* = \mathbf{H}^*\mathbf{T}^*. \tag{3.8}$$

This appears to be the first mathematical formulation of what is considered by many to be Wolff's law of trabecular architecture in remodeling equilibrium, namely that the principal stress directions are coincident with the principal directions of the trabecular architecture. It is also generally agreed that the direction associated with the largest (smallest) Young's modulus in the cancellous bone should be associated with the direction in which the massiveness of the trabecular architecture is greatest (least). If the Young's moduli are ordered by $E_1 > E_2 > E_3$ then this condition is satisfied if $H_1 > H_2 > H_3$.

Since the principal axes of $\mathbf{T}^*$ and $\mathbf{H}^*$ are coincident by Wolff's law, it can be shown that the principal axes of $\mathbf{E}^*$ are also coincident with those of $\mathbf{T}^*$ and $\mathbf{H}^*$. To see why this is true, consider a principal coordinate system of $\mathbf{H}^*$. This coordinate system is also a principal coordinate system of $\mathbf{T}^*$. Since the shear stresses are all zero in this coordinate system, it follows that the shearing strains are also zero, hence the coordinate system is also a principal coordinate system of $\mathbf{E}^*$. These results are summarized by any two of the following three relations:

$$\mathbf{T}^*\mathbf{H}^* = \mathbf{H}^*\mathbf{T}^*, \quad \mathbf{T}^*\mathbf{E}^* = \mathbf{E}^*\mathbf{T}^*, \quad \mathbf{E}^*\mathbf{H}^* = \mathbf{H}^*\mathbf{E}^*. \tag{3.9}$$

## 5. An evolutionary Wolff's law for trabecular architecture

The constitutive relations for the evolutionary form of Wolff's law are

$$\mathbf{T} = \beta_1\mathbf{1} + \beta_2\mathbf{E} + \beta_3\mathbf{H} + \beta_4\mathbf{H}^2 + \beta_5(\mathbf{HE} + \mathbf{EH}) + \beta_6(\mathbf{H}^2\mathbf{E} + \mathbf{EH}^2), \tag{3.10}$$

$$\dot{\mathbf{H}} = \alpha_1\mathbf{1} + \alpha_2\mathbf{H} + \alpha_3\mathbf{H}^2 + \alpha_4\mathbf{E} + \alpha_5(\mathbf{HE} + \mathbf{EH}) + \alpha_6(\mathbf{H}^2\mathbf{E} + \mathbf{EH}^2), \tag{3.11}$$

$$\dot{e} = \dot{e}(e, \mathrm{tr}\mathbf{E}, \mathrm{tr}\mathbf{H}, \mathrm{tr}\mathbf{H}^2, \mathrm{tr}\mathbf{H}^3, \mathrm{tr}\mathbf{EH}, \mathrm{tr}\mathbf{EH}^2), \tag{3.12}$$

where all the $\alpha$'s and $\beta$'s are functions of $e, \mathrm{tr}\mathbf{H}, \mathrm{tr}\mathbf{H}^2$ and $\mathrm{tr}\mathbf{H}^3$ and some may be functions of strain ($\mathrm{tr}\mathbf{E}, \mathrm{tr}\mathbf{EH}$ and $\mathrm{tr}\mathbf{EH}^2$) if they are consistent with the restriction of a linear dependence upon strain.

An example of the application of this evolutionary form of Wolff's law will now be described in order to illustrate the model. An illustration of the formulation of the boundary value problem considered is shown in Fig. 24. Figure 24 (left) shows the remodeling equilibrium situation associated with a stress state $\mathbf{T}^0$ that exists for $t < 0$. Figure 24 (right) shows the situation at $t = 0^+$ when a new stress state $\mathbf{T}^*$ is applied and held constant for all subsequent time.

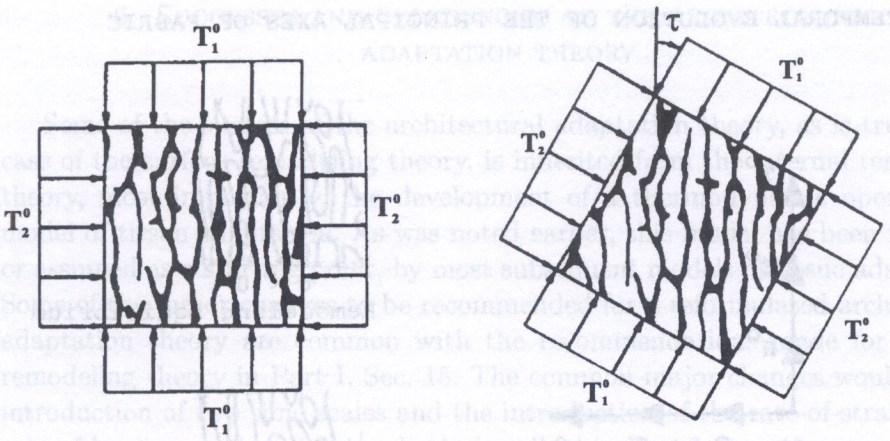


FIG. 24. An illustration of the formulation of the boundary value problem considered. (left) The remodeling equilibrium situation associated with a stress state $\mathbf{T}^0$ that exists for $t < 0$. (right) The situation at $t = 0^+$ when a new stress state $\mathbf{T}^*$ is applied and held constant for all subsequent time. The subsequent evolution of the trabecular architecture is illustrated in Fig. 25.

To aid the reader in the understanding of Eqs. (3.10) to (3.12) to solve the problem described in Fig. 24, Fig. 25 is employed. Figure 25 is a sequence of four illustrations showing the temporal evolution of the trabecular architecture from an RE situation characterized by states of stress, strain and fabric denoted as $\mathbf{T}^0$, $\mathbf{E}^0$ and $\mathbf{H}^0$, respectively, to an RE situation characterized by states of stress, strain and fabric denoted as $\mathbf{T}^*$, $\mathbf{E}^*$ and $\mathbf{H}^*$, respectively. Figure 25 (top) illustrates the remodeling equilibrium situation that exists for $t < 0$. The principal axes of $\mathbf{T}^0$, $\mathbf{E}^0$ and $\mathbf{H}^0$ are coincident. Figure 25 (upper middle) illustrates the situation when remodeling is initiated at $t = 0^+$. The applied stress is now represented by the temporally constant stress tensor $\mathbf{T}^*$, whose principal axes make an angle in the 1–3 plane with the principal axes of the previously applied stress tensor $\mathbf{T}^0$. Furthermore, the temporally varying strain tensor $\mathbf{E}(t)$ has instantaneously assumed a new value while the fabric tensor $\mathbf{H}^0$ remains at its $t < 0$ value. Figure 25 (lower middle) illustrates the situation at a typical time $t$ as remodeling is proceeding. The principal axes of strain $\mathbf{E}$ and fabric $\mathbf{H}$ make angles with the horizontal axes in the 1–3 plane. As time increases, the principal axes of strain $\mathbf{E}$ and fabric $\mathbf{H}$ move into coincidence with the principal axes of the applied stress $\mathbf{T}^*$. Figure 25 (bottom) illustrates the new remodeling equilibrium situation that is achieved as $t$ tends to infinity. A new RE situation has been established; it is characterized by states of stress, strain and fabric with coincident principal axes denoted as $\mathbf{T}^*$, $\mathbf{E}^*$ and $\mathbf{H}^*$, respectively, and by a solid volume fraction $e^*$.

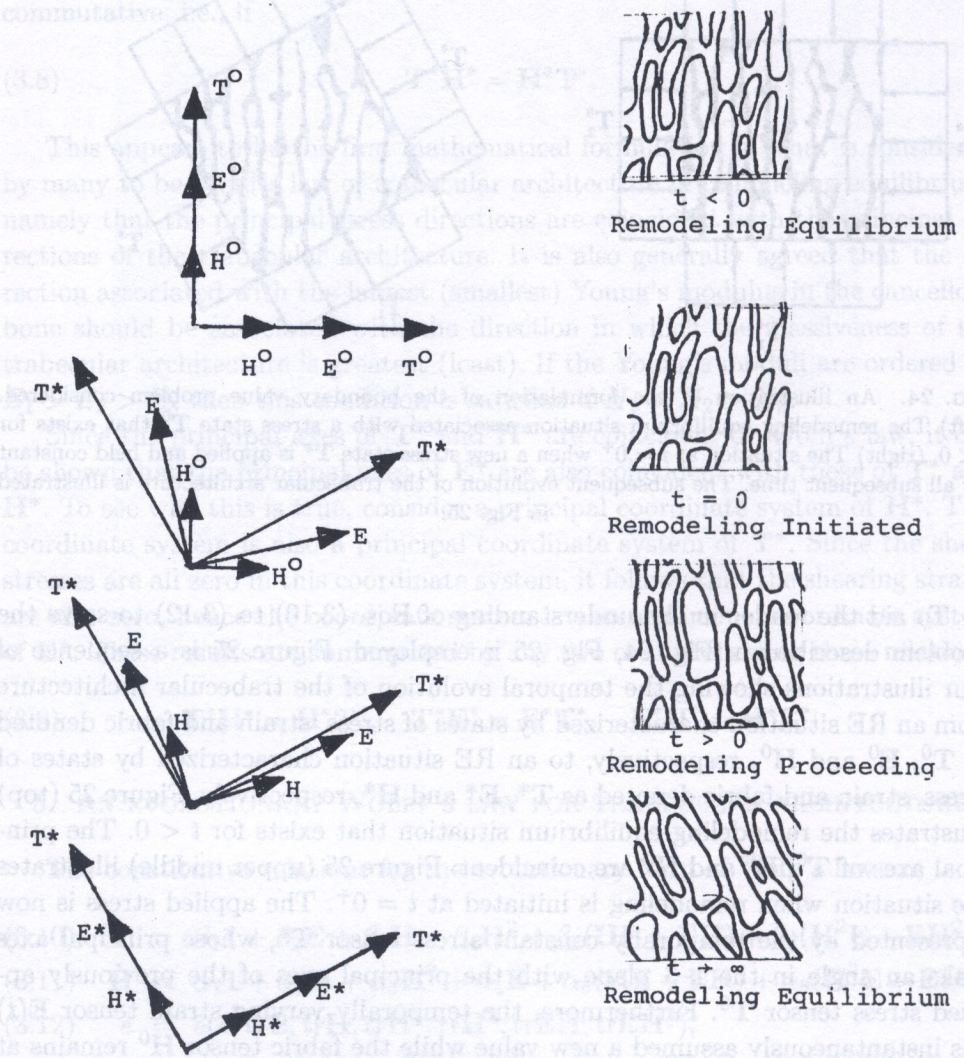


FIG. 25. This sequence of four illustrations shows the evolution of the trabecular architecture from an RE situation characterized by states of stress, strain and fabric denoted as $\mathbf{T}^0$, $\mathbf{E}^0$, and $\mathbf{H}^0$, respectively, to an RE situation characterized by states of stress, strain and fabric denoted as $\mathbf{T}^*$, $\mathbf{E}^*$, and $\mathbf{H}^*$, respectively. (top) The remodeling equilibrium situation that exists for $t < 0$. (upper middle) The situation when remodeling is initiated at $t = 0^+$. (lower middle) The situation at a typical time $t$ as remodeling is proceeding. (bottom) A new RE situation is restored as t tends to infinity.

## 6. Successes and deficiencies of the architectural adaptation theory

Some of the success of the architectural adaptation theory, as is true in the case of the surface remodeling theory, is inherited from the internal remodeling theory, most importantly, the development of a thermodynamic open-system model of tissue adaptation. As was noted earlier, this model has been followed, or assumed as a starting point, by most subsequent models of tissue adaptation. Some of the major changes to be recommended for a reformulated architectural adaptation theory are common with the recommendations made for internal remodeling theory in Part I, Sec. 15. The common major changes would be the introduction of two time scales and the introduction of the rate-of-strain or the rate-of-loading as the stimulus, both described in Part I, Sec. 15.

The use of the fabric tensor to characterize the architecture of cancellous bone has been treated with skepticism by some (Kuo and Carter, 1991; Jacobs, *et al.*, 1997), but in the last decade its effectiveness in representing the local architecture of cancellous bone has been demonstrated by many investigators (Turner *et al.*, 1990; Goulet *et al.*, 1994; van Rietbergen *et al.* 1996, 1998; Zysset *et al.*, 1998; Zysset, 2002). It is rather universally recognized that porosity or solid volume fraction is the primary measure of local material structure in a porous material. This means that in the purely geometric kinematic description of the arrangement of the pore structure the porosity is the zero order term and fabric tensors of even order are the higher order measures. Porosity does not, however, reflect any directionality of the specimen's pore microstructure. The fabric tensors for solid materials with pores are constructed using one of the methods described by Odgaard (1997 or 2001). Now there appears to be a general agreement that a fabric tensor is the best second measure of local material microstructure in bone. The general problem of the quantification of structural anisotropy in materials with distinctive microstructure like geological and biological materials is considered in a series of papers by Kanatani (1983; 1984 a, b; 1985). The problem of the determination of structural anisotropy of solid materials with pores by the methods of quantitative stereology was considered by Hilliard (1967). In some situations higher order fabric tensors are necessary; this will be considered below.

The theory of architectural adaptation does not depend upon the precise details of the definition of the fabric tensor. It is required only that the fabric tensor be a positive definite tensor that is a quantitative stereological measure of the microstructural architecture, a measure whose principal axes are coincident with the principal microstructural directions and whose eigenvalues are proportional to the massiveness of the microstructure in the associated principal direction. The many ways to construct a fabric tensor for bone are described by

ODGAARD (1997; 2001). These methods include the stereological methods known as the mean intercept length method, the volume orientation method and star volume distribution method. In cancellous bone, the unit vectors may represent the orientation of the interface surface area or the inclusion volume orientation, HILLIARD (1967).

The experimental procedure for the surface area orientation measurement of cancellous bone is described by WHITEHOUSE (1974 a, b), HARRIGAN and MANN (1984) and TURNER *et al.* (1990). The work of these authors, and ODGAARD (1997; 2001), ODGAARD *et al.* (1997), VAN RIETBERGEN *et al.* (1996, 1998) and others, has shown that the fabric tensor is a good measure of the structural anisotropy in cancellous bone tissue. The methodology of making measurements is easily adapted to an automated computational system as shown by HARRIGAN and MANN (1984) and TURNER *et al.* (1990).

In developing the relationship (3.7) between the elastic constant tensor and the fabric tensor, it was assumed that the matrix material of the porous elastic solid was isotropic and that the anisotropy of the porous elastic solid was completely determined by the fabric tensor representing the architecture of the material microstructure (see COWIN, 1985 and TURNER and COWIN, 1987). It was then shown that the material symmetries of orthotropy, transverse isotropy and isotropy correspond to the cases of three, two and one distinct eigenvalues of the fabric tensor, respectively. The symmetry of the material is orthotropic if the three eigenvalues of $\mathbf{H}$ are distinct, transverse isotropy if only two are distinct and isotropy if all three eigenvalues are equal. The paper of TURNER *et al.* (1990) reports on the experimental determination of the coefficients in the stress-strain-fabric relationship in the case of cancellous bone. See also VAN RIETBERGEN *et al.* (1996, 1998).

As noted above, the result (3.7) is based on the assumption that the matrix material is isotropic and that the anisotropy of the solid porous material is determined by the fabric tensor. In the case of cancellous bone the validity of that assumption has been experimentally verified by the work of ODGAARD *et al.* (1997). These authors concluded that the elastic and fabric main directions coincide in cancellous bone; cancellous bone is an elastic, highly porous material. ODGAARD *et al.* (1997) make the following remark: "Cowin's fabric mechanics relations (COWIN, 1985, 1986) (equation (3.7)) implicitly assume mechanical and fabric main directions must be aligned. This may seem an intuitively acceptable assumption, but experiment support has not previously been given". The fact that the mechanical and fabric main directions coincide in (3.7) is a direct algebraic consequence of the constitutive assumption that the stress is an isotropic function of the strain tensor and the normalized fabric tensor only. An explicit meaning of this assumption is that the mechanical anisotropy of the material is determined predominantly by architectural features measured by the normalized

fabric tensor measure and it is influenced less by other features, such as the actual symmetry of the matrix material. This same assumption is explicit in the related computation work of VAN RIETBERGEN(1996), and thus in ODGAARD *et al.* (1997).

A few words about whether the assumption that the second order fabric tensor is an adequate representation of the distribution of material of one phase relative to the material of the second phase and whether fabric tensors of higher order representing this distribution are necessary. Specifically, it is assumed that tensors of fourth order are not necessary. This is not always true; in certain situations the effect of the fourth order tensors can be of the same magnitude as the second order tensors. An example of this in the case of granular materials is given by MEHRABADI *et al.* (1988). In the case of solid materials with pores, specifically the case of a solid with isolated fluid-filled pores, it has been shown that, for oblate pores filled with fluid of low compressibility, the contribution of a fourth order fabric tensor is comparable with the one of the second order tensor (SHAFIRO and KACHANOV, 1997 and KACHANOV, 1999).

There is another misunderstanding of architectural adaptation theory recorded in JACOBS *et al.* (1997). These authors write that "The simplifying restriction to orthotropic material behavior common to other anisotropic remodeling formulations is not required (COWIN *et al.*, 1992)". The architectural adaptation theory of COWIN *et al.* (1992), described above is not restricted in the way suggested. When the architecturally adapting material is not in remodeling equilibrium, there are no restrictions on the material symmetry. When the architecturally adapting material is in remodeling equilibrium, the material symmetry must be either orthotropic, transversely isotropic or isotropic. This situation with respect to material symmetry in COWIN *et al.* (1992) is no more restricted than it is in the JACOBS *et al.* (1997) theory.

CARTER, ORR, and FYHRIE (1989) present a model for relating mechanical load history to the angle of intersection of trabeculae at a point in cancellous bone. The authors employ an initial mechanical state which is a two-dimensional, homogeneous, isotropic elastic continuum representation of the proximal femur. They apply a rule for determining an "equivalent normal stress" in a computationally iterative fashion to predict the angle of intersection of trabeculae. In their model this angle depends upon the magnitudes of different loadings, the number of cycles each loading is repeated, and an exponent that they take to be one or four. At several points in their text CARTER *et al.* (1989) contrast their approach to the development of a theory of trabecular bone remodeling with the approach taken by COWIN (1986):

A. On page 235 of CARTER *et al.* it is suggested "...that it may not be possible to correctly represent the local stimulus which determines bone orientation using the stress tensor calculated from a single loading condition, or any type of

'equilibrium' stress tensor (COWIN, 1986) that is representative of the loading history".

B. On page 241: "An important difference between our equivalent normal stress approach to estimating bone orientations and the trajectorial theory advanced by Wolff (1892), PAUWELS (1980), and COWIN (1986) is that we believe that the local stimulus to bone remodeling cannot, in general, be represented by a single stress tensor".

C. Also on page 241: "The trajectorial theory advanced by many previous investigators (VON MEYER, 1867; WOLFF, 1892; ROUX, 1880, 1895; HAYES and SNYDER, 1981; COWIN, 1986; FYHRIE and CARTER, 1986) can therefore be viewed as an approximation and is a degenerate case of the multiple-loading theory".

These remarks might leave the reader with incorrect impressions concerning the nature and assumptions underlying the bone remodeling theory proposed by COWIN (1986). Discussion is restricted here to two such points.

**Point 1**. Quote A suggests that the angle of intersection between individual trabeculae can be determined from a stress analysis of the authors' type, but not from one of the type employed by COWIN (1986). There is a fallacy in the suggestion of CARTER *et al.* that their stress analysis, or the continuum model proposed by COWIN (1986), can predict the angle of intersection of individual trabeculae.

The reason for the inability of these two models to make such a prediction is that the assumption of material continuity is not satisfied at the scale the prediction is made. That is to say that, in continuum models for cancellous bone, the continuum assumption restricts the resolution so that a material feature as small as the angle of intersection between trabeculae cannot be predicted because homogenization has been applied to make a continuum model.

The debate over the prediction of the angle of intersection of individual trabeculae from a stress analysis is not new. It began in 1866 when it was observed that the directions of the trabeculae in the proximal femur coincided closely with the directions of normal stress extrema predicted by a stress analysis of a homogeneous and continuous elastic object of the same shape as the bone, and loaded in the same way (COWIN, 2001). It was well known that the directions of normal stress extrema must be orthogonal. These observations led WOLFF (1892) to his rigid interpretation of the law that bears his name, the interpretation that requires real trabeculae to intersect orthogonally. Acknowledging the data which established that real trabeculae do not always intersect orthogonally, MURRAY (1936) pointed out the fallacy in Wolff's rigid interpretation by observing that the prediction of orthogonality in the directions of normal stress extrema is based on the assumption that the bone tissue density is continuous while, in reality, the density of trabecular architecture

is discontinuous. The fallacy that underlies the rigid interpretation of Wolff's law promulgated by WOLFF (1892) is to apply the results of a stress analysis, based on the assumption of a continuous material, to the prediction of discontinuous or discrete features whose characteristic length is smaller than the minimum length for which the assumption of material continuity is satisfied.

The resolution of the fallacy lies in the establishment of the length over which the material properties of cancellous bone microstructure are to be averaged to form a continuum model. It is only at that length, and at no smaller length scales, that the theoretically predicted directions of normal stress extrema can be compared with real trabecular architecture. The minimum value for this length is at least several trabecular widths. HARRIGAN *et al.* (1988) observed that the precise length is dependent on the stress gradient and suggested that, if the results of a stress analysis "...vary by more than 20–30% over a distance spanning three to five trabeculae, the results are suspect". A *resolution length restriction* for the trajectorial theory is that the directionality in the trabecular architecture of bone coincides with the predicted directions of normal stress extrema (i.e., the principal stress trajectories) only for lengths equal to or larger than the length on which trabecular bone can be considered as a continuous material (COWIN, 1989). This restriction prevents the trajectorial theory from the contradiction with nature embodied in Wolff's rigid interpretation, while it preserves the basic idea of the trajectorial theory.

CARTER *et al.* introduced the concept of an "equivalent normal stress" determined by a non-tensorial composition rule for combining a number of tensorial normal stress components, each normal stress being associated with a single loading condition. The extrema of the "equivalent normal stress" as a function of spatial direction are not, in general, orthogonal as they must be for a normal stress that is a tensorial component. The authors suggest that real trabeculae intersect at angles determined by the difference between the extrema directions of the "equivalent normal stress". Since these directions can, in general, be nonorthogonal, the authors suggest that real trabeculae need not intersect orthogonally. The authors do not discuss the fact that their "equivalent normal stress" rule predicts the angle of trabecular intersection to be dependent upon the number of cycles of the various loadings experienced by the bone, as well as upon the exponent that they take to be either one or four.

The fallacy in Wolff's viewpoint (COWIN, 2001) is repeated in the approach of CARTER *et al.*, even though the theory proposed by CARTER *et al.* is interpreted by them as predicting non-orthogonal intersection of individual trabeculae, rather than the orthogonal intersection of individual trabeculae argued by WOLFF (1892). The fallacy incorporated in both the interpretations

of WOLFF and of CARTER *et al.* is that, when the angles of intersection of real trabeculae are compared with the theoretically predicted directions of normal stress extrema, the cancellous bone is assumed to be both continuous and discontinuous on the same length scale. The prediction of directions of normal stress extrema requires the *assumption of a continuous material.* However, when the intersections of real trabeculae of a specimen are viewed with the eye, the viewer is visually acknowledging *the discontinuity of the material* structure. The fallacy (or contradiction) is that the theory assumes continuity and the visual inspection assumes discontinuity, on the same length scale.

**Point 2.** The approach of COWIN (1986), which characterizes remodeling equilibrium by a stress or strain tensor, does not exclude the possibility of the consideration of multiple loading stress histories.

It is possible to misinterpret the phrase "single loading condition" or "single stress tensor" in the quotes A and B given above from CARTER *et al.* The possibility for an incorrect interpretation arises from the authors' use of the adjective "single" to modify "stress tensor". The characterization of remodeling equilibrium by a stress tensor does not require or imply that only a single loading has been considered. A stress tensor can be determined at each point in a bone due to a single loading if the reasonable assumption that bone is a linearly elastic material is made. If multiple loadings are considered (OXNARD and YANG, 1981), the stress tensors for each single loading can be added together at any instant of time to obtain the stress tensor for the multiple loading. This composition is an application of the superposition principle of linear elasticity. When the time history of stress is considered for multiple loadings, the tensorial character preserving composition rules developed in the theories of hereditary phenomena (e.g. viscoelasticity, dielectric behavior, etc.) can easily be adapted so that the tensorial character of stress is preserved for multiple loading stress histories. Therefore, whether it is a single loading, or a multiple loading, or a multiple loading history, it is always possible to preserve the tensorial character of stress. The existence of a remodeling equilibrium stress tensor does not imply a single loading situation. The "equivalent normal stress" rule suggested by Carter *et al.* does not preserve the tensorial character and, from the restricted viewpoint of that rule, the authors' statements reject any combination of stress tensors that are not composed by their rule as a stimulus for bone remodeling. The quote *C* given above from CARTER *et al.* is open to a similar misinterpretation; the authors would have been clearer if they had prefaced the sentence that is quote *C* with the phrase "From the perspective of our nonlinear, nontensorial theory..." The way the sentence of quote C reads it could be misinterpreted as suggesting, in error, that the theories of many previous investigators are restricted to single loading situations.

## Appendix A. Special vectors and tensors in six dimensions

The developments in these notes will frequently concern the relationship between symmetric second rank tensors in three dimensions. The symmetric second rank tensors of interest will include stress and stress rate and strain and strain rate, among others. The most general form of a linear relationship between second rank tensors in three dimensions involves a three-dimensional fourth rank tensor. In general the introduction of tensors of rank higher than two involves considerable additional notation. However, since the interest here is only in three-dimensional fourth rank tensors that relate three-dimensional symmetric second rank tensors, a simple notational scheme can be introduced. The basis of the scheme is to consider a three-dimensional symmetric second rank tensor also as a six-dimensional vector and then three-dimensional fourth rank tensors may be associated with second rank tensors in a space of six dimensions. When this association is made, all of the algebraic machinery associated with the linear transformations and second rank tensors is available for the three-dimensional fourth rank tensors.

The definition of a second rank tensor in a space of three dimensions $\mathbf{T}$ is written in the form

$$\mathbf{T} = \sum_{j=1}^{j=3}\sum_{i=1}^{i=3} T_{ij}\mathbf{e}_i \otimes \mathbf{e}_j = \sum_{\beta=1}^{\beta=3}\sum_{\alpha=1}^{\alpha=3} T_{\alpha\beta}\mathbf{e}_\alpha \otimes \mathbf{e}_\beta, \tag{A.1}$$

where $\mathbf{e}_i$ and $\mathbf{e}_j$ are the (Latin) base vectors in a 3-dimensional vector space and where $\mathbf{e}_\alpha$ and $\mathbf{e}_\beta$ are the (Greek) base vectors in the same 3-dimensional vector space. Executing the summation in the Latin system,

$$\begin{aligned}\mathbf{T} = {} & T_{11}\mathbf{e}_1 \otimes \mathbf{e}_1 + T_{22}\mathbf{e}_2 \otimes \mathbf{e}_2 + T_{33}\mathbf{e}_3 \otimes \mathbf{e}_3 + T_{23}(\mathbf{e}_2 \otimes \mathbf{e}_3 + \mathbf{e}_3 \otimes \mathbf{e}_2) \\ & + T_{13}(\mathbf{e}_1 \otimes \mathbf{e}_3 + \mathbf{e}_3 \otimes \mathbf{e}_1) + T_{12}(\mathbf{e}_1 \otimes \mathbf{e}_2 + \mathbf{e}_2 \otimes \mathbf{e}_1).\end{aligned} \tag{A.2}$$

If a new set of base vectors defined by

$$\begin{aligned}\hat{\mathbf{e}}_1 &= \mathbf{e}_1 \otimes \mathbf{e}_1, \\ \hat{\mathbf{e}}_2 &= \mathbf{e}_2 \otimes \mathbf{e}_2, \\ \hat{\mathbf{e}}_3 &= \mathbf{e}_3 \otimes \mathbf{e}_3, \\ \hat{\mathbf{e}}_4 &= \frac{1}{\sqrt{2}}(\mathbf{e}_2 \otimes \mathbf{e}_3 + \mathbf{e}_3 \otimes \mathbf{e}_2), \\ \hat{\mathbf{e}}_5 &= \frac{1}{\sqrt{2}}(\mathbf{e}_1 \otimes \mathbf{e}_3 + \mathbf{e}_3 \otimes \mathbf{e}_1), \\ \hat{\mathbf{e}}_6 &= \frac{1}{\sqrt{2}}(\mathbf{e}_1 \otimes \mathbf{e}_2 + \mathbf{e}_2 \otimes \mathbf{e}_1),\end{aligned} \tag{A.3}$$

are introduced as well as a new set of tensor components defined by

$$\begin{aligned} \hat{T}_1 &= T_{11}, \quad \hat{T}_2 = T_{22}, \quad \hat{T}_3 = T_{33}, \\ \hat{T}_4 &= \sqrt{2}T_{23}, \quad \hat{T}_5 = \sqrt{2}T_{13}, \quad \hat{T}_6 = \sqrt{2}T_{12}, \end{aligned} \tag{A.4}$$

then (A.2) may be rewritten as

$$\hat{\mathbf{T}} = \hat{T}_1\hat{\mathbf{e}}_1 + \hat{T}_2\hat{\mathbf{e}}_2 + \hat{T}_3\hat{\mathbf{e}}_3 + \hat{T}_4\hat{\mathbf{e}}_4 + \hat{T}_5\hat{\mathbf{e}}_5 + \hat{T}_6\hat{\mathbf{e}}_6, \tag{A.5}$$

or

$$\hat{\mathbf{T}} = \sum_{i=1}^{i=6} \hat{T}_i\hat{\mathbf{e}}_i = \sum_{\alpha=1}^{\alpha=6} \hat{T}_\alpha\hat{\mathbf{e}}_\alpha, \tag{A.6}$$

which is the definition of a vector in six dimensions. Consider next a fourth rank tensor $\mathbf{c}$ in three dimensions defined by

$$\begin{aligned} \mathbf{c} &= \sum_{m=1}^{m=3}\sum_{k=1}^{k=3}\sum_{j=1}^{j=3}\sum_{i=1}^{i=3} c_{ijkm}\mathbf{e}_i\otimes\mathbf{e}_j\otimes\mathbf{e}_k\otimes\mathbf{e}_m \\ &= \sum_{\delta=I}^{\delta=III}\sum_{\gamma=I}^{\gamma=III}\sum_{\beta=I}^{\beta=III}\sum_{\alpha=I}^{\alpha=III} c_{\alpha\beta\gamma\delta}\mathbf{e}_\alpha\otimes\mathbf{e}_\beta\otimes\mathbf{e}_\gamma\otimes\mathbf{e}_\delta, \end{aligned} \tag{A.7}$$

and having symmetry in its first and second pair of indices, $c_{ijkm} = c_{jikm}$ and $c_{ijkm} = c_{ijmk}$, but not another symmetry in its indices; in particular $c_{ijkm} \neq c_{kmij}$ in general. The results of interest are for a fourth rank tensor in three dimensions with these particular symmetries because it is these fourth rank tensors that relate symmetric second rank tensors in three dimensions. Due to the special indicial symmetries just described, the change of basis (A.3) may be introduced in (A.7) and it may be rewritten as

$$c = \sum_{j=1}^{j=6}\sum_{i=1}^{i=6} \hat{c}_{ij}\hat{\mathbf{e}}_i\otimes\hat{\mathbf{e}}_j = \sum_{\beta=I}^{\beta=VI}\sum_{\alpha=I}^{\alpha=VI} \hat{c}_{\alpha\beta}\hat{\mathbf{e}}_\alpha\otimes\hat{\mathbf{e}}_\beta, \tag{A.8}$$

where the 36 components of $c_{ijkm}$, the fourth rank tensor in three dimensions (with the symmetries $c_{ijkm} = c_{jikm}$ and $c_{ijkm} = c_{ijmk}$) are related to the 36

components of $\hat{c}_{ij}$, the second rank tensor in six dimensions, by

$$
\begin{aligned}
&\hat{c}_{11} = c_{1111}, \quad \hat{c}_{22} = c_{2222}, \quad \hat{c}_{33} = c_{3333}, \quad \hat{c}_{23} = c_{2233},\\
&\hat{c}_{32} = c_{3322}, \quad \hat{c}_{13} = c_{1133}, \quad \hat{c}_{31} = c_{3311}, \quad \hat{c}_{12} = c_{1122},\\
&\hat{c}_{21} = c_{2211}, \quad \hat{c}_{44} = 2c_{2323}, \quad \hat{c}_{55} = 2c_{1313}, \quad \hat{c}_{66} = 2c_{1212},\\
&\hat{c}_{45} = 2c_{2313}, \quad \hat{c}_{54} = 2c_{1323}, \quad \hat{c}_{46} = 2c_{2312}, \quad \hat{c}_{64} = 2c_{1223},\\
&\hat{c}_{56} = 2c_{1312}, \quad \hat{c}_{65} = 2c_{1213}, \quad \hat{c}_{41} = \sqrt{2}c_{2311}, \quad \hat{c}_{14} = \sqrt{2}c_{1123},\\
&\hat{c}_{51} = \sqrt{2}c_{1311}, \quad \hat{c}_{15} = \sqrt{2}c_{1113}, \quad \hat{c}_{61} = \sqrt{2}c_{1211}, \quad \hat{c}_{16} = \sqrt{2}c_{1112},\\
&\hat{c}_{42} = \sqrt{2}c_{2322}, \quad \hat{c}_{24} = \sqrt{2}c_{2223}, \quad \hat{c}_{52} = \sqrt{2}c_{1322}, \quad \hat{c}_{25} = \sqrt{2}c_{2213},\\
&\hat{c}_{62} = \sqrt{2}c_{1222}, \quad \hat{c}_{26} = \sqrt{2}c_{2212}, \quad \hat{c}_{43} = \sqrt{2}c_{2333}, \quad \hat{c}_{34} = \sqrt{2}c_{3323},\\
&\hat{c}_{53} = \sqrt{2}c_{1333}, \quad \hat{c}_{35} = \sqrt{2}c_{3313}, \quad \hat{c}_{63} = \sqrt{2}c_{1233}, \quad \hat{c}_{36} = \sqrt{2}c_{3312}.
\end{aligned}
\tag{A.9}
$$

Using the symmetry of the second rank tensors, $\mathbf{T} = \mathbf{T}^{\mathrm{T}}$ and $\mathbf{J} = \mathbf{J}^{\mathrm{T}}$, as well as the two indicial symmetries of $c_{\mathrm{ijkm}}$, the linear relationship between $\mathbf{T}$ and $\mathbf{J}$,

$$
T_{ij} = \sum_{j=1}^{j=3} \sum_{i=1}^{i=3} c_{ijkm} J_{km},
\tag{A.10}
$$

may be expanded to read

$$
\begin{aligned}
T_{11} &= c_{1111}J_{11} + c_{1122}J_{22} + c_{1133}J_{33} + 2c_{1123}J_{23} + 2c_{1113}J_{13} + 2c_{1112}J_{12},\\
T_{22} &= c_{2211}J_{11} + c_{2222}J_{22} + c_{2233}J_{33} + 2c_{2223}J_{23} + 2c_{2213}J_{13} + 2c_{2212}J_{12},\\
T_{33} &= c_{3311}J_{11} + c_{3322}J_{22} + c_{3333}J_{33} + 2c_{3323}J_{23} + 2c_{3313}J_{13} + 2c_{3312}J_{12},\\
T_{23} &= c_{2311}J_{11} + c_{2322}J_{22} + c_{2333}J_{33} + 2c_{2323}J_{23} + 2c_{2313}J_{13} + 2c_{2312}J_{12},\\
T_{13} &= c_{1311}J_{11} + c_{1322}J_{22} + c_{1333}J_{33} + 2c_{1323}J_{23} + 2c_{1313}J_{13} + 2c_{1312}J_{12},\\
T_{12} &= c_{1211}J_{11} + c_{1222}J_{22} + c_{1233}J_{33} + 2c_{1223}J_{23} + 2c_{1213}J_{13} + 2c_{1212}J_{12},
\end{aligned}
\tag{A.11}
$$

The corresponding linear relationship between $\hat{\mathbf{T}}$ and $\hat{\mathbf{J}}$,

$$
\hat{T}_i = \sum_{j=1}^{j=6} \hat{c}_{ij} \hat{J}_j,
\tag{A.12}
$$

may be expanded to read

$$
\begin{aligned}
\widehat{T}_1 &= \hat{c}_{11}\hat{J}_1 + \hat{c}_{12}\hat{J}_2 + \hat{c}_{13}\hat{J}_3 + \hat{c}_{14}\hat{J}_4 + \hat{c}_{15}\hat{J}_5 + \hat{c}_{16}\hat{J}_6,\\
\widehat{T}_2 &= \hat{c}_{21}\hat{J}_1 + \hat{c}_{22}\hat{J}_2 + \hat{c}_{23}\hat{J}_3 + \hat{c}_{24}\hat{J}_4 + \hat{c}_{25}\hat{J}_5 + \hat{c}_{26}\hat{J}_6,\\
\widehat{T}_3 &= \hat{c}_{31}\hat{J}_1 + \hat{c}_{32}\hat{J}_2 + \hat{c}_{33}\hat{J}_3 + \hat{c}_{34}\hat{J}_4 + \hat{c}_{35}\hat{J}_5 + \hat{c}_{36}\hat{J}_6,\\
\widehat{T}_4 &= \hat{c}_{41}\hat{J}_1 + \hat{c}_{42}\hat{J}_2 + \hat{c}_{43}\hat{J}_3 + \hat{c}_{44}\hat{J}_4 + \hat{c}_{45}\hat{J}_5 + \hat{c}_{46}\hat{J}_6,\\
\widehat{T}_5 &= \hat{c}_{51}\hat{J}_1 + \hat{c}_{52}\hat{J}_2 + \hat{c}_{53}\hat{J}_3 + \hat{c}_{54}\hat{J}_4 + \hat{c}_{55}\hat{J}_5 + \hat{c}_{56}\hat{J}_6,\\
\widehat{T}_6 &= \hat{c}_{61}\hat{J}_1 + \hat{c}_{62}\hat{J}_2 + \hat{c}_{63}\hat{J}_3 + \hat{c}_{64}\hat{J}_4 + \hat{c}_{65}\hat{J}_5 + \hat{c}_{66}\hat{J}_6.
\end{aligned}
\tag{A.13}
$$

The advantage to the notation (A.12) or (A.13) as opposed to the notation (A.10) or (A.11) is that there is no matrix representation of (A.10) or (A.11) that retains the tensorial character while there is a simple, direct and familiar tensorial representation of (A.12) or (A.13). The Eqs. (A.12) or (A.13) may be written in matrix notation as the linear transformation

$$
\widehat{\mathbf{T}} = \widehat{\mathbf{C}}\hat{\mathbf{J}}. \tag{A.14}
$$

Recalling the rule for the transformation of vectors in a coordinate transformation, the transformation rule for $\widehat{\mathbf{T}}$ or $\hat{\mathbf{J}}$ may be written down by inspection,

$$
\hat{\mathbf{J}}^{(L)} = \widehat{\mathbf{Q}}\hat{\mathbf{J}}^{(G)} \qquad \text{and} \qquad \hat{\mathbf{J}}^{(G)} = \widehat{\mathbf{Q}}^T\hat{\mathbf{J}}^{(L)}, \tag{A.15}
$$

where the superscripts $L$ and $G$ refer to the bases denoted using the Latin or Greek alphabets for subscripts. Furthermore the second rank tensor $\widehat{\mathbf{C}}$ in the space of six dimensions transforms according to the rule

$$
\widehat{\mathbf{C}}^{(L)} = \widehat{\mathbf{Q}}\widehat{\mathbf{C}}^{(G)}\widehat{\mathbf{Q}}^T \qquad \text{and} \qquad \widehat{\mathbf{C}}^{(G)} = \widehat{\mathbf{Q}}^T\widehat{\mathbf{C}}^{(L)}\widehat{\mathbf{Q}}. \tag{A.16}
$$

In short, the second rank tensor $\widehat{\mathbf{C}}$ in the space of six dimensions may be treated exactly like a second rank tensor in the space of three dimensions as far as the usual tensorial operations are concerned.

The relationship between components of the second rank tensor in three dimensions and the vector in 6 dimensions contained in (A.4) may be written in $n$-tuple notation for $\mathbf{T}$ and $\mathbf{J}$ ($\widehat{\mathbf{T}}$ and $\hat{\mathbf{J}}$),

$$
\begin{aligned}
\widehat{\mathbf{T}} &= [\widehat{T}_1, \widehat{T}_2, \widehat{T}_3, \widehat{T}_4, \widehat{T}_5, \widehat{T}_6]^T = [T_{11}, T_{22}, T_{33}, \sqrt{2}T_{23}, \sqrt{2}T_{13}, \sqrt{2}T_{12}]^T,\\
\hat{\mathbf{J}} &= [\hat{J}_1, \hat{J}_2, \hat{J}_3, \hat{J}_4, \hat{J}_5, \hat{J}_6]^T = [J_{11}, J_{22}, J_{33}, \sqrt{2}J_{23}, \sqrt{2}J_{13}, \sqrt{2}J_{12}]^T.
\end{aligned}
\tag{A.17}
$$

These formulas permit the conversion of three-dimensional second rank tensor components directly to six-dimensional vector components and *vice versa*.

The $\sqrt{2}$ factor that multiplies the last three components of the definition of the six-dimensional vector representation of the three-dimensional second rank tensor, (A.4), assures the scalar product of the two six-dimensional vectors is equal to the trace of the product of the corresponding second rank tensors,

$$\widehat{\mathbf{T}} \cdot \hat{\mathbf{J}} = \mathrm{tr}\mathbf{T}\mathbf{J} = \mathbf{T} : \mathbf{J}. \tag{A.18}$$

The transformation rules (A.15) and (A.16) for the vector and second rank tensors in six dimensions involve the six-dimensional orthogonal tensor transformation $\widehat{\mathbf{Q}}$. The tensor components of $\widehat{\mathbf{Q}}$ are given in terms of $\mathbf{Q}$ by

$$\widehat{\mathbf{Q}} = \begin{bmatrix} \widehat{Q}_{11} & \widehat{Q}_{12} & \widehat{Q}_{13} & \widehat{Q}_{14} & \widehat{Q}_{15} & \widehat{Q}_{16} \\ \widehat{Q}_{21} & \widehat{Q}_{22} & \widehat{Q}_{23} & \widehat{Q}_{24} & \widehat{Q}_{25} & \widehat{Q}_{26} \\ \widehat{Q}_{31} & \widehat{Q}_{32} & \widehat{Q}_{33} & \widehat{Q}_{34} & \widehat{Q}_{35} & \widehat{Q}_{36} \\ \widehat{Q}_{41} & \widehat{Q}_{42} & \widehat{Q}_{43} & \widehat{Q}_{44} & \widehat{Q}_{45} & \widehat{Q}_{46} \\ \widehat{Q}_{51} & \widehat{Q}_{52} & \widehat{Q}_{53} & \widehat{Q}_{54} & \widehat{Q}_{55} & \widehat{Q}_{56} \\ \widehat{Q}_{61} & \widehat{Q}_{62} & \widehat{Q}_{63} & \widehat{Q}_{64} & \widehat{Q}_{65} & \widehat{Q}_{66} \end{bmatrix} \tag{A.19}$$

$$= \begin{bmatrix} Q_{11}^2 & Q_{21}^2 & Q_{31}^2 & \sqrt{2}Q_{21}Q_{31} \\ Q_{12}^2 & Q_{22}^2 & Q_{32}^2 & \sqrt{2}Q_{22}Q_{32} \\ Q_{13}^2 & Q_{23}^2 & Q_{33}^2 & \sqrt{2}Q_{23}Q_{33} \\ \sqrt{2}Q_{13}Q_{12} & \sqrt{2}Q_{22}Q_{22} & \sqrt{2}Q_{32}Q_{33} & Q_{22}Q_{33} + Q_{32}Q_{23} \\ \sqrt{2}Q_{11}Q_{13} & \sqrt{2}Q_{21}Q_{22} & \sqrt{2}Q_{31}Q_{33} & Q_{21}Q_{33} + Q_{23}Q_{31} \\ \sqrt{2}Q_{11}Q_{12} & \sqrt{2}Q_{21}Q_{22} & \sqrt{2}Q_{31}Q_{32} & Q_{21}Q_{32} + Q_{22}Q_{31} \end{bmatrix}$$

$$\begin{bmatrix} \sqrt{2}Q_{11}Q_{31} & \sqrt{2}Q_{11}Q_{21} \\ \sqrt{2}Q_{12}Q_{32} & \sqrt{2}Q_{12}Q_{22} \\ \sqrt{2}Q_{13}Q_{33} & \sqrt{2}Q_{13}Q_{23} \\ Q_{12}Q_{33} + Q_{32}Q_{13} & Q_{12}Q_{23} + Q_{13}Q_{22} \\ Q_{11}Q_{33} + Q_{13}Q_{31} & Q_{11}Q_{23} + Q_{21}Q_{13} \\ Q_{11}Q_{32} + Q_{12}Q_{31} & Q_{11}Q_{22} + Q_{12}Q_{21} \end{bmatrix}.$$

To see that $\widehat{\mathbf{Q}}$ is an orthogonal matrix in six dimensions requires some algebraic manipulation. The proof rests on the orthogonality of the three-dimensional $\mathbf{Q}$:

$$\mathbf{Q}\mathbf{Q}^T = \mathbf{Q}^T\mathbf{Q} = 1, \ \Rightarrow \widehat{\mathbf{Q}}\widehat{\mathbf{Q}}^T = \widehat{\mathbf{Q}}^T\widehat{\mathbf{Q}} = \hat{1}. \tag{A.20}$$

In the special case when $\mathbf{Q}$ is given by

$$\mathbf{Q} = \begin{bmatrix} \cos\alpha & -\sin\alpha & 0 \\ \sin\alpha & \cos\alpha & 0 \\ 0 & 0 & 1 \end{bmatrix}. \tag{A.21}$$

$\hat{\mathbf{Q}}$ has the representation

$$\text{(A.22)}\quad \hat{\mathbf{Q}} = \begin{bmatrix} \cos^2\alpha & \sin^2\alpha & 0 & 0 & 0 & \sqrt{2}\cos\alpha\sin\alpha \\ \sin^2\alpha & \cos^2\alpha & 0 & 0 & 0 & -\sqrt{2}\cos\alpha\sin\alpha \\ 0 & 0 & 1 & 0 & 0 & 0 \\ 0 & 0 & 0 & \cos\alpha & -\sin\alpha & 0 \\ 0 & 0 & 0 & \sin\alpha & \cos\alpha & 0 \\ -\sqrt{2}\cos\alpha\sin\alpha & \sqrt{2}\cos\alpha\sin\alpha & 0 & 0 & 0 & \cos^2\alpha - \sin^2\alpha \end{bmatrix}$$

It should be noted that while it is always possible to find $\hat{\mathbf{Q}}$ given $\mathbf{Q}$ by use of (A.19), it is not possible to determine $\mathbf{Q}$ unambiguously given $\hat{\mathbf{Q}}$. Although $\hat{\mathbf{Q}}$ is uniquely determined by $\mathbf{Q}$, the reverse process of finding a $\mathbf{Q}$ given $\hat{\mathbf{Q}}$ is not unique in that there will be a choice of sign necessary in the reverse process. To see this non-uniqueness note that both $\mathbf{Q} = \mathbf{1}$ and $\mathbf{Q} = -\mathbf{1}$ correspond to $\hat{\mathbf{Q}} = \hat{1}$. There are 9 components of $\mathbf{Q}$ that satisfy 6 conditions given by $(A.20)_1$. There are therefore only three independent components of $\mathbf{Q}$. However, there are 36 components of $\hat{\mathbf{Q}}$ that satisfy the 21 conditions given $(A.20)_2$ and hence 15 independent components of $\hat{\mathbf{Q}}$. Thus, while (A.19) uniquely determines $\hat{\mathbf{Q}}$ given $\mathbf{Q}$, the components of $\hat{\mathbf{Q}}$ must be considerably restricted in order to determine $\mathbf{Q}$ given $\hat{\mathbf{Q}}$, and selections of signs must be made.

## References


1. R.B. Ashman, S.C. Cowin, W.C. Van Buskirk, J.C. Rice, *A continuous wave technique for the measurement of the elastic properties of cortical bone*, J. Biomechanics, **17**, 349–361, 1984.
2. D.R. Carter, T.E. Orr, D.P. Fyhrie, *Relationships between loading history and femoral cancellous bone architecture*, J. Biomechanics, **22**, 231–244, 1989.
3. S.C. Cowin, D.M. Hegedus, *Bone remodeling I: A Theory of adaptive elasticity*, J. of Elasticity, **6**, 313–325, 1976.
4. S.C. Cowin, R.R. Nachlinger, *Bone remodeling III; uniqueness and stability in adaptive elasticity theory*, J. of Elasticity, **8**, 285–295, 1978.
5. S.C. Cowin, W.C. Van Buskirk, *Internal bone remodeling induced by a medullary pin*, J. Biomechanics, **11**, 269–275, 1978.

6. S.C. Cowin, W.C. Van Buskirk, *Surface bone remodeling induced by a medullary pin*, J. Biomechanics, **12**, 269–276, 1979.

7. S.C. Cowin, K. Firoozbakhsh, *Bone remodeling of diaphyseal surfaces under constant load: theoretical predictions*, J. Biomechanics, **14**, 471–484, 1981.

8. S.C. Cowin, *The relationship between the elasticity tensor and the fabric tensor*, Mechanics of Materials, **4**, 137–147, 1985.

9. S.C. Cowin, R.T. Hart, J.R. Balser, D.H. Kohn, *Functional adaptation in long bones: establishing in vivo values for surface remodeling rate coefficients*, J. Biomechanics, **18**, 665–684, 1985.

10. S.C. Cowin, *Wolff's law of trabecular architecture at remodeling equilibrium*, J. Biomechanical Engineering, **108**, 83–88, 1986.

11. S.C. Cowin, *A Resolution restriction for Wolff's law of trabecular architecture*, Bull. Hosp. Jt. Dis. Orthop. Inst., **49**, 206–213, 1989.

12. S.C. Cowin, L. Moss-Salentijn, M.L. Moss, *Candidates for the mechanosensory system in bone*, J. Biomechanical Engineering, **113**, 191–197, 1991.

13. S.C. Cowin, A.M. Sadegh, G.M. Luo, *An Evolutionary Wolff's law for trabecular architecture*, J. Biomechanical Engineering, **114** 129–136, 1992.

14. S.C. Cowin, Y. Arramon, G.M. Luo, A.M. Sadegh, *Chaos in the discrete-time algorithm for bone density remodeling rate equations*, J. Biomechanics, **26**, 1077–1089, 1993.

15. S.C. Cowin, S. Weinbaum, Yu Zeng, *A case for bone canaliculi as the anatomical site of strain generated potentials*, J. Biomechanics, **28**, 1281–1296, 1995.

16. S.C. Cowin, *Strain or deformation rate-dependent finite growth in soft tissues*, J. Biomechanics, **29**, 647–649, 1996.

17. S.C. Cowin, *Bone Poroelasticity*, J. Biomechanics, **32**, 218–238, 1999.

18. S.C. Cowin, M.L. Moss, *Mechanosensory mechanisms in bone*, [in:] Textbook of Tissue Engineering, ($2^{nd}$ edition) R. Lanza, R. Langer, W. Chick [Eds.], Academic Press, San Diego, 723–738, 2000.

19. S.C. Cowin, *The false premise in Wolff's law*, [in:] Bone Mechanics Handbook, S.C. Cowin [Ed.], CRC Press, Boca Raton, FL, 2001.

20. S.C. Cowin, *Mechanosensation and fluid transport in living bone*, Journal of Musculoskeletal and Neuronal Interactions (JMNI), 2, 256–260, 2002.

21. K. Firoozbakhsh, S.C. Cowin, *Devolution of inhomogeneities in bone structure: predictions of adaptive elasticity theory*, J. Biomechanical Engineering, **102**, 287–293, 1980.

22. K. Firoozbakhsh, S.C. Cowin, *An analytical model of Pauwels functional adaptation mechanism for bone*, J. Biomechanical Engineering, **103**, 246–252, 1981.

23. H.M. Frost, *Dynamics of bone remodeling*, [in:] Bone Biodynamics, H.M. Frost [Ed.], Little and Brown, Boston 1964.

24. Y.C. Fung, *Biomechanics; motion, flow, stress and growth*, Springer, New York 1990.

25. D.P. Fyhrie, D.R. Carter, *A unifying principle relating stress to trabecular bone morphology*, J. Orthop. Res., **4**, 304–317, 1986.

26. A.E. Goodship, L.E. Lanyon, J.H. McFie, *Functional adaptation of bone to increased stress*, J. Bone Jt Surg., **61-A**, 539–546, 1979.

27. R.W. Goulet, S.A. Goldstein, M.J. Ciarelli, J.L. Kuhn, M.B. Brown, L.A. Feldkamp, *The relationship between the structural and orthogonal compressive properties of trabecular bone*, J. Biomechanics, **27**, 375–389, 1994.

28. T. Harrigan, R.W. Mann, *Characterization of microstructural anisotropy in orthotropic materials using a second rank tensor*, J. Mat. Sci., 19, 761–769, 1984.

29. T.P. Harrigan, M. Jasty, R.W. Mann, W.H. Harris, *Limitations on the continuum assumption in cancellous bone*, J. Biomechanics, **21**, 269–276, 1988.

30. R.L. Hart, *Bone modeling and remodeling: theories and computation*, [in:] Bone Mechanics Handbook, S.C. Cowin [Ed.], CRC Press, Boca Raton, FL, 2001.

31. R.F.S. Hearmon, *An introduction to applied anisotropic elasticity*, Oxford University Press, Oxford.1961

32. D.M. Hegedus, S.C. Cowin, *Bone remodeling, II: small strain adaptive elasticity*, J. of Elasticity, **6**, 337–352, 1976.

33. G. Hermann, H. Liebowitz, *Mechanics of bone fracture*, [in:] Fracture: An Advanced Treatise, Vol. 7, H. Liebowitz [Ed.], Academic Press, 771-840, New York 1972.

34. J.E. Hilliard, *Determination of structural anisotropy*, Stereology – Proc. 2nd Int. Congress for Stereology, Chicago 1967, Springer, 219, Berlin 1967.

35. R. Huiskes, H. Weinans, J. Grootenboer, M. Dalstra, B. Fudala, T.J. Slooff, *Adaptive bone remodeling theory applied to prosthetic-design analysis*, J. Biomechanics, **20**, 1135–1150, 1987.

36. C.R Jacobs, J.C. Simo, G.S. Beaupré, D.R. Carter, *Adaptive bone remodeling incorporating simultaneous density and anisotropy considerations*, J. Biomechanics, **30**, 603–613, 1997.

37. Z.G.K Jaworski, M. Liskova-Kiar, H.K. Uhthoff, *Effect of long term immobilization on the pattern of bone loss in older dogs*, J. Bone Jt Surg., 62-B, 104–110, 1980.

38. M. Kachanov, *Solids with cracks and non-spherical pores: proper parameters of defect density and effective elastic properties*, Int. J. Fracture, **97**, 1–32, 1999.

39. K. Kanatani, *Characterization of structural anisotropy by fabric tensors and their statistical test*, J. Japanese Soil Mech. Found. Engrg., **23**, 171, 1983.

40. K.I. Kanatani, *Distribution of directional data and fabric tensors*, Int. J. Engr. Sci., **22**, 149–164, 1984a.

41. K. Kanatani, *Stereological determination of structural anisotropy*, Int. J. Engr. Sci., **22**, 531–546, 1984b.

42. K. Kanatani, *Procedures for stereological estimation of structural anisotropy*, Int. J. Engrg. Sci., **23**, 587–596, 1985.

43. A.D. Kuo, D.R. Carter, *Computational methods for analyzing the structure of cancellous bone in planar sections*, J. Orthop. Res., **9**, 918–931, 1991.

44. B.K.F. Kummer, *Biomechanics of bone*, [in:] Biomechanics, Y.C. Fung, N. Perrone, M. Anliker [Eds.], Prentice Hall, 237–271, 1972.

45. L.E. LANYON, A.E. GOODSHIP, C.J. PYE, J.H. MACFIE, *Mechanically adaptive bone remodeling*, J. Biomechanics, **15**, 141–154, 1982.

46. L.E. LANYON, C.T. RUBIN, *Static versus dynamic loads as an influence on bone remodeling*, J. Biomechanics, **17**, 897–906, 1984.

47. S.G. LEKHNITSKII, *Theory of elasticity of an anisotropic elastic body*, Holden Day, San Francisco 1963.

48. G.M. LUO, S.C. COWIN, A.M. SADEGH, Y. ARRAMON, *Implementation of strain rate as a bone remodeling stimulus*, J. Biomechanical Engineering, **117**, 329–338, 1995.

49. R.B. MARTIN, D.R. BURR, *Structure, Function and Adaptation of Compact Bone*, Raven Press, New York 1989.

50. M.M. MEHRABADI, S. NEMAT-NASSER, H.M. SHODJA, G. SUBHASH, *Some basic theoretical and experimental results on micromechanics of granular flow*, [in:] Micromechanics of Granular Materials, S. SATAKE, J.T. JENKINS [Eds.], Elsevier, Amsterdam 1988.

51. J. MONNIER, L. TRABUCHO, *Existence and uniqueness of solution to an adaptive elasticity model*, Mathematics and Mechanics of Solids, **3**, 217–228, 1998a.

52. J. MONNIER, L. TRABUCHO, *An Existence and uniqueness result in bone remodeling theory*, Comp. Meth. Appl. Mech. Engng., **151**, 539–544, 1998b.

53. P.D.F. MURRAY, *Bones, a study of the development and structure of the vertebrate skeleton*, Cambridge U.P., 1936.

54. J.A. O'CONNOR, L.E. LANYON, H. MACFIE, *The influence of strain rate on adaptive bone remodeling*, J. Biomechanics, **15**, 767–781, 1982.

55. A. ODGAARD, J. KABEL, B. VAN RIETBERGEN, M. DALSTRA, R. HUISKES, *Fabric and elastic principal directions of cancellous bone are closely related*, J. Biomechanics, **30**, 487–495, 1997.

56. A. ODGAARD, *Three-dimensional methods for quantification of cancellous bone architecture*, Bone, **20**, 315–328, 1997.

57. A. ODGAARD, *Quantification of cancellous bone architecture*, Bone Mechanics Handbook, S.C. COWIN [Ed.], CRC Press, Boca Raton, FL, 2001.

58. C.E. OXNARD, H.C. YANG, *Beyond biometrics: studies of complex biological patterns*, Symposia of the Zoological Society of London, 46, 127–l67, 1981.

59. F. PAUWELS, *Gesammelte abhandlungen zur funktionellen anatornie des Bewegungsapparates*, Springer Verlag, 1965.

60. P.J. PRENDERGAST, D. TAYLOR, *Prediction of bone adaptation using damage accumulation*, J. Biomechanics, **27**, 1067–1076, 1994.

61. P.J. PRENDERGAST, *An analysis of theories in biomechanics*, Engng. Trans., **49**, 117–133, 2001.

62. W. ROUX, *The problems, methods, and scope of developmental mechanics, An introduction to the "Archiv für Entwickelungsmechanik der Organismen"*, (translated by W.M. WHEELER), Wood's Hole Biol. Lect., (1895), pp. 149–90, 1885.

63. C.T. RUBIN, L.E. LANYON, *Regulation of bone formation by applied dynamic loads*, J. Bone Jt. Surg., **66A**, 397, 1984.

64. B. SHAFIRO, M. KACHANOV, *Materials with fluid filled pores of various shapes: effective elastic properties and fluid pressure polarization*, Int. J. Solids Structures, **34**, 3517–3540, 1997.

65. T.H. SMIT, J.M. HUYGHE, S.C. COWIN, *A double poroelastic model of cortical bone: estimation of the linear isotropic parameters*, J. Biomechanics, **35**, 829–836, 2002.

66. S. TIMOSHENKO, *Strength of Materials*, 3rd. ed., Vol. 1, Chapter VIII, Van Nostrand, 1955.

67. L. TRABUCHO, *An existence result in bone remodeling* [in:] *IUTAM Syposium on Synthesis in Bio-Solid Mechanics*, P. PETERSEN and M.P. BENDSØE [Eds.], Kluwer, Dordrecht, 235–246, 1999.

68. M.C. TSILI, *Theoretical solutions for internal bone remodeling of diaphyseal shafts using adaptive elasticity theory*, J. Biomechanics, **33**, 235–239, 2000.

69. C.H. TURNER, S.C. COWIN, *On the dependence of the elastic constants of an anisotropic porous material upon porosity and fabric*, J. Materials Sci., **22**, 3178–3184, 1987.

70. C.H. TURNER, S.C. COWIN, J.Y. RHO, R.B. ASHMAN, J.C. RICE, *The fabric dependence of the orthotropic elastic properties of cancellous bone*, J. Biomechanics, **23**, 549–561, 1990.

71. H.K. UHTHOFF, Z.F.G. JAWORSKI, *Bone loss in response to long term immobilization*, J. Bone Jt Surg., 60-B, 420–429, 1978.

72. C. VAN COCHRAN, *Primer of Orthopaedic Biomechanics*, Churchill Livingstone, New York 1982.

73. B. VAN RIETBERGEN, A. ODGAARD, J. KABEL, R. HUISKES, *Direct mechanical assessment of elastic symmetries and properties of trabecular bone architecture*, J. Biomechanics, **29**, 1653–1657, 1996.

74. B. VAN RIETBERGEN, A. ODGAARD, J. KABEL, R. HUISKES, *Relationships between bone morphology and bone elastic properties can be accurately quantified using high-resolution computer reconstructions*, J. Orthop. Res., **16**, 23–28, 1998.

75. L. WANG, S.P. FRITTON, S.C. COWIN, S. WEINBAUM, *Fluid pressure relaxation mechanisms in osteonal bone specimens: modeling of an oscillatory bending experiment*, J. Biomechanics, **32**, 663–672, 1999.

76. L. WANG, S.C. COWIN, S. WEINBAUM, S.P. FRITTON, *Modeling tracer transport in an osteon under cyclic loading*, Ann. Biomed. Engng., **28**, 1200–1209, 2000.

77. S. WEINBAUM, S.C. COWIN, YU ZENG, *A model for the excitation of osteocytes by mechanical loading-induced bone fluid shear stresses*, J. Biomechanics, **27**, 339–360, 1994.

78. W.J. WHITEHOUSE, *The quantitative morphology of anisotropic trabecular bone*, J. Microscopy, **101**, 153–168, 1974.

79. W.J. WHITEHOUSE, E.D. DYSON, *Scanning electron microscope studies of trabecular bone in the proximal end of the human femur*, J. Anatomy, **118**, 417–444, 1974.

80. J. WOLFF, *Das gesetz der transformation der Knochen*, Berlin, Hirschwald, 1892.

81. J. WOLFF, *The law of bone remodelling*, Springer, Berlin 1986.

82. S.L.Y. Woo, S.C. Kuei, W.A. Dillon, D. Amiet, F.C. White, W.H. Akeson, *The effect of prolonged physical training on the properties of long bone-a study of Wolff's law*, J. Bone Jt Surg., 63-A, 780–787, 1981.

83. L. You, S.C. Cowin, M. Schaffler, S. Weinbaum, *A model for strain amplification in the actin cytoskeleton of osteocytes due to fluid drag on pericellular matrix*, J. Biomechanics, **34**, 1375–1386, 2001.

84. D. Zhang, S.C. Cowin, S. Weinbaum, *Electrical signal transmission in a bone cell network: the influence of a discrete gap junction*, Ann. Biomed. Engng., **26**, 644–659, 1998.

85. P.K. Zysset, R.W. Goulet, S.J. Hollister, *A global relationship between trabecular morphology and homogenized elastic properties*, Journal of Biomechanical Engineering, **120**, 640–646, 1998.

86. P.K. Zysset, *A review of morphology-elasticity relationships in human trabecular bone: theories and experiments*, J. Biomechanics, 2002 (in press).

Note added in proof, June 15, 2003.

The following references contain further developments of the theory described in this review and critique.

M. Epstein, G.A. Maugin, *Thermomechanics of volumetric growth in uniform bodies*, International Journal of Plasticity, **16**, 951–978, 2000.

V.A. Lubarda, A. Hoger, *On the mechanics of solids with a growing mass*, International Journal of Solids and Structures, **39**, 4627–4664, 2002.

S. Ramtani, M. Zidi, *Damaged bone remodeling theory: thermodynamical approach*, Mechanics Research Communications, **26**, 701–708, 1999.

S. Ramtani, M. Zidi, *A theoretical model of the effect of continuum damage on a bone adaptation model*, Journal of Biomechanics, **34**, 471–479, 2001.

S. Ramtani, M. Zidi, *Damaged bone adaptation under steady homogeneous stress*, ASME Journal of Biomechanical Engineering, **124**, 1–6, 2002.

M. Zidi, S. Ramtani, *Stability analysis and finite element simulation of bone remodeling model*, ASME Journal of Biomechanical Engineering, **122**, 1–4, 2000.

*Received September 25, 2002.*